H24/3424

MONASH UNIVERSITY
THESIS ACCEPTED IN SATISFACTION OF THE
REQUIREMENTS FOR THE DEGREE OF
DOCTOR OF PHILOSOPHY
ON..... 13 May 2003 .....

.....[redacted].....

Sec. Research Graduate School Committee

ERRATA

p. 6 para 2, line 2" "mechanism and" for " mechanism "ant"
p. 14, last bullet point: "acting as an impurity" for "acting as ab impurity"
p. 17 para 1, line 4: "that a decrease" for "that an decrease"
p. 25, para 3, line 2: " the initial value" for "initial vale"
p. 35, Tabel 2.2, column 4, row 2, bullet point 2: "Applied only to Cr-Mo-V" for "Applied I Cr-Mo-V"
p. 39, para 1, line 8: "reported a decrease of hardness" for "reported an increase of hardness"
p. 41, para 1, line 2: "carbides" for "carbohydrates"
p. 54, Figure 3.3 caption: "after Croker, 1997" for " after Croker 1998"
p. 60 para 1, line 15:"Alexander and Klueh, 1990" for "Alexander and Klueh, 1991"
p. 74, Table 4.3, title"... of sub-size correlation" for " ... of sub-seize correlation"
p. 88, para 1, line 4: "susceptible to temper... for "susceptible t temper"
p. 90, para 2, line 6: "from Charpy" for "form Charpy"
p. 90 , para, 2, line 7: "have caused" for ' have causesd"
p. 91, Figure 5.6 caption: "indicating fully" brittle..." for indicating fulyl brittle.."
p. 96, para 2, line 2:"also plotted as black squares" for " also plotted as red squares"
p. 103, para 2, line 4: "last column tabulates" for " last column of tabulates"
p. 106, para 1, last line: " ... of large cracks" for "large crack"
p. 107, para 1, line 2: "Weibull, 1951" for "Weibull, 1952"
p.107, para 1, line 6: "Ritchie, Knott and Rice" for "Rice, Knott and Ritchie"
p. 111, para 1, last line: "Norton and Strang, 1969" for "Norton, 1969".
p. 130, para, 2, line 1: "Both carbon replicas (Fig. 6.4) and thin foils (Fig. 6.3)" for "Both carbon replicas (Fig. 6.3) and thin foils (Fig. 6.4)"
p. 131, para 2, line 4: "Mitchell and Moss, 1998" for " Mitchell and Moss, 1994"
p. 139, para 2, line 4: " the Fe/Mo ration" for " the Fe/ Mp ratio"
p. 151, reference Cheruvu...: "Metallurgical" for " Metallurgicla"
p. 152, reference Foulds 1992: "In service Steam" for " In-Service Stem"
p. 155, reference Knott, 1998: "Probabilistic assessments" for" "Probilistic Assessments"
p. 155, reference Jones, 1994: "crack growth" for "cracj growth"
p. 155, Kadoya, 1991: " repair and.. " for " repair nad..."
p. 158, Moss:et al.: "Plant" for "Palnt"
p. 175, publication 3, line 2: "...and evaluation of plant" for " ...and evaluation if plant"

ADDENDUM

p. 65, Table 4.2, legend: insert "SE- service-exposed, DE- de-embrittled".
p. 68, para 1, line 8: delete "The present result indicates that the ductile failure by microvoid coalescence had occurred prior to the onset of brittle failure by cleavage" and insert "The brittle cleavage had occurred prior the ductile failure mode, which is supported by Fig.s4.5, 4.6.
p. 71, para 1, line 15: Insert "with the exception of stage 3" and read
"It is noteworthy that the ΔFATT values for the de-embrittled specimens with the exception of stage 3..."
p. 90 para 2: delete "which seems to fit the experimental data better than the FATT actually measured from Charpy V-Notch test" and read "Thus the correlations based on the small punch energy values yielded the FATT values of 82.2 °C.
p.92, para 3, line 4: delete "It is clear that the slope for the linear fits are different for all three cases of the rotor material studied here"
p.93: delete: "The re-embrittled condition ....." up to "... to the maximum embrittlement level".
p. 93, Figure 5.7, legend insert an empty square with the notation "De-embrittled"
p. 121, Table 6.1 insert ± 0.05 into the columns 3, 4, 5, 6 and 7 of the Table.
p. 123 Table 6.2 should look:

Table 6.2 Number of carbide particles per unit volume as calculated from image analysis of SEM images from different stages

Stage	*1*	*3*	*12*
No of particles (cm^{-3})	0.28	0.235	0.19

p. 130, para 2, last line: delete "(see inset)"
p. 134, para 2: insert "volume" and read "The volume fraction of the carbides..."
p. 134, para 2 delte "in Fig. 6.7" and read ".... As depicted in Table 6.2".
p. 135, para 2: add at the end: "However, Mo_2C precipitation is generally considered to have a deleterious effect on temper embrittlement resistance, because Mo is removed from the solid solution. Both stage 1 and 3 show extensive fine scale Mo_2C precipitation and yet are severely embrittled. The requirement for Mo in solid solution points to a strain filed effect around Mo atoms pinning P. This point awaits further clarification by the APFIM as will be considered in Chapter 8."
p. 136, bullet point 1: delete "However, Mn was found to have the opposite effect".
p. 137, last bullet point: delete "...was not negligible" and insert " ...was significant"
p. 141 Fig. 7.1 caption "P Grain Boundary Concentration..."
p. 144, bullet point 2: delete "causes" and read "The relationship of P and Mo is complex and affects the migration..."
p. 147, bullet point 3m line 4: delete "the advantages/disadvantages of using either of the methods further explored".
p.170, Appendix B: Thickness = 10 mm.

Fracture Toughness and Microstructure Correlations in a Power Generating Rotor

Alexandra Shekhter

B.Sc.(Hons.) (Mat.Sci.)

A Thesis Submitted for the Degree of Doctor of Philosophy

School of Physics and Materials Engineering
Monash University
Victoria 3800
Australia

December 2002

Dedicated to my father Vladimir Chekhter, whose dream made me fulfill my aspirations.

Посвящается моему отцу, Владимиру Шехтеру, чья мечта позволила воплотить в жизнь мои стремления.

Per aspera ed astra...

Synopsis

In Australia and throughout the world there exist many pressure vessels and turbine rotors where safety is reliant on the conservative nature of design codes. Moreover, the toughness of the materials used in the manufacture of pressure equipment reduces with time in service. The material investigated in this study (1.0Cr-1.0Mo-0.25V wt %[1] steel) has been widely used for turbine generating rotors. These components are the most critical to the safe operation of power plant. These alloys and the nature of their service schedule have a potential for temper embrittlement, resulting in toughness degradation and a decrease in the critical flaw sizes for brittle fracture. Therefore, in-service inspections and remaining life assessment must determine the safety of these components.

The aim of this project was to derive new mechanical property correlations and microstructural indicators for improved assessment of the structural integrity of low alloy steel pressure equipment. The research program focused on a high pressure-intermediate pressure (HP-IP) rotor steel in the ex-service, de-embrittled and re-embrittled conditions.

In this work, fracture toughness estimated by miniature test techniques as well as full and sub-size specimen variations was related to component toughness. For example, the small punch test (SPT) is emerging as a valuable technique to measure toughness for many heavy section components. The aim was to correlate SPT data and conventional fracture toughness test data from embrittled steels for subsequent use as

toughness parameters in structural integrity assessment. Ultimately, this type of assessment may allow for in-service crack growth and materials degradation analysis.

Mechanical testing was carried out to obtain validated relationships between fracture appearance transition temperature (FATT) and fracture toughness (K_{Ic}). New correlations between SPT data, K_{Ic} fracture toughness data were also developed.

Optical microscopy in conjunction with analytical scanning electron microscopy (ASEM), analytical transmission electron microscopy (ATEM) and three-dimensional atom probe field ion microscopy (3DAP/FIM) were conducted to characterise the microstructure. Results compared microstructure between rotor stages and service temperature, degree of embrittlement and edge-to-core within a given stage.

After conducting the initial impact screening tests, three locations of the rotor were selected for further mechanical investigation: stage 1 (operating temperature 565 °C), stage 3 (operating temperature 511 °C), and stage 12 (operating temperature 351 °C). This choice was justified by measured FATT values for stage 3 and 1 representing two extremes of embrittlement, stage 1 being the hottest stage (the point of steam inlet) and 3- the most embrittled. Following the Charpy V-Notch Testing (CVN), SPT and K_{Ic} testing of an ex-service rotor steel it was concluded that the SPT and CVN impact testing for stages 1, 3 and 12 in service-exposed, de-embrittled and re-embrittled conditions produced transition temperature values that were within the limits of the confidence interval approach. The results provided an empirical estimate of K_{IC} values which were comparable to the experimentally measured values. Based on this, three-

[1] Throughout the thesis compositions are in weight percent unless indicated otherwise

way or triangular correlations between CVN-K_{Ic}-SPT results, small punch test could be used to directly estimate the fracture toughness and critical crack size and, in future, could become a remaining life assessment tool.

The microstructural examination revealed that there was little or no difference in microstructure between the edge and core of individual rotor disks or stages, and this was supported by similarities in the impact test data. However, detailed TEM characterisation suggested that microchemical information of the phases varied for the three stages as they were exposed to different thermal histories. The role of alloying elements in scavenging P was also examined by experiments to locate P in the microstructure. It was apparent that P partitioning along M_3C carbide and matrix interfaces was significant. Moreover, combining the results from SEM, TEM and 3DAP/FIM allowed the formulation of mass balances for most of the elements between the phases. This provides a useful indicator for the assessment of the service history/remaining lifetime. The combined results of the assessment of miniature and full size fracture toughness correlations and microstructural examination could prove potentially useful in deriving new more efficient routes for remaining life assessment for the Australian power generation industry..

Declaration

This thesis contains no material that has been accepted previously for the award of any other degree or diploma in any University or other institution. To the best of my knowledge and belief, it contains no material published previously or written by any other person, except where due reference is made in the text.

Alexandra Shekhter

December 2002

Acknowledgements

I would like to gratefully acknowledge the following people and organisations for their support and contributions towards production of this thesis:

- My supervisor, Associate Professor Simon Ringer, for his guidance, enthusiasm and support throughout the duration of this project. His mentorship has proven to be truly valuable to me. I am also grateful to Professor Barry Muddle for his motivation and encouragement during the latter part of my candidacy
- Mr. Andrew Croker and Mr. David Carr of Materials Division, Australian Nuclear Science and Technology Organisation for all the help and expertise with the small punch test and K_{Ic} fracture toughness tests and for general discussions. I would also like to thank all staff at the Materials Assessment group, especially Mrs. Sam Humphries, Ross Finlay and Paul Stathers for making my stay at ANSTO very productive and enjoyable.
- Dr. Mike Drew of the Pacific Power Intl. for organising the rotor material, Dr. Roger Griffiths (BP) and Electricity Corporation of New Zealand for providing support for this project
- HRL Technology for help with the elevated temperature tensile testing
- ARC for proving financial support over the years without which this would not be possible
- All of technical, support and academic staff, especially Dr. Elena Pereloma in the School of Physics and Materials Engineering at Monash University.
- All my friends, especially Chamini, Ilana, Chris, Sally and Katherine for their encouragement and friendship
- My husband Vadim, Mum and Dad for their belief in me no matter what
- A special thank you to my mother-in-law Svetlana, who looked after my son during the most difficult times of the writing-up, and to my son Benjamin for coming along during the final stage of my candidacy and being incredibly patient with me.

Glossary

3D/APFIM	*Three-Dimensinal Atom Probe Field Ion Microscope*
CVN	*Charpy V-Notch*
DBTT	*Ductile-to-Brittle Transition Temperature*
FATT	*Fracture Appearance Transition Temperature*
FEA	*Finite Elements Analysis*
LSE	*Lower Shelf Energy*
RLA	*Remaining Life Assessment*
SEI	*Secondary Electron Image*
SPT	*Small Punch Test*
SPTT	*Small Punch Transition Temperature*
USE	*Upper Shelf Energy*

TABLE OF CONTENTS

Chapter 1: Introduction

This chapter introduces the project and presents the thesis layout

1.1 Remaining Life Assessment of Turbine Generating Rotors

The ability of plant to operate safely and economically requires the assessment of structural integrity of individual critical components and estimation of the remaining life. Whilst life assessment technology is complex, it must be developed to optimise both maintenance planning and life extension.

The object of the remaining life analysis of older pressure equipment is to ensure that the reliability can be maintained at a high level even after an extended period of operation, ie 15-30 years (Berg *et al.*, 1982). The results of mechanical testing and materials characterisation are employed to improve the quality of the remaining life prediction of older pressure equipment. At critical locations of actual components, microstructural changes and microcracking can be observed using surface examination techniques. These results provide valuable support to the evaluation of the expanded lifetime. It is therefore of utmost importance that during the lifetime of the power station, operational data should be carefully documented (Bertilsson, *et al*, 1985).

Figure 1.1 is a pneumatic diagram of a steam power plant. It is clear that a variety of materials of construction are needed to withstand a wide range of conditions in the plant, depending upon the local conditions of pressure, temperature, and chemical environment (Puzak, *et al.*, 1952) The capacity, reliability, efficiency, availability, and safety of plants depend critically on the integrity of the components and materials employed (Viswanathan, 1989). A number of damage phenomena, such as

embrittlement, creep, hydrogen attack, and hydrogen embrittlement, can impair plant integrity.

Turbine rotors are amongst the most critical and highly stressed components of power plants. Failures of rotors have resulted in a wide spectrum of eventualities ranging from catastrophic bursts to lengthy forced outages imposing severe economic penalties on the affected utilities (Viswanathan, 1989). There have been only a few instances of catastrophic bursts of rotors. However, great concern exists for the potential for such bursts because of the consequences of such incidents (Viswanathan, 1993). Rotors made prior to 1970 are of concern because of their composition compared to current rotors. In addition, rotors manufactured in the 1960's and 1970's are increasingly reaching their design life limits. There has also been an increasing awareness of the inadequacy of the original design database and of unanticipated in-service degradation of the rotor materials (Iwadate, 1985). To forestall the possibility of catastrophic burst, several rotors are retired annually, based essentially on the recommendations of the turbine manufacturers (Rana, 1994). Changes in operating procedures and more frequent inspections are also resorted to, resulting in heavy operating and maintenance costs. In addition to avoiding premature failures prior to the end of design life many utilities would like to extend the life of the rotors beyond their design life for economic reasons (Viswanathan, 1993).

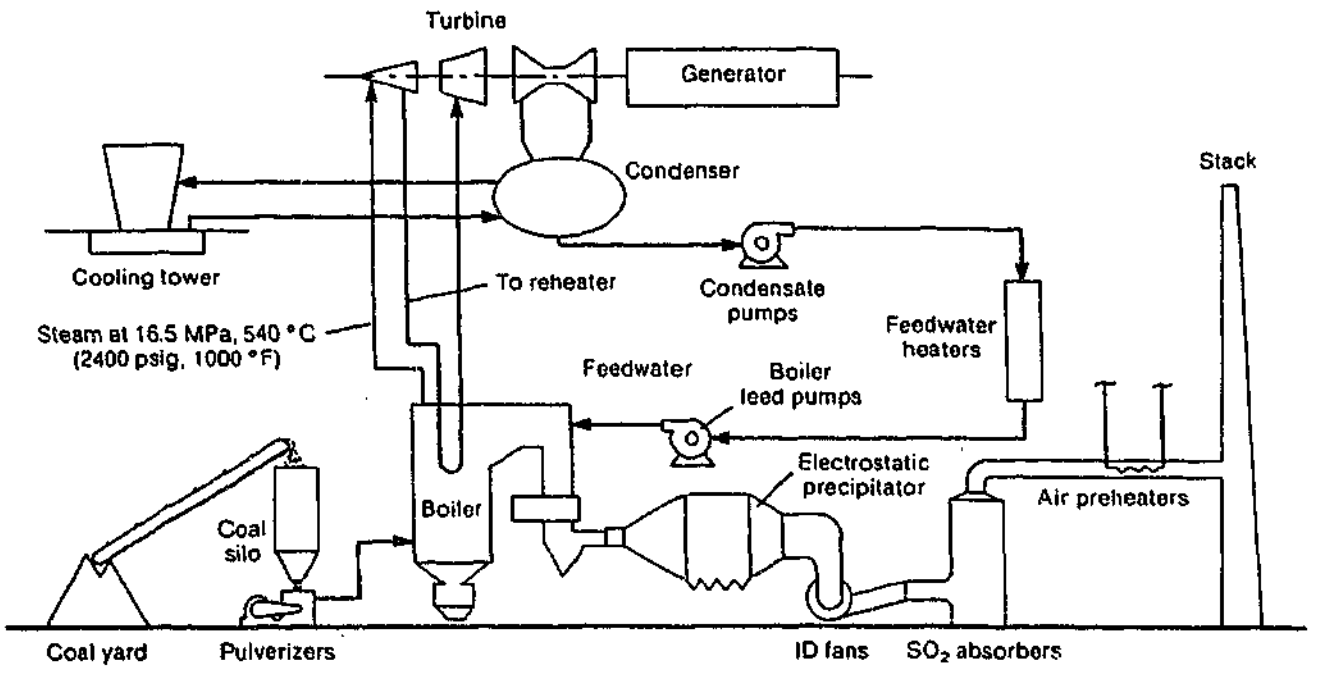

Figure 2.1 Schematic diagram for a steam power plant

1.2 Australian Power Generation Industry

In Australia approximately 30% of fossil fuel power generation plants, representing 25% of the total generating capacity, are over 20 year old. Additionally, the changing generation environment, with utility corporatisation, privatisation and increasing transmission link-up, has resulted in competition between generating sources and increased cyclic operation. This will lead to increased life consumption rates. A somewhat similar situation exists with other high performance pressure plants used in the petroleum and chemical industries with some operating plants over 40 years old (Moss, *et al*, 1995).

In Australia and throughout the world there exists many pressure vessels and turbine rotors where safety is reliant on the conservative nature of design codes. Moreover, the toughness of the materials used in the manufacture of pressure equipment reduces with

time in service. The material investigated in this study (1.0Cr-1.0Mo-0.25V steel) has been widely used for turbine generating rotors. These components are the most critical to the safe operation of power plant. These alloys are potentially susceptible to temper embrittlement, resulting in toughness degradation and a decrease in the critical flaw sizes for brittle fracture. Therefore, in-service inspections and remaining life assessment must determine the safety of these components. These issues have brought about the present study, since they create the need for an efficient and accurate methodology for assessing the structural integrity of pressure equipment, to enable the safe and most economical scheduling of run, repair and replacement of plant. Progress in this area has the potential to improve the competitiveness of power and petro-refining industries by:

- reducing component failures and unscheduled maintenance down-time (which reduce profits),
- allowing for more accurate planning of outages and providing longer lead times for new plant construction,
- in some cases, avoiding the need to construct new plant, which is desirable because of escalating construction costs and the potential environmental impact of new plant, improving the ability of operators to meet safety requirements (and therefore obtain operating licenses) (Cane, 1986).

Therefore, there is a clear need to assess the current rotor life and possibly extend it beyond the design life with the aid of an efficient remaining life analysis that would not impair the operation of the plant due to time constraints and destructive nature.

1.3 Thesis Outline

The aim of the project was to contribute towards the development of a methodology for estimation of remaining life in temper embrittled low alloy turbine generating rotor with the emphasis on miniaturisation approach. The structure of the study presented in this thesis is as follows:

Chapter 2 comprises a literature review that provides a background to the areas of work relevant to this investigation. Included is a complete history of the analysis of the temper embrittlement damage mechanism ant the fabrication and service experience of power generating rotors. The existing methods both mechanical and microstructural are also discussed in detail.

Chapter 3 outlines the experimental procedures relevant to the work undertaken. The rotor steel composition and heat treatments employed are fully described. Also provided in the chapter are the descriptions of the mechanical methods used in this study with the appropriate references to the appendices for the cut-up documentation and specimen specifications. Techniques and operational parameters relevant to the material microstructural examination are also summarised.

Chapter 4 details the investigation into the initial impact screening procedures and also the studies the effect of miniaturisation on the impact properties of the service-exposed material. The impact screening of numerous locations across the rotor allowed the mechanical and microstructural investigations to focus on three critical locations. Charpy V-Notch Testing and fractographic analyses were performed on the service-

exposed materi.. in order to study the effect of the specimen size on the impact properties and to correlate the full size and miniature size data.

Chapter 5 consists of the results of the three kinds of mechanical testing: Charpy V-Notch Testing, Small punch tests and full size K_{Ic} fracture toughness measurements for the service-exposed, de-embrittled and re-embrittled rotor material. The correlations between these tests are also presented and discussed and a new possible correlation method based on the miniature specimen technique for structural integrity assessment is discussed. The calculations of the remaining life assessment parameter – critical crack size are presented and compared to that of the rotor failed in service.

Chapter 6 examines the microstructure of the service-exposed rotor material by optical metallography, FEG SEM and TEM. It also provides a detailed EDXS analysis of the M_3C carbide that dominated all three stages of the rotor. Included in the chapter are results of stereological calculations of the precipitate number density and 3D APFIM results of the carbide-matrix P segregation.

Chapter 7 attempts to unite the mechanical and microstructural outcomes and summarises the major achievements that arose from this study.

Chapter 8 suggests a number of areas for future exploration.

Chapter 2: Literature Survey

This chapter reviews the existing state of knowledge and outlines the target areas of the present research

2.1 Damage Mechanisms

Pressure equipment such as power generation plant components are subjected to the complex array of damage mechanisms, consisting of primarily of creep and creep embrittlement at higher temperatures, hydrogen attack and embrittlement at temperatures below 150°C, and temper embrittlement in the intermediate 350-540°C temperature range. These mechanisms typically affecting the in-service performance of pressure equipment such as steam turbines are summarised in Table 2.1. The excessive action of one or the combination of these mechanisms may lead to pronounced acceleration of failure. The present study focuses on temper embrittlement in low alloy steels with particular emphasis on turbine generating rotors. Therefore, selected aspects of the fabrication and service of these components that influence susceptibility to temper embrittlement are now discussed.

Table 2.1 Damage Mechanisms Affecting Pressure Equipment

Damage Mechanisms	*Temperature Range*	*Main Characteristics*
Creep and Creep Embrittlement	>500 °C	Component Deformation
Hydrogen Attack Hydrogen Embrittlement	below 150 °C	Blistering Crack Formation Lower Threshold for Crack Propagation
Temper Embrittlement	345-540 °C	Loss of Toughness

2.2 Temper Embrittlement

Temper embrittlement reduces the critical flaw sizes in the material, and changes the fracture mechanism from ductile to brittle cleavage, which leads to a critical deterioration of the toughness of the steel component (Newhouse and Holtz, 1968). Charpy V-Notch (CVN) testing is the most commonly used method to evaluate the ductile-to-brittle transition in steels, and the temperature at which this transition occurs is usually determined. A steel that has been embrittled will show an increase in its transition temperature and it is natural to use the shift in transition temperature as a measure of embrittlement. The ductile-to-brittle transition temperature (DBTT) is defined as the temperature where the Charpy V-Notch energy is equal to the mean value of the upper and lower shelf energies (Dieter, 1988). An alternative parameter, the fracture appearance transition temperature (FATT) is defined as the temperature where the fracture surface has 50% ductile and 50% brittle appearance.

Temper embrittlement is a major cause of toughness degradation in rotor steels. An example of toughness degradation in 2.5 Cr-1Mo steel from a hydro-desulphurisation unit after seven years of service is illustrated in Figure 2.1. Numerous components otherwise in sound condition become candidates for retirement if they are severely embrittled. The problem is encountered as a result of exposure of steel in the temperature range 345-540°C. Tempering, postweld heat treatments, or service exposure in this range must be avoided. The problem may be overcome by heat treating above this range followed by rapid quenching (Newhouse and Holtz, 1968).

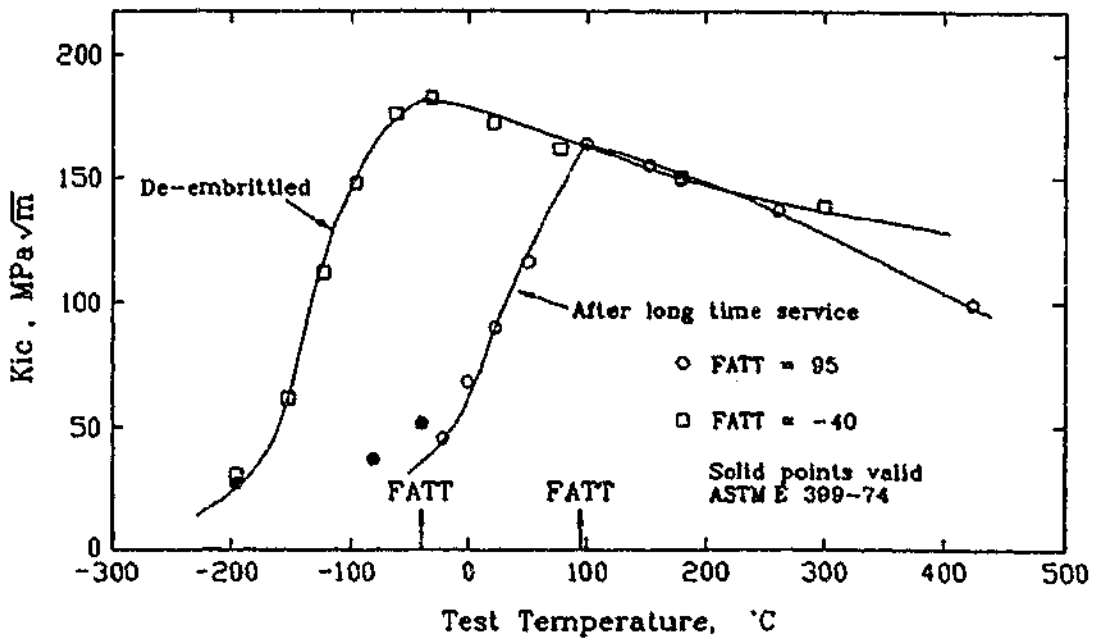

Figure 2.1 Effect of long term service (7 years) on the fracture toughness of a 2.5 Cr- 1 Mo steel taken from a hydro-desulphuriser (after Moss and Kelly, 1994).

Unfortunately, in the case of massive components such as rotors, no rate of cooling is fast enough and some residual embrittlement may be inevitable. Subsequent to heat treatment exposure of the component during service in the critical range can also lead to embrittlement (Viswanathan, 1989).

Many pressure equipment components are invariably exposed to the critical temperature during service and hence embrittlement cannot be avoided. Some examples include boiler headers, steam pipes, turbine castings, pressure vessels, blades and HP-IP rotors.

2.2.1 Effect of Phosphorus and Other Impurity Elements on Temper Embrittlement

It is well established at this time that the segregation of tramp elements - Sb, P, Sn, and As - to prior austenite grain boundaries in steel is the principal cause of temper embrittlement. Until the development of Auger Electron Spectroscope (AES) in the mid-1960's, no conclusive evidence of such segregation could be obtained. Harris (1968) and Palmberg and Matcus (1969) were pioneers in demonstrating segregation of antimony and phosphorus to grain boundaries using the AES technique. Viswanathan (1971) obtained evidence of the segregation of P to grain boundaries in Ni-Cr steel. A comparison of the grain-boundary AES from the Ni-Cr steel in the embrittled and non-embrittled conditions is shown in Figure 2.2.

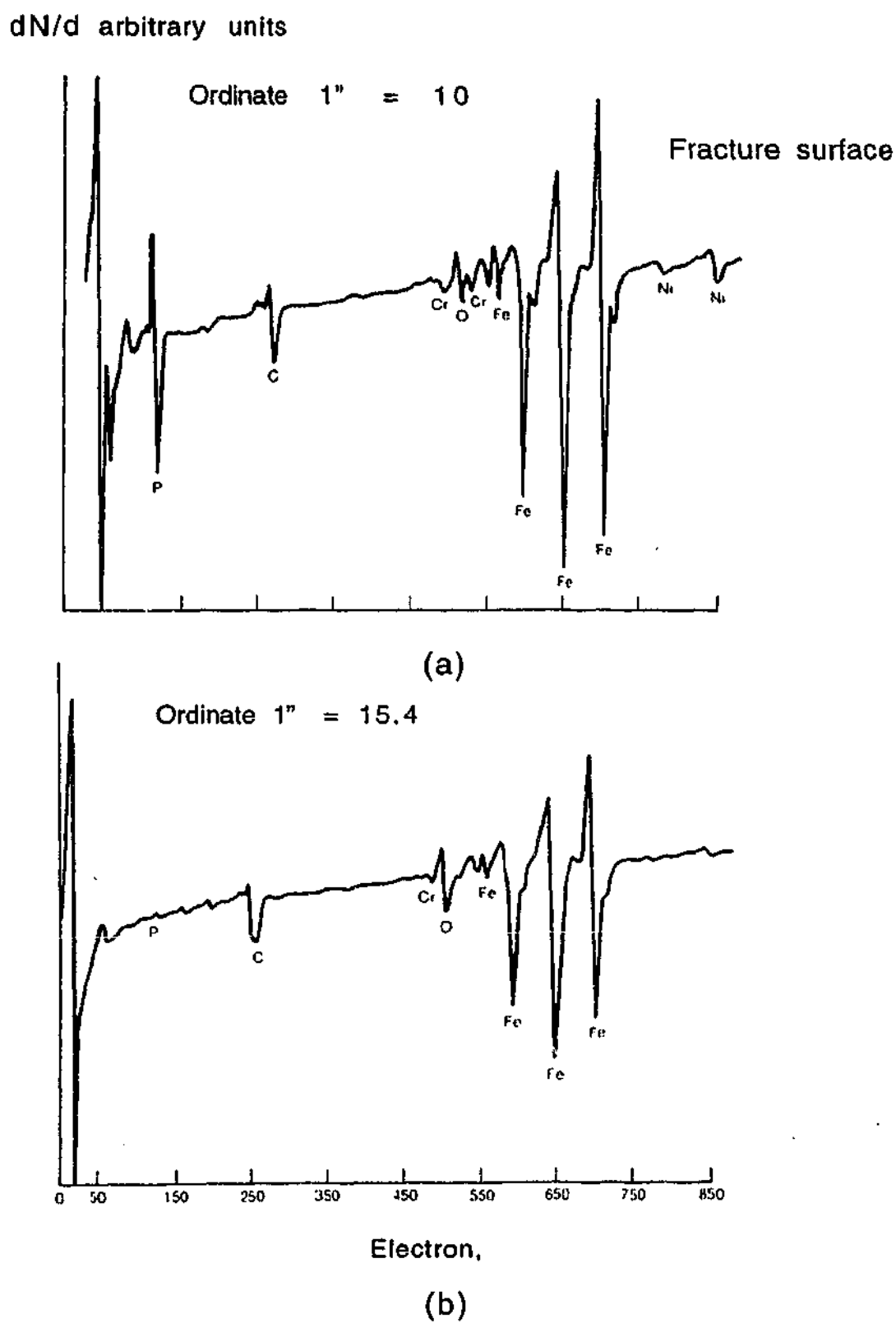

Figure 2.2 Auger spectra from the fracture surface of a Ni-Cr steel in the (a) embrittled and (b) non-embrittled conditions (after Viswanathan, 1989).

The spectra provide evidence for segregation of P and Sn. Based on these and numerous subsequent investigations (Abe, 1990; Sevc; 1994; Bulloch, 1999), the following issues regarding temper embrittlement are now well established (Bruemmer, 1987; Faulkner *et al.*, 1996):

- Segregation of both impurity elements and alloying elements to selected prior austenite grain boundaries occurs. The concentrations of the former are much higher, sometimes approaching 200 to 300 times their bulk concentrations.
- Segregation is usually confined to one or two atomic layers and decays exponentially away from the grain boundaries (Viswanathan and Joshi, 1975).
- Segregation occurs only in ferrite in the critical region from 315 to 540 °C and not during austenitising treatments (Smith and Low, 1974).
- Segregation can be reversed at temperatures above the critical range (Bulloch, 1999).
- The extent of segregation is higher in steel with a tempered-martensite structure compared with a tempered-bainite structure, and also increases with increasing level of martensite or decreasing tempering temperature (Kim *et al.*,1998).
- Segregation occurs preferentially and non-uniformly, presumably because of differences in grain-boundary structure (Viswanathan *et al.*, 1987).
- The complex relationship between molybdenum and phosphorous results in Mo acting as ab impurity element suppressant (Gould, 1968).

Both electronic and elastic misfit interactions of the tramp-element atoms in the host lattice have been investigated as the driving forces for segregation. (Seah and Hondros, 1973). The theoretically calculated grain-boundary-enrichment ratio is inversely

proportional to the atomic solubility of the element in the parent lattice (Fig. 2.3). Based on this research, the predicted tendency for segregation in steel would decrease in the order Sb, P, Sn, As, Cr. Hondros (1965, 1968) also found that the solubility was inversely proportional to the term $\frac{d\gamma}{dC}$ in the Gibbs absorption formula

$$\tau_2 = -\frac{C}{kT}\frac{d\gamma}{dC} \qquad \text{(Equation 2.1)}$$

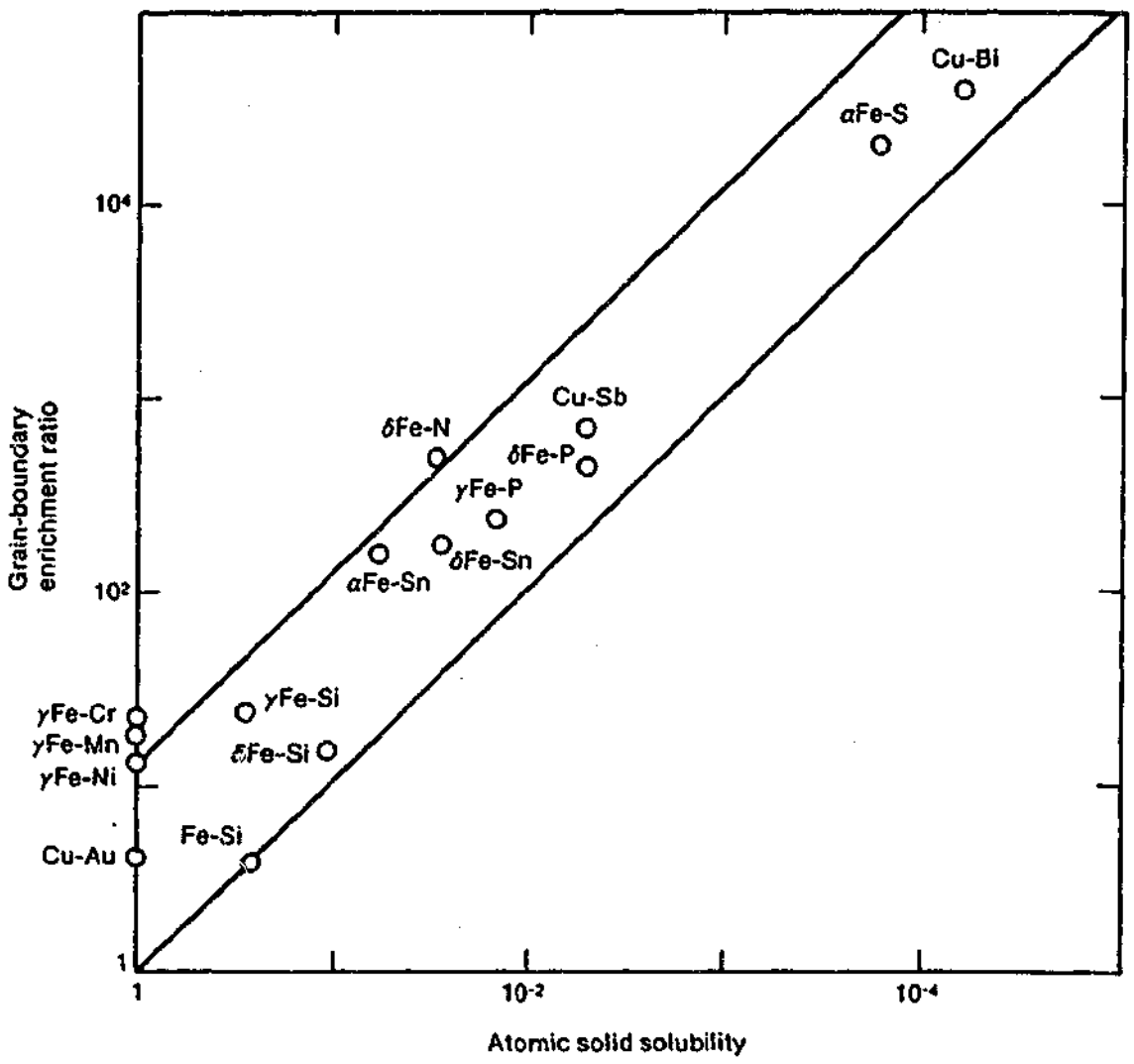

Figure 2.3 Correlation of predicted grain boundary enrichment ratios for various solutes with the inverse of solid solubility (after Seah and Hondros, 1973).

where τ_2 is the grain-boundary concentration of the impurity element in excess of the bulk concentration C, $\frac{d\gamma}{dC}$ is the reduction in grain-boundary energy with the concentration of the impurity at absolute temperature T, and k is Boltzmann's constant.

This equation states that any solute which lowers γ tends to be segregated at equilibrium (Hondros and McClean, 1968). It was also shown that highly segregated element such as phosphorous had large values of $\frac{d\gamma}{dC}$ whereas elements such as chromium had much lower values of $\frac{d\gamma}{dC}$. Most experimental results to date indicate that the segregation of phosphorous in steel obeys equilibrium thermodynamics as represented by equation 2.1 and that it can be explained mainly on the basis of the reduction in grain-boundary energy resulting from segregation.

A reduced grain-boundary energy implies reduced fracture-surface energy, thus rendering the grain boundaries susceptible to intergranular fracture. Since temper embrittlement is related to changes at the grain boundaries, it is always manifested as intergranular fracture (Low, 1964; McMahon, 1964). Tensile strength and ductility remain essentially unaffected (Kalderon *et al.*, 1972). Although extremely severe embrittlement can be detected as a reduction in tensile strength and ductility (Holtzmann, 1996).

2.2.2 Effect of Molybdenum

Molybdenum has been found to decrease the susceptibility to embrittlement. Newhouse and Holtz (1968) analysed a large set of data on rotor steels and concluded that an decrease in the molybdenum content tended to increase the susceptibility to embrittlement. Comon *et al.* (1968) also concluded that in the range of 0.24 to 1.23 % molybdenum additions were beneficial.

Qu and McMahon (1983) concluded that molybdenum could act as an effective scavenger for phosphorus and other embrittling impurities. Few details of the mechanism of the scavenging effect are available although the widely accepted theory is that molybdenum is acting as an embrittlement suppressant by having a strong effect on the solubility of phosphorus in iron. However, the scavenging is lost when molybdenum is precipitated in carbides as a result of continued tempering during service at elevated temperatures. The formation of carbides by molybdenum results in the release of phosphorous which is then free to segregate to grain boundaries (Yu and McMahon, 1980).

2.2.3 Temper embrittlement: Concluding remarks

It is clear that temper embrittlement adversely influences the toughness of the turbine generating rotors. It results in a decrease of the rotor life under base load and cyclic operation due to increased risk of brittle fracture, and is one of the major causes of the early retirement of rotors. It also has a major effect on the operating procedure. To

keep transient stresses low, stringent controls have to be exercised with respect to the start-stop procedures. For instance, during each cold start, the rotors are pre-warmed to a temperature above the fracture appearance transition temperature (FATT), over a period of several hours prior to the imposition of full load. The controlled start-up and shut-down requirements lead to increased capital costs and operational costs for the plant and decreased flexibility and availability. The temper embrittlement problem and the consequent degradation of toughness thus have a significant effect on the reliability, availability, and efficiency of a steam turbine, and its ability to operate under cyclic loads.

2.3 Steam Turbine Rotors: Fabrication and Service Experience

2.3.1 Composition and Heat Treatment

Figure 2.4 is a schematic diagram of a HP/IP rotor. The evolution of steel compositions for high-temperature rotor applications has been reviewed in the literature. (Timo, *et al*, 1982). The early use of carbon steels was superseded by Ni-Mo-V steels in the mid-1940's.

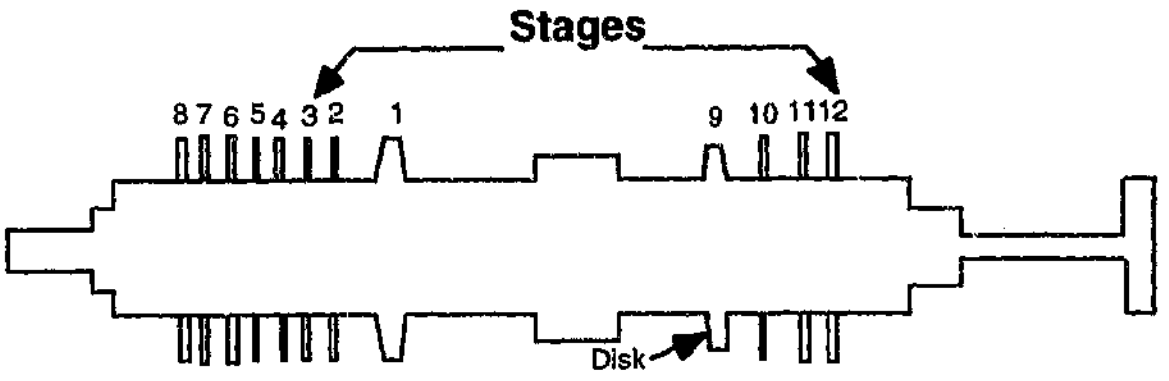

Figure 2.4 A schematic of a HP/IP rotor

With increasing demands on creep strength a 1Cr-1Mo-0.25V steel was introduced in the early 1950's and has remained in the industry standard ever since, although a few higher-alloy steel rotors (12%) have been placed in service (Timo, *et al* 1982).

Achievement of the desired properties in Cr-Mo-V steel rotors is made possible by careful control of heat treatment and composition. Examination of continuous cooling transformation diagram (Fig. 2.5) for Cr-Mo-V steel shows that for the normal range of a air cooling rates employed for rotors, the predominant transformation product would be upper bainite. Oil quenching may shift the transformation product increasingly toward lower bainite, but its is unlikely that the cooling rates needed for formation of martensite are ever encountered.

In the United States, the usual practice has been to air cool the rotors from the austenitizing temperature in order to achieve a highly creep-resistant, but somewhat less tough, upper bainitic microstructure. On the other hand, European manufacturers have resorted to oil and steam quenching of rotors from the austenitizing temperature, to achieve a better compromise between creep strength and toughness (Timo, *et al.*, 1982).

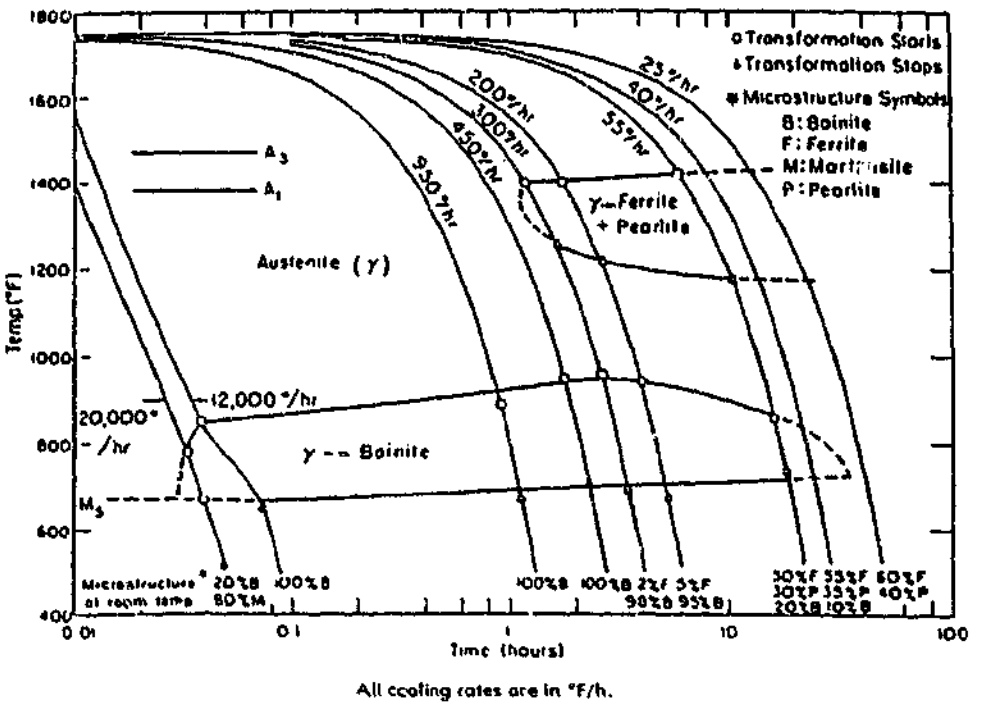

Figure 2.5 Continuous Cooling Transformation Diagram for Cr-Mo-V steel (after Werner, 1956).

The final heat treatment of the forging usually consists of austenitizing at about 955°C followed by tempering in the range 675 to 705°C. The austenitizing and tempering treatments are chosen so as to achieve the desired strength without sacrificing the ductility. In general, improvements in creep rupture strength are only achieved at the expense of the steel's low temperature fracture toughness. The turbine makers in different countries have adopted differing philosophies with respect to the relative importance of the two properties and the achievement of their optimum combination through compositional and heat treatment variations.

The element that contributed most significantly to the strength of Cr-Mo-V steels is vanadium. The effect of vanadium arises primarily form the formation of a stable and fine dispersion of V_4C_3 - type carbides, and the V:C ratio leads to excessive V_4C_3 precipitation, accompanied by high rupture strength and very low rupture ductility.

Molybdenum suppresses ferrite formation and promotes bainite formation. It also contributes to strengthening via solid-solution effects and by precipitation of Mo_2C. Chromium contributes to solution oxidation resistance in steam (Viswanathan, 1975). Service-exposed FATT was observed to increase with increasing maximum tensile strength and phosphorous content and to decrease with increasing chromium and molybdenum content. The higher levels of chromium and molybdenum are thought to be responsible for the FATT data of the modern European forgings being superior to the results for the equivalent UK conventional steels by up to around 20° C. The typical impurity concentrations for Cr-Mo-V steels are shown in Figure 2.6.

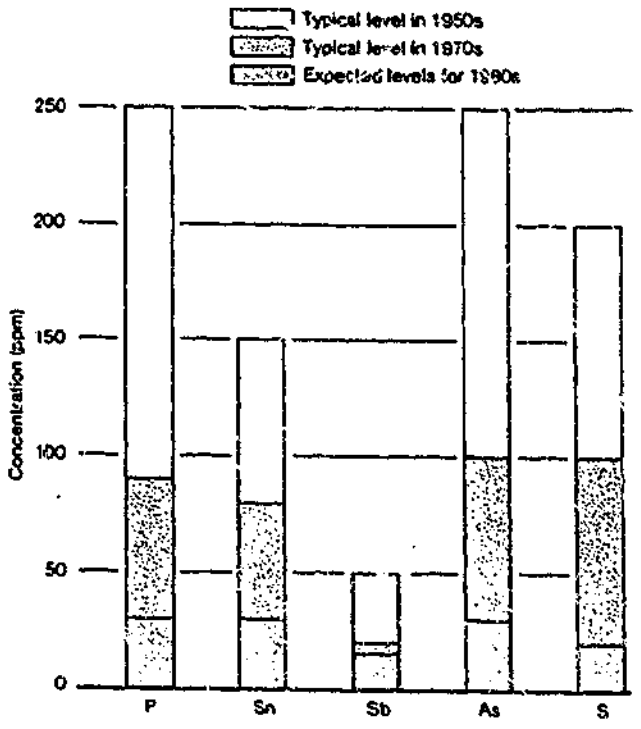

Figure 2.6 Trends in impurity levels in Cr-Mo-V steels (after Viswanathan and Jaffee, 1983).

2.3.2 Manufacture-induced inhomogeneities and toughness degradation in-service

During heat treatment, the surface of rotors cools more rapidly than the bore material. This generally results in a microstructure consisting entirely of upper bainite at the surface, with increasing ferrite content mixed-in with the bainite as the bore is approached. Furthermore, during the cooling cycle from tempering, the surface will cool more rapidly compared to the bore material, resulting in more embrittlement at the bore than at the surface. Compositional gradients can further exacerbate these effects. The microstructural variations and the temper embrittlement variations described above generally result in a FATT which is higher compared to the peripheral surface FATT. The extent of this variation will obviously depend upon the rotor size, rotor type, the heat treatment procedure, chemical composition and segregation (Viswanathan and Gehl, 1992).

2.4 Existing Methods for Assessment of Temper Embrittlement

With the risk of the brittle failure of the rotor, the toughness becomes the most important design parameter. The following sections provide an overview of the existing methods for the assessment of toughness of the pressure equipment, both destructive and non-destructive.

2.4.1 Conventional Mechanical Testing

Based on the results of extensive research efforts over the last decade, the factors controlling temper embrittlement and the mechanisms involved are now better understood (Viswanathan, 1989). With the improved steel making technology available today, it is possible to control the levels of impurity elements, such as P, S, Sn, As, and Sb , to a degree where temper embrittlement can be appreciably minimised. However, for older, higher impurity steel rotors/disks (for instance, of the 1950's vintage) that can severely embrittle, there is a need to estimate the toughness degradation that has occurred in order to assess the reliability, remaining life, and future operational parameters for the rotor.

Full Size Fracture Toughness

A value of adequate toughness in Cr-Mo-V rotors is provided by the ASTM A470 class specification which limits the FATT to 120°C maximum (Viswanathan and Jaffee, 1983). The fracture mechanics approach assumes that all components contain pre-existing cracks or crack-like defects (flaws), which then grow in service to reach a critical size, at which catastrophic failure of the component will occur. In performing the life analysis of a rotor using the fracture mechanics approach, the main area of concern is the near-bore region (Viswanathan and Jaffee, 1983). This is due to the fact that the maximum tangential stress occurs at the bore, and decreases rapidly away from the bore, as shown in Figure 2.7.

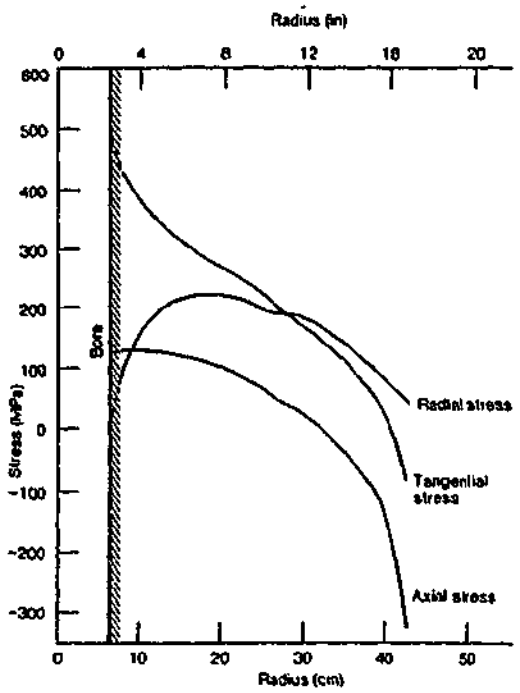

Figure 2.7 Radial varition of stress in HP/IP rotor (after Cook *et al.*, 1978).

The most important material parameter in assessing rotor integrity is the fracture toughness, which is expressed in terms of plain strain fracture toughness K_{Ic}, or stress-strain fracture toughness J_{Ic}. The definition and methods of determining K_{Ic} are set out in ASTM test procedure E 399. The value of K_{Ic} at the location of the highest stress and at that temperature where the transient stresses peak, determines the critical crack-size (Viswanathan and Foulds 1994). Variations in temperature, stress, and material inhomogeneity along and across the rotor dictate that the critical size value, a_c, for the rotor should be computed for the worst combination of these variables. This is done by using the lower scatterband values of K_{Ic} as shown in Figure 2.8.

The plain strain fracture toughness K_{Ic} can then be used directly to determine whether or not catastrophic fracture will occur from a defect of known size in a structure under load. Fracture will occur if relationship of the following type is satisfied:

$$K_{Ic} \leq Q\sigma\sqrt{\pi a} \qquad \text{Equation 2.2}$$

where Q is a geometric factor, σ is stress, and a is crack length.

Another approach has been developed, involving the J integral method, by means of a specimen loaded in the elastic-plastic regime (ASTM 813). The J_{IC} criterion was introduced and developed by Begley and Landes (1972), is based largely on the path-independent J-integral proposed by Rice (1968).

This criterion attempts to characterise the elastic-plastic field. Begley and Landes have checked that the initial vale of J_{IC} measured with a small specimen at the maximum load, or more accurately at the onset of slow-crack growth is in good agreement with the fracture toughness K_{IC} measured with a large specimen. (Marandet and Sanz, 1977).

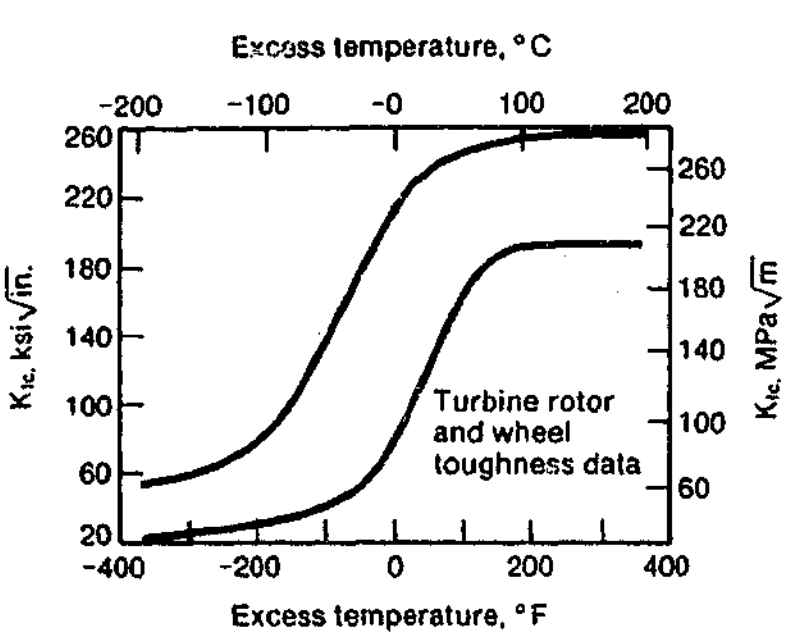

Figure 2.8 Correlation of K_{Ic} values with excess temperature for rotor and disk steels, defined as the temperature of interest minus the FATT at that temperature.

In the temperature range where fracture occurs suddenly by cleavage, the results obtained by different authors (Begley and Landes, 1977; Marandet and Sanz, 1977) make it clear that there is a satisfactory agreement between K_{Ic} values determined under the conditions required by the ASTM 399 and K_{Ic} values derived from J_{Ic} according to the following relationship:

$$K_{Ic} = \sqrt{E(1-\upsilon^2)} * J_{Ic} \qquad \text{Equation 2.3}$$

where E is the elastic modulus and υ is the Poisson's ratio. Marandet and Sanz (1977) undertook a systematic investigation on the effect of specimen size on J_{Ic} fracture toughness, as applied to rotor steels, and proved this approach to be competitive with the K_{Ic} approach. Small specimen J_{Ic} testing requires much smaller test pieces than comparable K_{Ic} test pieces.

Charpy V-Notch Testing

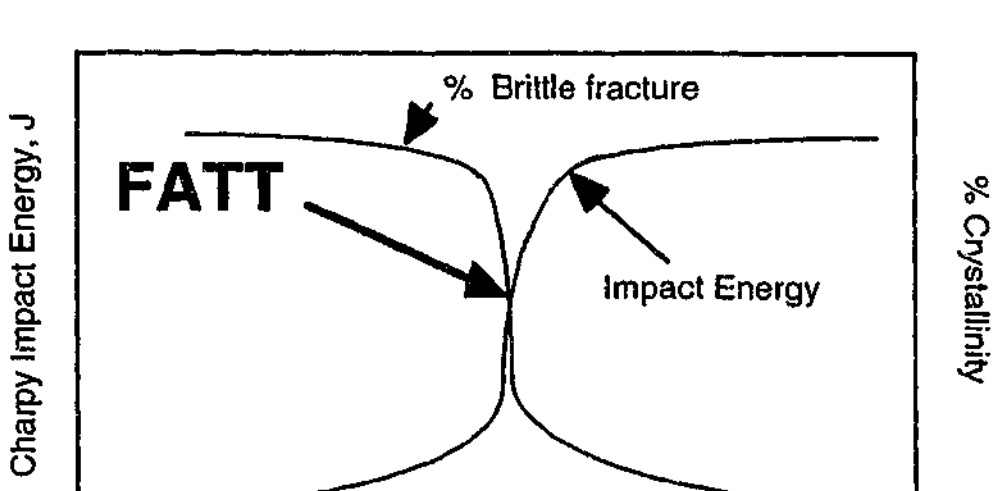

Figure 2.9 Charpy V-Notch Testing Transition Curve

Charpy V-Notch (CVN) testing is the most basic method for the assessment of the ductile-to-brittle transition for pressure equipment steelsSeveral transition temperatures can be derived from this test and these can be then used as criteria to assess the degree of embrittlement. Some researchers employ the approach of a fixed energy value (e.g. 20 J) transition temperature (Yu and McMahon, Jr., 1981). Others use a Ductile-to-Brittle Transition Temperature (DBTT) defined as a temperature value corresponding to a mean value between upper and lower energy shelves (Abe, *et al.*, 1987).

Temper embrittlement susceptibility is often assessed by measuring the shift in the 50 % Charpy fracture appearance transition temperature (Δ 50% FATT) between a non-embrittled and a potentially embrittled condition, as shown in Figure 2.9. Strong justification for the use of a single Charpy specimen can be found in the early work of Newhouse (1963), who found that the FATT of the steels could be estimated from the percentage of fibrosity or impact of a single specimen tested at a given temperature. In study by Yu and McMahon Jr., 1983, the temper embrittlement behaviour of two retired rotors (Buck and Joppa) and one failed rotor (Gallatin) was assessed using the Charpy tests and an FATT approach. The results indicated an FATT of >150°C. Comparisons between a service-exposed material condition and a potentially non-embrittled material are made on the basis of FATT (Viswanathan and Bruemmer, 1985; Viswanathan, 1991; Viswanathan and Gehl, 1991; Bulloch, 1993). Charpy impact testing and a derived FATT are often employed to examine the remaining life assessment by assessing the variation of FATT/DBTT with service exposure time (Viswanathan and Gehl, 1991; Yu and McMahon, Jr., 1983). FATT is also a parameter

that is used to evaluate the kinetics of phosphorous segregation on the grain boundaries (Viswanathan and Jaffe, 1983; Swaminathan *et al*, 1994) and to investigate the effect of operating temperature on hardness, grain size and full size fracture toughness K_{Ic} or J_{Ic} (Swaminathan, *et al, 1994*; Viswanathan, 1991; Holtzman *et al.*, 1996).

Small Punch Testing

Small punch test is a miniaturised specimen technique that allows the use of considerably less material than full size fracture toughness and Charpy testing. Small punch specimen technology has evolved out of necessity for a small volume of material to evaluate the effects of irradiation on materials properties (Corwin and Lucas, 1986). A comprehensive study by Baik *et al.*, 1983 represents one of the earliest attempts to correlate the results from small punch testing with FATT. Following these findings several Japanese researchers began a systematic study to improve the small punch technique for the purpose of assessing the mechanical properties (Mao *et al.*, 1987; Takahashi *et al.*, 1988).

In the small punch test, a finished small punch specimen is placed between the punch guide and die (Viswanathan, 1994). A hemispherical punch is advanced upward through the guide to deform the specimen against the receiving die, in a mechanical testing machine. The punch displacement rate is controlled during the test. A load vs displacement curve is thus developed, the area under which denotes the energy absorbed during the test.

By conducting tests at different temperatures, a curve of absorbed energy vs temperature can be developed which is very similar in shape to that of a Charpy energy vs temperature curve, with the difference that the small punch test curve is shifted laterally to lower temperatures along the temperature axis compared to the Charpy curve (Viswanathan and Gehl, 1992). The midpoint of the energy curve can be used to define a ductile to brittle transition temperature, T_{sp}. Each value is thickness corrected to normalise results to 0.5 mm thickness as there is a degree of thickness variability between the specimens.

Various aspects of small punch test were summarised by Lucas in 1990 review for irradiation testing. An example of transition behaviour exhibited in a small punch test is shown in Fig. 2.10.

There has been considerable debate over recent years on the subject of the destructive or non-destructive nature of the small punch test. Supporters of the small punch test being non-destructive associate this with the fact that only small amounts of material are required for the small punch tests. Nevertheless, the small punch test involves removal of material from the component, and this supports the "destructive nature" of the test.

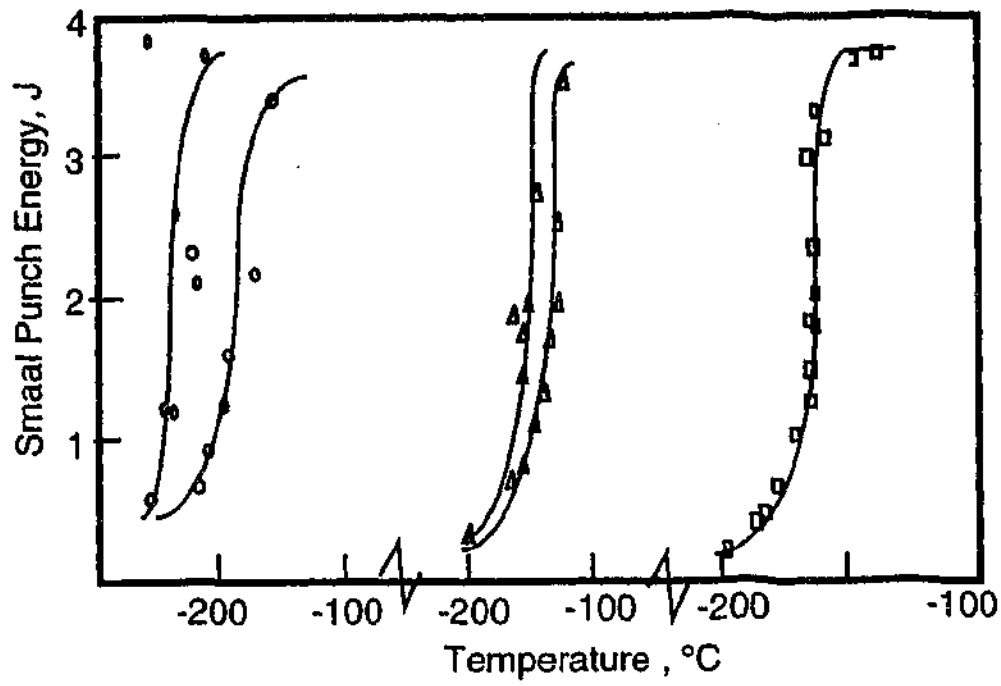

Figure 2.10 Examples of transition behaviour characterised by small punch test tests (after Lucas, 1990).

The development and subsequent application of miniature sample removal SSam™ (Mercaldi, 1989) to a fossil power plant component in service facilitated a new era in a small punch test exploration. The collated experience led to a design of a small punch test device (Foulds and Jewett, 1991; Foulds *et al.*, 1991) capable of removing the amount of material sufficient for small punch testing and obtaining a transition curve.

Correlation Between Destructive Methods

The amounts of material available for full size fracture toughness and Charpy V-Notch testing are often limited. This motivated researchers to develop correlations between various mechanical tests in order to simplify the assessment of toughness and the remaining life. Early on correlations that were developed focused on Charpy tests. Jones (1972) reported a relationship correlating FATT and K_{Ic} values in the lower bound region. Rolfe-Novak (1970) and Iwadate *et al.*, (1977) developed correlations

that applied in the upper-shelf region. Viswanathan (1989) summarised correlation approaches applicable to the lower-shelf, upper-shelf and transition region.

Foulds *et al* (1991) have successfully applied the small punch test procedure to determine the T_{sp} for 12 retired rotor samples. The T_{sp} values obtained correlated well with the Charpy FATT values as shown in Figure 2.11. Foulds and Viswanathan have proposed that the following factors are important in relating the results of these approaches:

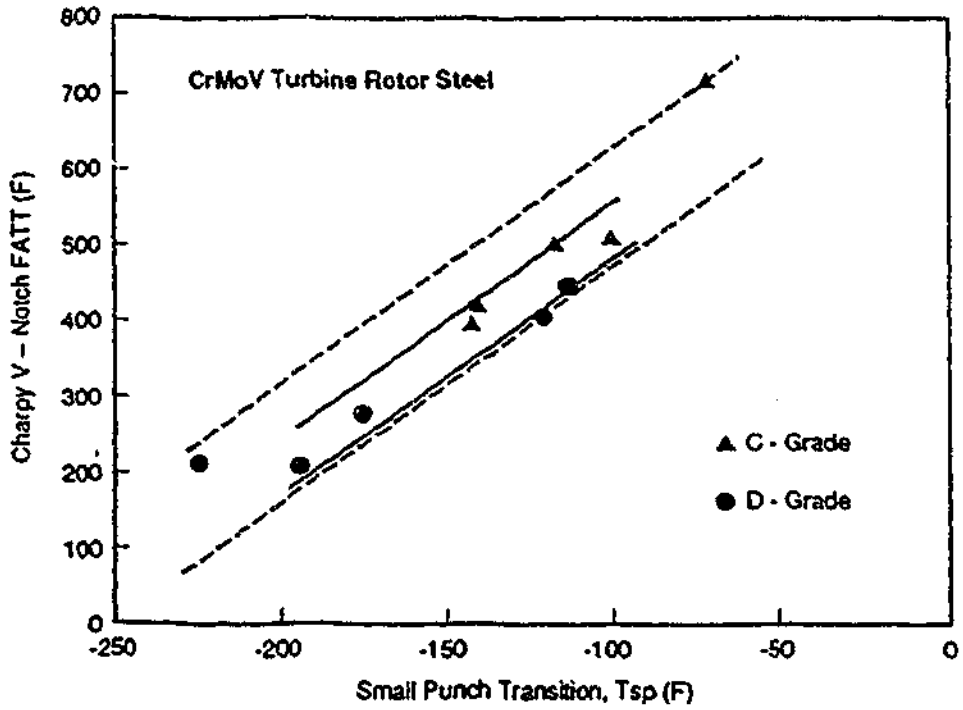

Figure 2.11: Plot of standard Charpy FATT versus small punch T_{SP} for Cr-Mo-V material tested showing the scatter band for the data analysed (after Viswanathan and Gehl, 1992).

- while the transition temperature from a series of small punch tests is observed to be significantly lower than the FATT, there is a material specific correlation between T_{SP} and FATT that can be empirically established;
- experimental data indicate that fracture energy-based results are best obtained with the hemispherical punch head, as compared to earlier experiments with specimens having different geometries (Foulds *et al.* , 1991);
- the correlation procedure is based largely on the size of the database used to derive such a correlation.

For Cr-Mo-V rotor steels, the linear regression applied to a database compiled from 17 rotors of grades C and D produced the following mean or best-estimate FATT:

$$FATT\ (^{\circ}C) = 457.61 + 2.536\ T_{SP}\ (^{\circ}C) \qquad \text{Equation. 2.4}$$

This correlation method has been successfully applied to components in service (Viswanathan and Foulds, 1994).

Charpy V-Notch testing is the most commonly used method to evaluate the ductile-to-brittle transition in steels through FATT. Moreover, many older generation engineers are still familiar with only the impact-transition curve approach. However, the most important material parameter in assessing rotor integrity is the fracture toughness, which is expressed in terms of plane strain fracture toughness K_{Ic}, or stress-strain fracture toughness J_{Ic}. Furthermore, there is a large body of FATT data available to equipment manufacturers for the components manufactured in the past for which there was no K_{Ic} data generated.

A large body of Charpy V-Notch impact-test data is already available because the Charpy impact transition curve has been the most common basis for specifying toughness, and correlations between Charpy V-Notch testing and K_{Ic} have been extensively reviewed in the literature. In this work only selective correlation approaches were examined with the emphasis on possible implication of such correlations in further miniaturisation such as small punch testing (SPT).

Mao *et al.* (1991) developed a testing procedure to estimate both K_{Ic} and J_{Ic} fracture toughness using small punch tests. They used ductile steels and brittle ceramics to assess J_{Ic} and K_{Ic} respectively. Their research yielded a derivation of quantitative relationships between small punch test results and K_{Ic} and J_{Ic}. This would seem to have limited applicability here although the approach is further proof of the validation of cross-correlation.

2.4.2 Non-Destructive Methods

In recent years, a variety of non-destructive and relatively non-destructive techniques for determining FATT have been explored with varying degrees of success. Some of the more promising techniques are listed in Table 2.2 and are reviewed with respect to their advantages and limitations by Viswanathan and Foulds (1994). The majority of the FATT determination techniques listed in Table 2.2 have been explored for application to temper-embrittled Cr-Mo-V and Ni-Cr-Mo-V rotor steels. The methods include the bulk chemistry-based P method (Viswanathan and Gehl, 1991), the bulk chemistry-based regression correlations method (Kaplan, *et al.*, 1991), the grain boundary evolution-based etching method (Viswanathan *et al.*; 1988; Kadoya *et al.*, 1991), and the electrochemical method (Tanemura *et al.*, 1988). The chemistry-based method, the etching method, and the electrochemical method have the advantage that they can be applied in a truly nondestructive manner (without any sample removal). However, these fully nondestructive methods of toughness determination are indirect and can lead to excessively conservative estimates of FATT. In such cases, miniature removal of the material is desirable.

Table 2.2 Non-Destructive Techniques (after Viswanathan and Foulds, 1994)

Technique	*Prediction Method*	*Prediction Scatter*	*Advantage*	*Limitations*
Composition based correlation	Regression equation correlating composition, grain size, strength and exposure time with FATT	±19°C in FATT	• Relatively narrow scatter • May not require sampling • Inexpensive to implement	• Indirect, non-mechanical test • Correlation only for 318°C, and 371°C exposure
Bulk P content	Linear correlation between bulk P content and the maximum FATT anticipated in service	±28°C in FATT	• Relatively narrow scatter • May not require sampling • Inexpensive to implement	• Indirect, non-mechanical test • Applied inly to Cr-Mo-V steels • P measurement scatter • P variation in rotor • Predicts maximum FATT only
Picric Acid Etch	Correlation between the maximum change in FATT anticipated in service and grain boundary etch depth	±14°C in ΔFATT	• Requires very little material • Could be developed for in-situ application	• Indirect non-mechanical test • Requires material sampling • Significant scatter in measurement of etch depth • Predicts maximum ΔFATT only
Electrochemical etch	Correlation between the ΔFATT/pre-service FATT ratio and the polarisation behaviour as influenced by grain boundary repassivation	± 0.25 °C in ΔFATT/pre-service FATT at low levels of polarization	• Requires very little material • Could be developed for in-situ application	• Significant scatter in measurement of polarization behaviour • ΔFATT prediction requires knowledge of pre-service FATT

Composition Based Correlation

Several compositional correlations have been suggested for Ni-Cr-Mo-V steels, but the body of data pertaining to Cr-Mo-V steels is much more limited. A combined compositional parameter known as the J factor, equal to (P+Sn)*(Mn+Si), has been found to correlate well with embrittlement susceptibility (Viswanathan and Gehl, 1991). A relationship between the post-service FATT is shown in Fig. 2.12.

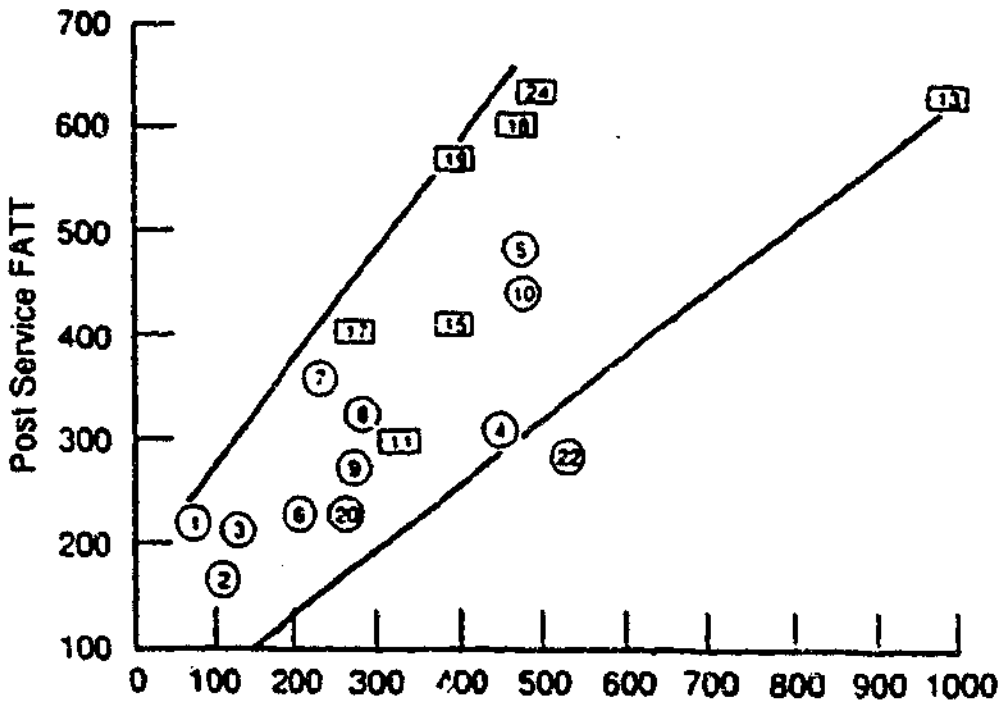

Figure 2.12 Variation of post service FATT (corrected for temperature and location) with the J-factor for Cr-Mo-V rotors (after Viswanathan and Gehl, 1991)

Microstrucutral Methods

Auger Electron Spectroscopy

Since temper embrittlement is caused by the segregation of certain impurity and alloying-element species to grain boundaries, considerable effort has been focussed on the quantitative analysis of the grain-boundary composition, which then can be related to the ΔFATT. Auger analysis of three retired rotors has provided clear evidence of segregation of both phosphorous and tin. A correlation between phosphorous segregation and the ΔFATT was observed, as shown in Figure 2.13. This relationship could be used to estimate FATT for in service rotors based on Auger analysis of small samples. However, the method's deficiencies include a large experimental error, difficulties associated with the location of the analyses (ie the determination of the prior austenite grain boundaries) and the complicated nature of the technique.

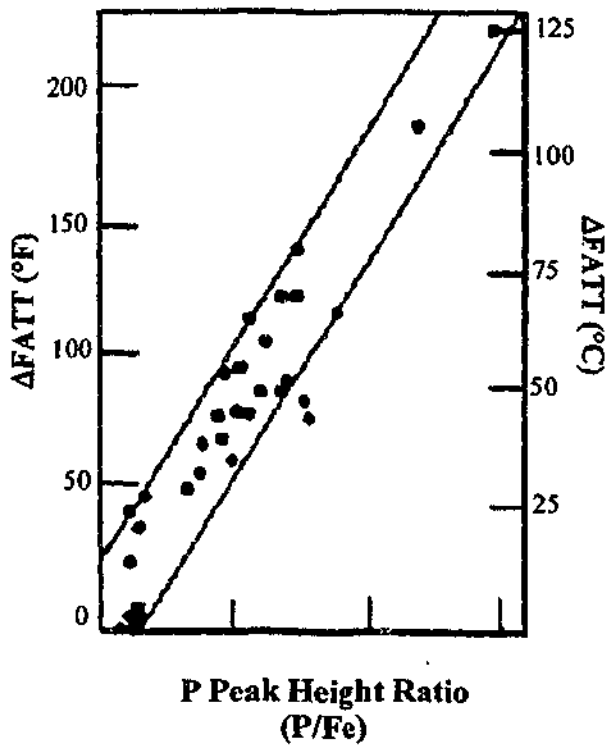

Figure 2.13 Correlation of ΔFATT with phosphorous segregation, based on Auger analysis, for Cr-Mo-V steel (after Viswanathan, 1989).

Chemical Etching

Segregated phosphorous at the grain boundaries of rotor steels may be detected by etching with a saturated aqueous solution of picric acid (Viswanathan and Bruemmer, 1985). Specimens having a greater value of ΔFATT were consistently more heavily etched. Figure 2.14 shows a relationship obtained between ΔFATT and the ratio of grain sizes D_0/D_a , where D_0 is the prior austenite grain size revealed by Nital etching, and D_a is the notional grain size revealed by picric acid etching.

Carbides morphology and distribution

Microstructural characterisation is a promising technique for assessment of temper embrittlement. However, the complexity of the interaction between the fine (nano) scale microstructural processes makes quantification of microscopy and microanalysis data difficult. A method for assessing the degree of temper embrittlement, recently developed by Moss and Kelly (1994), and based on earlier work by Stevens *et al.* (1985, 1986), and Nishizaka *et al.* (1985) involves a microscopical characterisation of the type and distribution of carbides together with an analysis of precipitates following their extraction form the steel alloy.

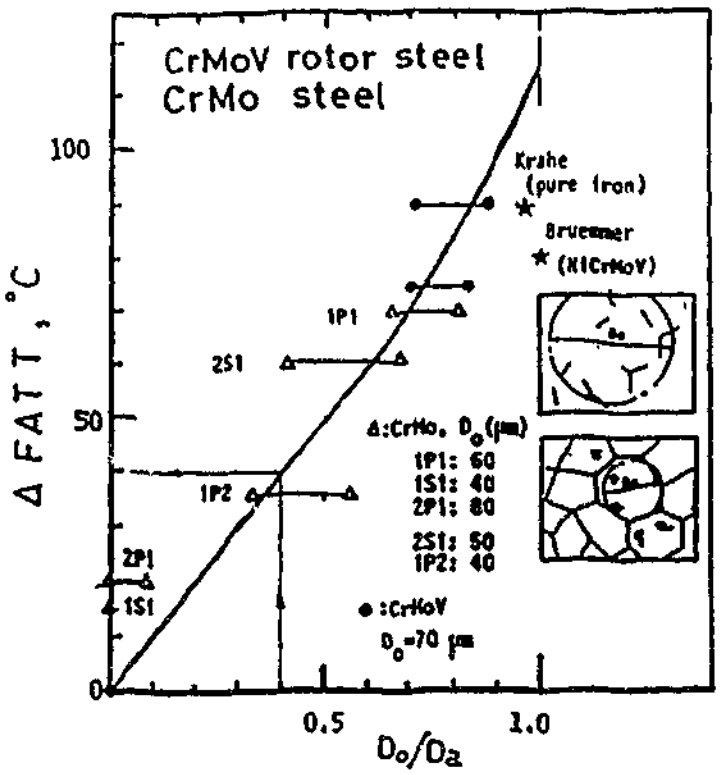

Figure 2.14 Relationship between grain size ratio (D_0/D_a) and ΔFATT (after Viswanathan and Bruemmer, 1985).

Following identification of the carbides types using ATEM, X-ray analysis of precipitates extracted from a known volume was performed, so as to determine the relative carbide proportion and the total mass fraction of carbide. This can be used to back calculate the amount of (e.g.) Mo remaining in solution in the matrix. This allows an estimate of the potential scavenging effect for P and, together with other microstructural parameters, can indicate the susceptibility to temper embrittlement. Mitchell and Moss (1998) examined seven turbine generating rotors, including in-service and retired units. They reported an increase of hardness that was possibly due to carbide-induced loss of Mo in solid solution.

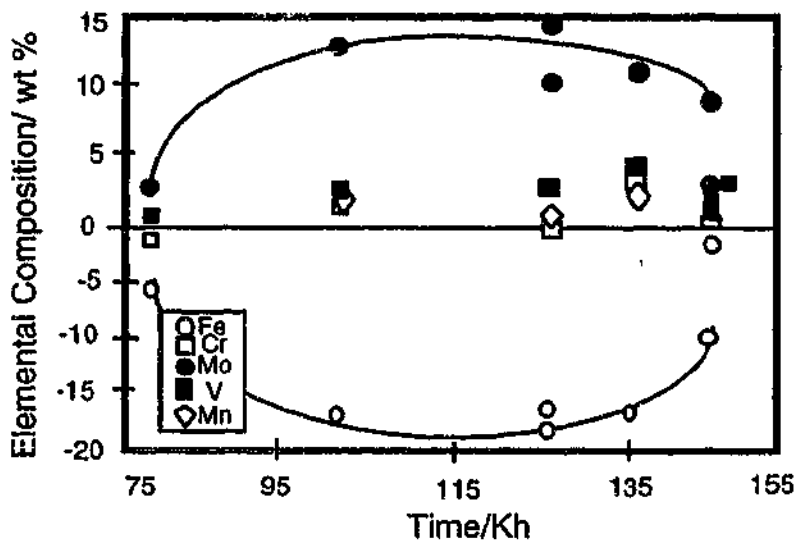

Figure 2.15. Change in average carbide compositions as a function of service exposure (after Mitchell and Moss, 1998).

Composition and morphology of MC, M_2C and M_3C carbides were investigated and were found to vary with exposure time. Figure 2.15 shows a change in average carbide compositions as a function of service exposure time.

Atom Probe Field Ion Microscopy (APFIM)

The introduction of APFIM during recent years has motivated an exploration of the effects of phosphorous and molybdenum on temper embrittlement. It allows for examination of the mechanisms and kinetics of segregation at the atomic level. Miller *et al.* (1995) performed a characterisation study of three Russian pressure vessel steels. High P levels were found at the lath boundaries and it was found to be confined to an extremely narrow region indicative of monolayer segregation. Their results also indicated that the P coverage in the three unradiated steels were similar and the phosphorus coverage increased by a factor of 2 after neutron-irradiation.

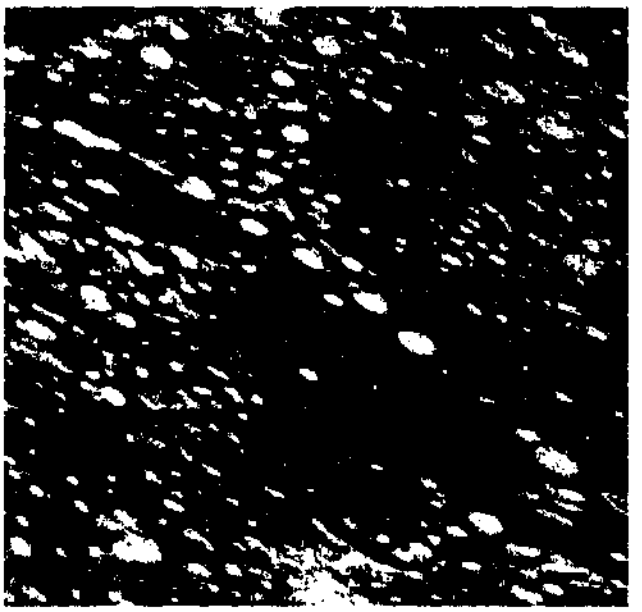

Figure 2.16 Field ion micrograph of a decorated lath boundary in a neutron-irradiated Weld 28 steel (after Miller *et al*,1995).

Figure 2.16 illustrates the lath boundaries that were found to be decorated with Mo carbohydrates and significant enrichments of phosphorus.

Miller *et al.* (2000) also reported a successful attempt of investigating the mechanisms that produce embrittlement in low copper materials used in reactor pressure vessels.

2.6 Aims and Objectives of the Project

The following factors seem to contribute to contemporary relevance of the problem of temper embrittlement:

- rotor age and vintage
- cyclic operation
- trends of increased privatisation
- the need to assess and possibly extend the design life

There has been extensive research performed on the structural integrity assessment of pressure equipment over the past three decades (Rice, 1968; Viswanathan, 1989). The findings provide invaluable knowledge of the approach to the remaining life analysis of power generation equipment. However, these efforts have been concentrated on the compilation of data based on the large range of pressure equipment, using in the majority of cases destructive mechanical testing.

Further to this, in most research investigations the test samples had been removed at a variety of locations with different exposure temperatures (Viswanathan and Gehl, 1991). Only in selected rotors had the effect of temperature on embrittlement been assessed by testing samples extracted at various locations along the rotor. The most complete data sets excluding the present research had been reported for the US Buck rotor and the Riverbend 6 rotor (Viswanathan, 1989). The present study appears to be the only complete set of impact and microstructural data collected for a single Australian retired rotor.

In this work, the main emphasis is placed on the miniaturisation or semi non-destructive technique of the testing specimens necessary for a successful remaining life estimation. It is proposed to unite the results from three kinds of mechanical testing and develop a three-way or triangular correlation. Such correlation would ultimately allow operators to conduct an on-site fracture toughness estimation and not be limited by the ASTM material requirements.

Scavenging of phosphorus and the variation of microchemical information of the precipitates between rotor stages also warrant further exploration. The microstructural information would permit assessing the kinetics of embrittlement as well as serving as complementary to mechanical testing correlations.

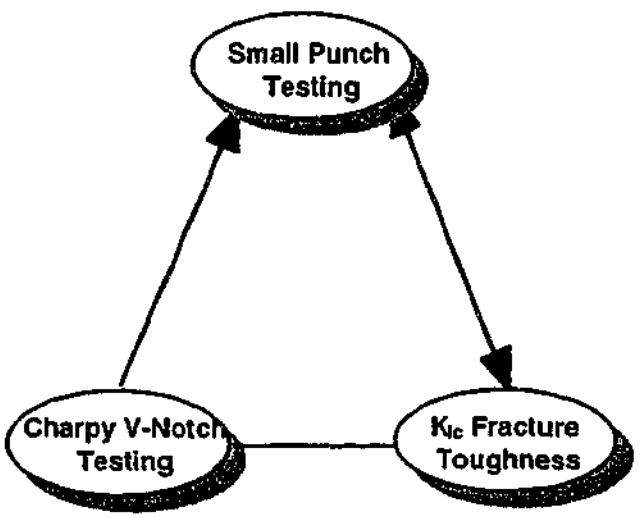

Figure 2.17 Triangular Mechanical Testing Correlations

More specifically the aims of this thesis are:

- the study and comparison of the results of the mechanical testing and microstructural analysis for a single HP/IP retired rotor for material taken from various locations of the retired rotor over a range of operating temperatures,
- the measurement of fracture toughness (K_{Ic}) and small punch test (SPT) data to correlate the results of the different kinds of mechanical testing,
- the derivation of new correlations, which quantify these relationship between full scale fracture toughness (K_{Ic}) test results and miniaturised SPT and Charpy tests for the entire range of service conditions,
- correlation of the mechanical test results for a single HP/IP rotor (full size and miniature size) with the results from a microstructural analysis, using analytical scanning and transmission electron microscopy,
- analysis of the Mo and P concentration in the matrix using selected 3DAP/FIM experiments and thus qualitative assessment of the kinetics of embrittlement.

Chapter 3: Experimental Methods and Techniques

The following chapter describes the material acquisition, techniques and methods employed for testing and examination

3.1 Cr-Mo-V Steel Rotor Components

The material investigated in this study was an ex-service Cr-Mo-V HP-IP turbine rotor steel. A detailed chemical composition of the rotor determined spectrographically is provided in Table 3.1. This rotor steel is typical of many rotors which remain in use. The retired HP-IP rotor had 8 high-pressure stages and 4 reaction stages, and was retired after 136,000 h of elapsed operation.

Eight stages (rotor disks) were available for the present work; designated stages 1 (hottest), 3,4,5,6,7,8, and 12 (coldest). Table 3.2 contains a list of approximate operating temperatures. These were calculated by Pacific Power Intl. using a Finite Element Method. Fig. 3.1 demonstrates the FEM rotor model and presents calculated temperatures.

Sectioning of a rotor stage is shown in Fig. 3.2. As suggested in the Fig. 3.2, quarters of the rims from each of the eight stages were machined so as to provide CVN specimens from the radial orientation in the service-exposed condition. This allowed for screening of the stages to determine the most embrittled stage.

Blocks were also cut out of the cores of stages 1, 3 and 12 so as to provide specimens for full size and sub-size Charpy V-Notch (CVN) tests, full size K_{Ic} fracture toughness tests, tensile tests, and small punch tests (SPT). Appendix A details the cut-up plan for Stages 1, 3 and 12. The radial notch orientation was consistent throughout the cut-up of the rotor.

Table 3.1 Rotor Chemical Composition

Element	*Composition of each of the stages locations*					
	Stage 1		*Stage 3*		*Stage12*	
	Core	*Rim*	*Core*	*Rim*	*Core*	*Rim*
Cr	1.19	1.24	1.22	1.23	1.23	1.21
Mo	0.82	0.83	0.86	0.84	0.84	0.83
V	0.22	0.23	0.22	0.23	0.23	0.23
C	0.30	0.29	0.31	0.3	0.29	0.28
Mn	0.58	0.65	0.48	0.66	0.64	0.63
Si	0.28	0.31	0.22	0.31	0.30	0.30
P	0.014	0.013	0.014	0.013	0.013	0.013
S	0.013	0.013	0.012	0.012	0.013	0.014
Cu	0.17	0.16	0.2	0.16	0.15	0.15
Ni	0.32	0.31	0.31	0.31	0.31	0.31
Nb	<0.01	<0.01	<0.01	<0.01	<0.01	<0.01
Ti	<0.01	<0.01	<0.01	<0.01	<0.01	<0.01
Al	0.01	0.01	<0.005	0.01	0.01	0.01
B	<0.0005	<0.0005	<0.0005	<0.0005	<0.0005	<0.0005
N	0.02	0.03	0.03	0.03	0.02	0.02
Sn	0.017	0.017	0.020	0.020	0.021	0.021
Sb	<0.005	<0.005	<0.005	<0.005	<0.005	<0.005
As	0.035	0.035	0.036	0.035	0.036	0.035

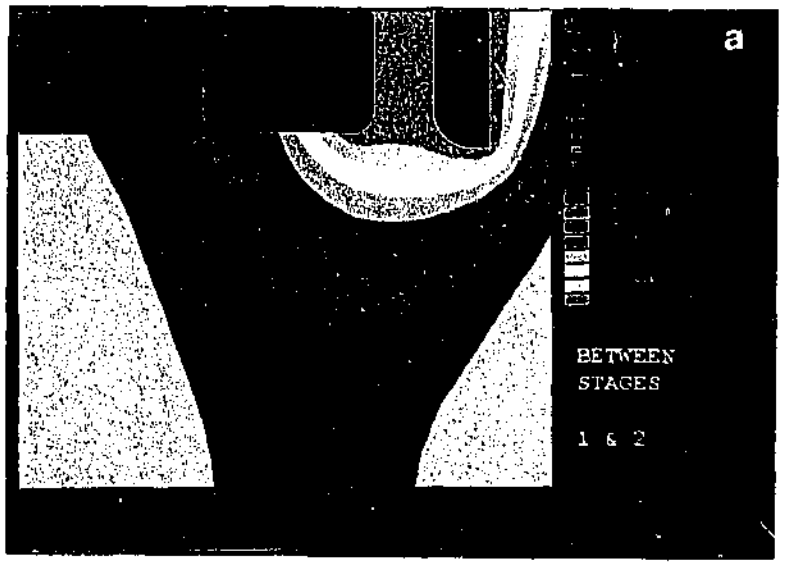

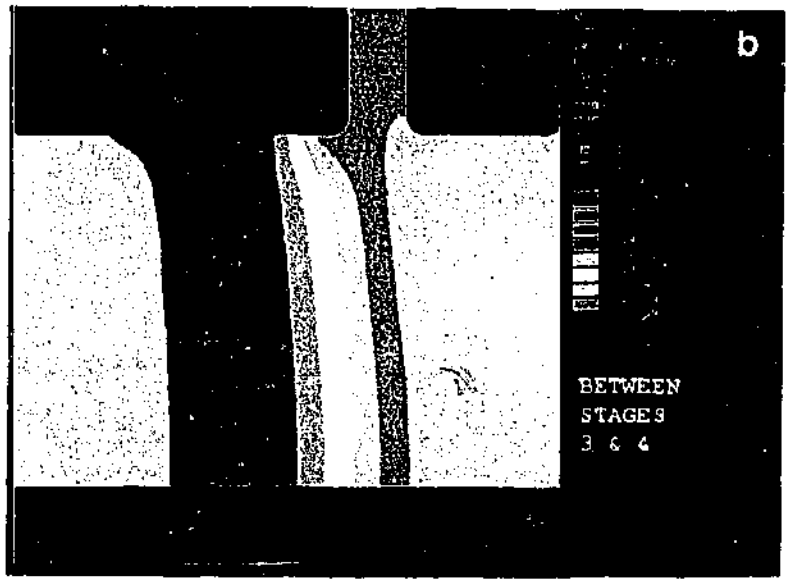

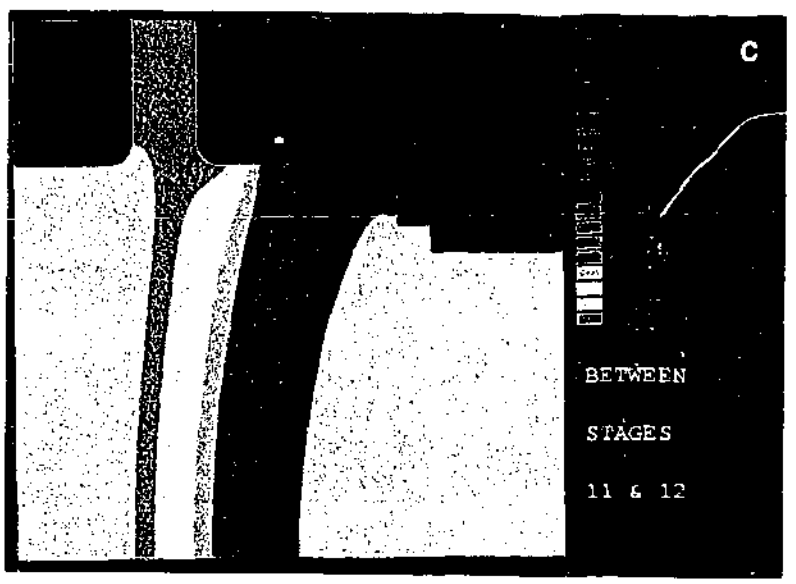

Figure 3.3 Temperature distribution between rotor stages (a) stage 1, (b) stage 3 and (c) stage 12

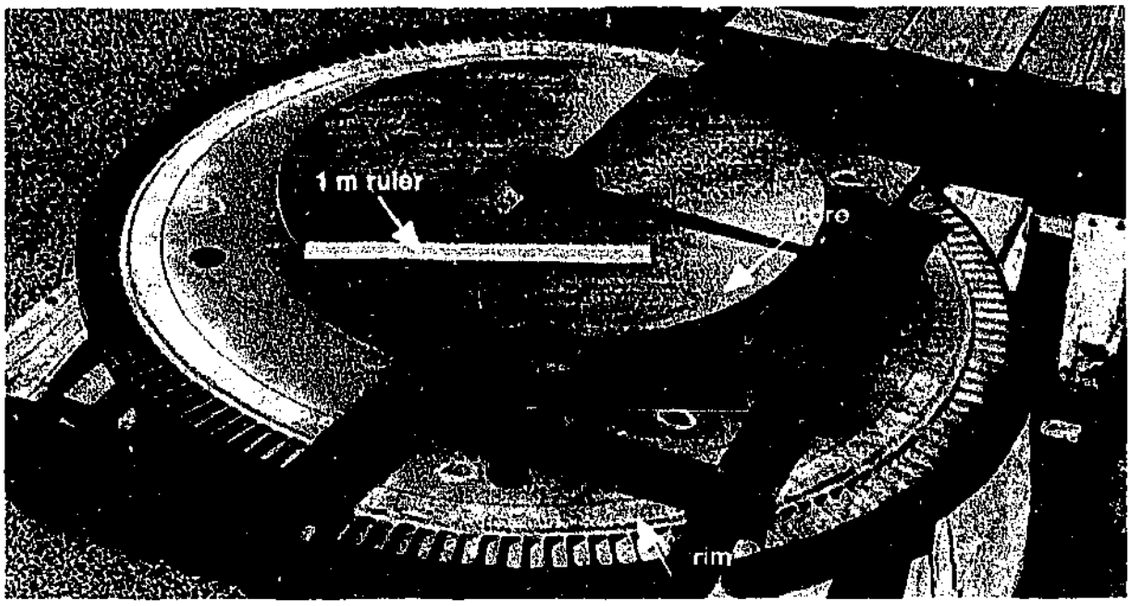

Figure 3.2 Sectioning of a rotor stage.

Table 3.2 Service Temperatures

Stage	*Operating Temperature (°C)*
1	565
3	505
4	480
5	470
6	440
7	420
8	400
12	200

3.2 Heat Treatments

Work on the rotor steel was designed around the following sample set:

- As-received (service exposed) condition,
- De-embrittled (using a standard de-embrittling heat treatment, as introduced by Low, (1964)),
- Re-embrittled (using a Gould heat treatment cycle, Gould *et al* (1968)).

De-embrittling heat treatment

In order to identify the degree of embrittlement one of the blocks for each mechanical test was subjected to a de-embrittling heat-treatment, consisting of tempering at 600°C for 2 hours followed by water quench. This treatment was introduced by Low (1968) and is known to remove all temper embrittlement incurred during rotor service life so as to indicate the non-embrittled FATT for a given composition and microstructure.

Re-embrittling heat treatment

To evaluate the susceptibility of embrittlement, blocks cut from the core of stages 1, 3 and 12, were subjected to accelerated step-cooling procedure, known as a Gould thermal cycle (Gould, 1968). This treatment has been devised to induce a greater amount of embrittlement than any isothermal exposure of equivalent time. These heat treatments were designed to combine the favourable kinetics of embrittlement at high temperatures with the favourable thermodynamics of segregation at lower temperatures. The step-cooling procedure that was employed is shown in Fig. 3.3.

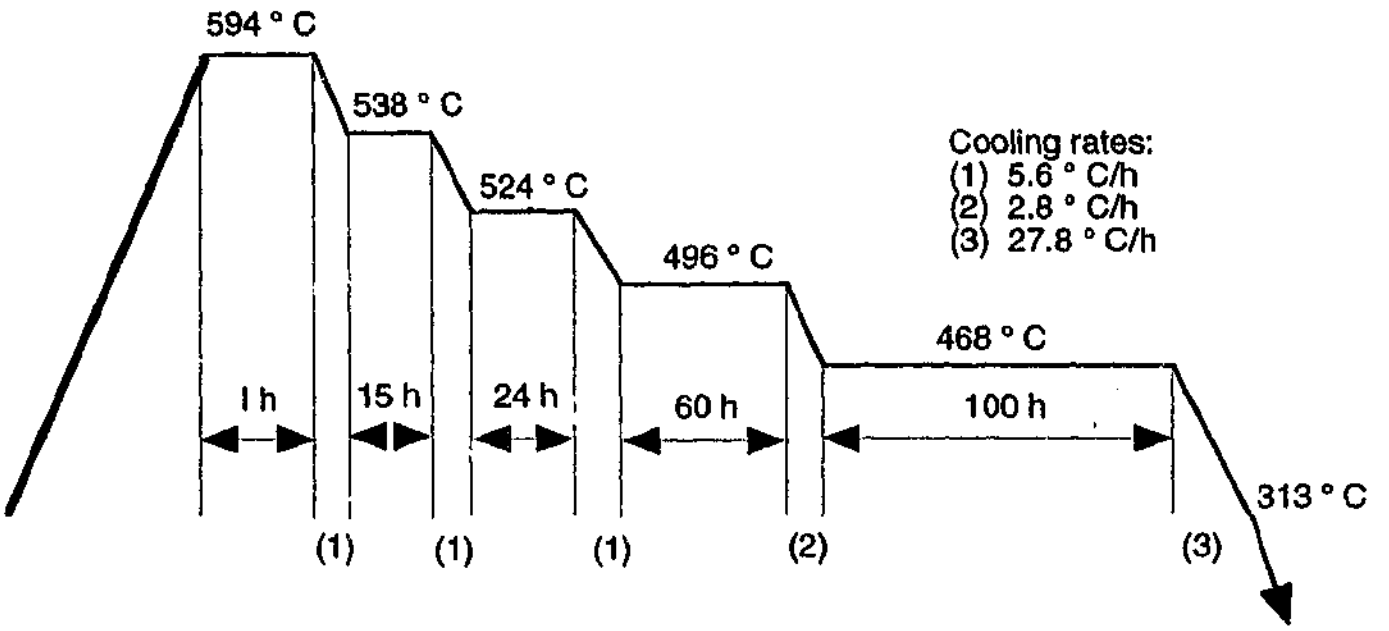

Figure 3.3: Step-cooling cycle

3.3 Mechanical Testing

Table 3.3 summarises the mechanical tests and the respective objectives of each test.

Table 3.3 Objectives of Mechanical Tests

Mechanical Test	*Objective*
Charpy V-Notch	to obtain the basic FATT
Tensile	to obtain the basic tensile properties, necessary for K_{Ic} and fracture toughness tests
K_{Ic}	to obtain a value of K_{Ic} and correlate it with FATT
Small Punch Test	to obtain a Small Punch Transition Temperature (SPTT), and then correlate it with the value, derived form Charpy tests and K_{Ic} values.

3.3.1 Charpy V-Notch Testing

The CVN testing was conducted in accordance with the ASTM E23-96, "Standard Test Methods for Notched Bar Impact Testing of Metallic Materials". The samples from two localities of the rotor were available: rim and core. Where tests were conducted at other than room temperature, the temperature of the specimen was controlled by immersion in a bath of silicone oil at the required temperature. Impact energies were measured in Joules. The percent of crystallinity of each specimen was estimated visually by examination under an optical microscope.

Two sample sizes were tested: standard full size and sub-size. Appendix B illustrates the dimensions and notch geometry of full and sub size Charpy specimens.

The percentage of crystallinity was determined in Charpy V-Notch tests with the aide of the stereomicroscope equipped with a grid-eyepiece. Comparison to other available methods, eg image analysis techniques, has proven the advantage of this method.

3.3.2 Tensile Testing

Tensile tests were conducted at room temperature in accordance with ASTM A 370-96, "Determination of Tensile Properties", using an INSTRON 4505 mechanical testing machine using a cross-head speed of 2.5 mm/min. Details of the tensile specimen geometry used are given in the Appendix B.

Elevated Temperature Tensile Testing

Tests at temperatures of 100-160 °C were conducted on an INSTRON testing machine equipped with an environmental chamber using cross-head speeds of 0.375-1 mm/min. Tests at temperatures of 180-280 °C were carried out on Schenck Universal Testing Machine equipped with high-temperature environmental chamber.

3.3.3 Small Punch Testing

The samples used in this test came from a broken full size Charpy sample and were oriented so that the fracture plane was the same as for the Charpy specimen, Fig. 3.4. Eighteen samples were cut flat and then prepared metallographically to ensure removal of any surface defects, scratches or deformation from the cutting process. Samples were stored in a desiccator to avoid corrosion. When mounting the samples in the testing rig, care was taken not to induce any plastic deformation in the sample due to small size of the samples.

The small punch tests were conducted according to ANSTO QA procedures (Croker, 1998) in light of the fact that there is no recognised standard for the small punch test. However, tests are based broadly on the methods proposed by JAERI (Takahashi, 1988) which have also been used by Foulds *et al.*,1994. These methods dictate punch and die geometry and loading rates. For the samples tested at a temperature other that room temperature the test was conducted in an insulated environmental chamber which was cooled with liquid nitrogen to achieve the temperature desired. The vessel has a temperature controller system and was fan forced so that a constant temperature within +/- 2°C of the nominated temperature is achieved throughout the chamber. Once the system had reached the required temperature it was held at this temperature for at least

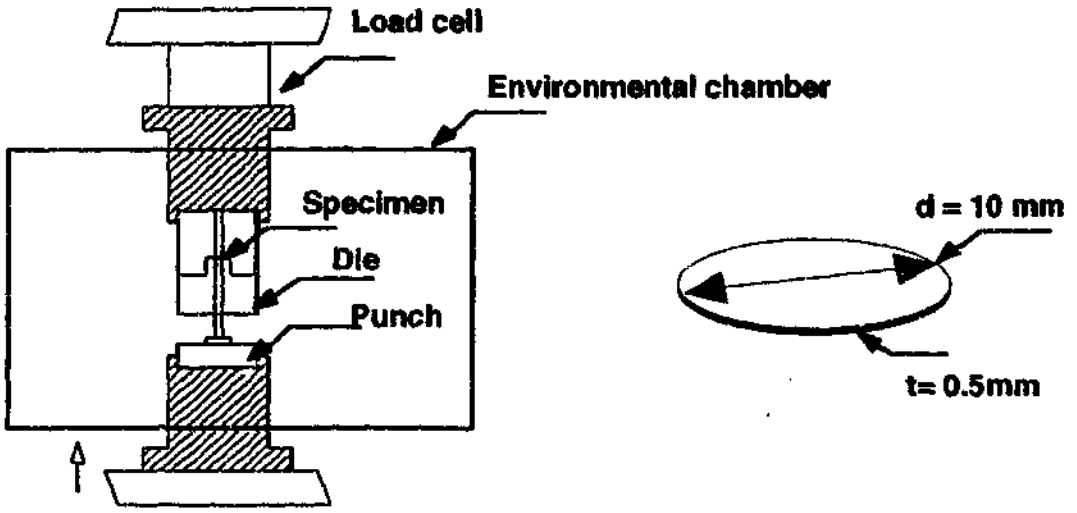

Figure 3.3 Schematic of small punch test setup (after Croker ,1998)

half an hour to equilibrate prior to commencing the test. Tests at -196°C were performed by immersion in a liquid nitrogen vessel fitted to the testing machine.

The crosshead speed was set to 0.2 mm per minute and load and displacement were monitored electronically by a personal computer (PC) via a General Purpose Interface Bus (GPIB) interface. The small punch testing rig and specimen geometry is shown in Fig. 3.4. Figure 3.5 shows a SPT jig and illustrates a liquid nitrogen run.

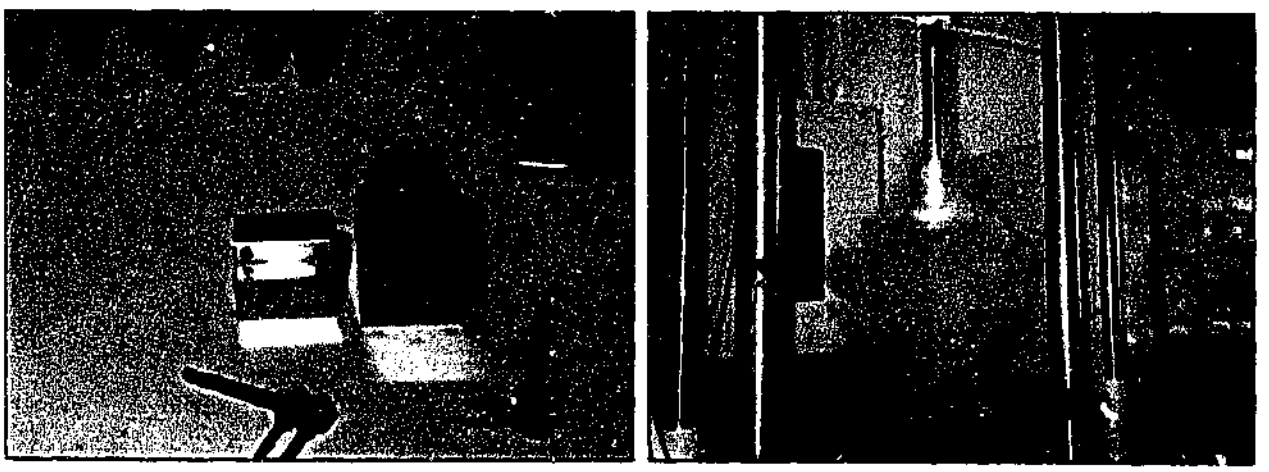

Figure 3.5 SPT jig (right) and SPT at -196 °C.

The small punch energy corresponds to the area under the curve of the load versus displacement graph up to the point of maximum load. The area under the curve was calculated from the electronic data using a simple spreadsheet and then thickness corrected to normalise all results to 0.5 mm thickness. The thickness corrected energy values used to plot the curve which are used to determine the Small Punch Transition Temperature, SPTT.

3.3.4 K_{Ic} Fracture toughness Testing

The K_{Ic} tests were performed in accordance with the ASTM E399-90 for the three-point bend single specimen technique. Three-point bend specimen dimensions and notch geometry are given in Appendix B. Fatigue loads were determined according to the equations given in ASTM 399-90 and are also presented in the Appendix C together with the photographs of various stages of K_{Ic} determination and the outline of the procedure involved.

3.4 Microscopy and Microanalysis

3.4.1 Optical Metallography

Samples for optical microscopy were hot mounted in bakelite, polished to a 1 μm finish and etched using 2% Nital (HNO_3). Light etching was carried out in 2 sec steps, totalling 15-20 sec, to progressively assess etch severity.

Colour etching was performed using a solution of (4% HNO_3 + 7%$(NO_2)_3C_6H_2OH$ + saturated $Na_2S_2O_3$). In this technique, selection of the temperature of etchants, etching time and temperature, and the humidity of the air used to dry the specimens are important factors in the attainment of a satisfactory delineation of different phases.

3.4.2 Electron Metallography

Discs of diameter 3 mm were machined and abraded to a thickness of ~40 μm and then thinned down in a Tenupol twin-jet eletropolishing unit using a solution of 5% perchloric acid in methanol. Electropolishing was carried out with an electrolyte temperature of –20 °C and an open circuit voltage of 30 V. Carbon extraction replicas were prepared for each stage using standard techniques.

Thin foils and carbon extraction replicas were examined in a Philips CM20 ATEM operating at 200 kV in scanning nanoprobe mode, with an Oxford Instruments ultra-thin-window energy dispersive X-ray spectroscopy (EDXS) detector, (Pentafet TG 6412 system) integrated with a Moran Scientific X-ray mapping package. Analytical parameters were held constant throughout the analyses with the probe size ≤ 5 nm. The microanalytical data was processed using the Cliff-Lorimer equation; since approximate

K-factors were used, it is difficult to assess the error in the precipitate compositions reported here, however, they are thought to be within 5-10%. Moreover, the systematic nature of the acquisitions makes the present data set sensitive to trends and variations between samples.

3.4.3 Scanning Electron Microscopy and Microanalysis

JEOL JSM 840-A analytical electron microscope, operating at 20kV fitted with an EDX system was used to examine the fracture surfaces. A JEOL high resolution electron microscope, operating at 15kV with the probe current of 10^{-11} A was used to examine polished and lightly etched sections.

Image analysis techniques were employed when calculating volume fractions of the precipitates. High resolution secondary electron images were scanned and analysed using the thresholding operation in the NIH Image v.1.62 image analysis software package.

3.4.4 APFIM

In the APFIM the specimen is in the form of a sharp tip. A positive potential is applied to the tip such that a very large electric field is present at the tip. The ambient gas surrounding the tip is usually Helium or Neon at a pressure of 1-3 x 10 to the minus 3 millibar. The gas atoms move towards the tip and strike it. The gas atoms may strike the surface many times, before an electron from the gas atom tunnels into the metal tip leaving the gas atom positively ionised. The gas atom is then accelerated away from the tip where it strikes a fluorescent screen. The net effect of many gas atoms is to create a pattern on the fluorescent screen showing spots of light which correspond to individual

atoms on the tip surface. The technique was invented by Erwin Müller in 1951. The atom probe is a related technique whereby a sudden voltage pulse is applied to the tip. This causes atoms on the surface of the tip to be ejected. The atoms travel down a drift tube where their time of arrival can be measured. The time taken for the atom to arrive at the detector is a measure ofthe mass of that atom. Thus compositional analysis of the sample can be carried out on a layer by layer basis (Miller, 2000A).

Samples for APFIM analysis were electropolished first in 25 % perchloric acid in acetic acid with a DC voltage of 5–10 V. Specimens were then observed under an optical microscope to examine the shape of the tip, and its suitability for APFIM analysis, magnification X50. If the tip was found not suitable for the analysis, tips were further sharpened in a solution of 5 % perchloric acid in 2-butoxyethanol using a DC voltage of ~10 V.

The 3DAP instrument consisted of a field ion microscope equipped with a CAMECA tomographic atom probe detection system. The sample tips were loaded into the specimen chamber and cooled to approximately 25K. Once the oxide layer was removed from the tip by field evaporation, a He field ion image was obtained. The tip was orientated to perform 3D atom probe analysis near the $\{111\}_{\alpha}$ pole, the He gas shut off and data collected at a temperature of 25 K with a voltage pulse fraction of 20 % in an ultra high vacuum of ~1 x 10^{-10} mbar. The data was visualised with the KINDBRISK SDV 3DAP data analysis software, a module of the Advanced Visualisation System (AVS), run on a Silicon Graphics Octane work station.

Chapter 4: Effect of Miniaturisation on the Impact Properties of Service-Exposed Material

The following chapter presents the initial impact results and summarises the relationship between standard and sub-size CVN specimens

4.1 Introduction

An assessment of the impact strength and fracture toughness of operating pressure equipment in the power generation and petro-refining industries is notoriously difficult due to difficulties in excising sample material in a non-destructive and/or non-disruptive way. Nevertheless, this remains an important field of scientific and technological study because of the ongoing need to extend the life of pressure equipment and assess structural integrity so as to deduce the implications of run, repair or replacement decisions. For these reasons, the use of miniaturised sampling and mechanical testing has received increased attention over the last decade (ASTM E23-96; Abe *et al*, 1987; Alexander and Klueh, 1991). Charpy V-Notch (CVN) impact testing has received particular attention because of the high strain rates and complex stress states that the test involves. Moreover, CVN impact testing is a rapid, relatively inexpensive and simple procedure that provides a qualitative measure of toughness. More recently, efforts have been initiated to develop test techniques and correlations that extract fundamental fracture toughness information from small volume specimens (Abe *et al*, 1987; Alexander and Klueh, 1991; Lucas *et al*, 1986; Corwin and Hougland, 1986). Given the requirements for the further miniaturisation of samples, the use of sub-size CVN specimens is of increasing significance.

Whilst ASTM E23–96 specifies the standard full-size dimensions of the CVN impact test specimen to be 10x10x50 mm, the standard also provides a variety of dimensions for sub-sized specimens. It does not, however, describe a general correlation method between the impact energy values obtained with specimens of different size. Furthermore, it does not exclude possible material-specific correlations between full-size and sub-size CVN specimens, although it is well established that smaller specimens

exhibit behaviour which is qualitatively similar to the full-size specimens (Abe *et al*,1987; Alexander and Klueh, 1991). At higher test temperatures, ductile modes of fracture occur and the energy absorbed tends toward an upper-shelf energy (USE) level. As the test temperature is decreased, a brittle mode of fracture predominates, with an accompanying reduction in the energy absorbed, tending towards a lower-shelf energy (LSE). Therefore, sub-size specimens show a ductile-to-brittle transition similar to that observed for full-size specimens (Alexander and Klueh, 1991). However, due to the reduction in both the specimen area and volume undergoing fracture, the stresses and strains vary with specimen size, and so the transition in fracture mode occurs at different temperatures (Abe *et al*,1987). This makes the comparison and correlation of the data generated with various specimen geometries difficult. In addition, the sub-size specimen geometries have not been standardised, with different researchers using different notch geometries for specimens having the same nominal dimensions (Alexander and Klueh, 1991).

In qualitatively assessing the degree of temper embrittlement, the use of CVN impact testing is almost universal, and there is an increasing tendency to use this data to estimate fracture toughness. This, together with the need to minimise the disruption and destruction of the equipment in acquiring samples, brings about a need for a detailed understanding not only of the effect of specimen size on FATT, but also of the effect of the degree of embrittlement itself. The following chapter attempts to assess quantitatively both of these questions in an in-service rotor steel. In this part of the research, we have tested and examined both sub and full-size CVN samples from selected stages of the rotor, which had been exposed to varying degrees of in-service embrittlement.

TABLE 4.1. Vickers hardness and FATT values for the alloys studied

Stage	*12*		*3*		*1*	
	Core	*Rim*	*Core*	*Rim*	*Core*	*Rim*
Hardness (VHN)	246	229	216	212	221	212

4.2 Mechanical Testing

4.2.1 Hardness Measurements

The result of hardness testing is summarised in Table 4.1.A slight but significant difference in Vickers hardness was also apparent, with the hardness of stage 12 exceeding the other stages and the core of each stage exceeding that of the rim, particularly for stage 12.

4.2.2 Charpy V-Notch Testing and Screening Procedures

Figures 4.1 (a-e) are plots of energy and crystallinity for standard full-size CVN specimens taken from rotor stages 1, 3, 4, 5, and 12, and include results from the corresponding sub-size specimens. A comparison between the two specimen sizes indicates that the sub-size specimens exhibit qualitatively similar behaviour to the standard full-size specimens, although the USE levels and FATTs are reduced.

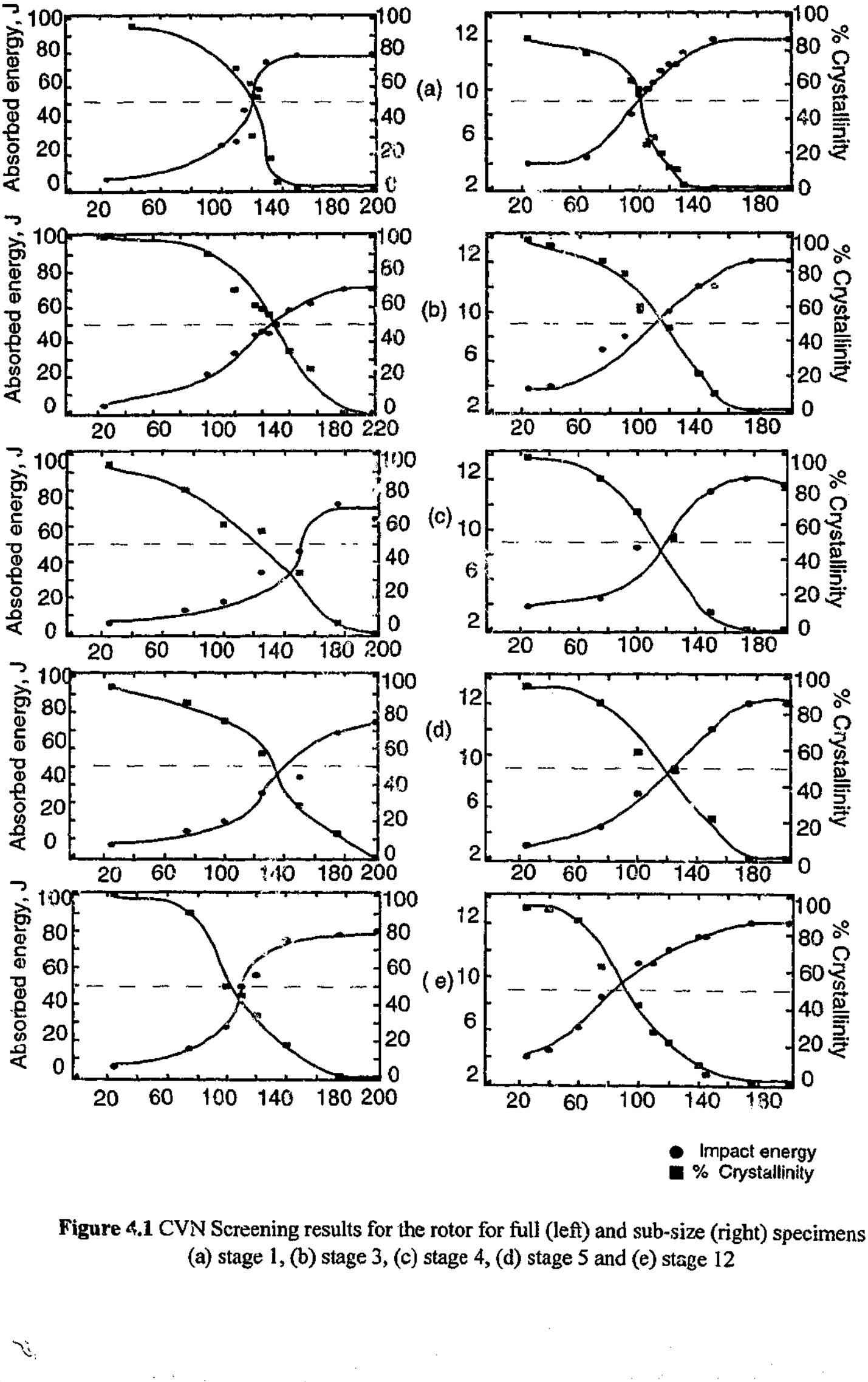

Figure 4.1 CVN Screening results for the rotor for full (left) and sub-size (right) specimens (a) stage 1, (b) stage 3, (c) stage 4, (d) stage 5 and (e) stage 12

Table 4.2 summarises the estimated operating temperatures for the three rotor stages and FATTs for both full and sub-size specimens. Figure 4.2 reveals the effect of operating temperature on the change in FATT between full and sub-sized specimens (ΔFATT) for service-exposed and de-embrittled material. The ΔFATT varies from almost zero for the de-embrittled stage 3 sample to as high as 32 °C for the embrittled stage 3 samples. The service-exposed specimens from stages 12 and 5 exhibited the lowest ΔFATT of approximately 17 °C. Stages 4, 3 and 1, which correspond to the higher operating temperatures, exhibited the higher ΔFATTs. To examine the influence of the degree of embrittlement, the ΔFATT for de-embrittled samples of stages 12, 3 and 1 was measured. The results indicate that the ΔFATT is dependent on the degree of embrittlement.

In order to obtain a correlation of the USE data for the full-size and sub-size specimens, the absorbed energy was normalised with respect to both the nominal fracture area Bb and the nominal fracture volume $(Bb)^{3/2}$, where B is the specimen width and b is the remaining ligament thickness beneath the notch (Abe *et al*, 1987). Results are provided in Figs. 4.3 and 4.4. Figure 4.3 compares the area-normalised energy for both full and sub-size specimens from stage 1. The normalisation converges from the LSE towards zero, however, there remains considerable variation between the USE values. Figure 4.4 provides the results of volume normalisation for stages 1, 3 and 12. Here, the shape of the full-size curves is replicated by the sub-size values, and their curves do not intersect.

Table 4.2 Rotor Operating Temperatures and corresponding FATTs of full and sub-size specimens.

Stage	*Oper-ating T,°C*	*FATT Full-size, °C*	*FATT Sub-size, °C*	*ΔFATT, SE °C*	*USE, Full-size, SE, J*	*ΔDBTT, SE, °C*	*ΔFATT, DE °C*	*ΔDBTT, DE, °C*
1	565	125	98	27	80	20	10	10
3	511	150	118	32	68	35	5	2
4	506	145	116	29	76	20	-	-
5	487	135	115	20	68	20	-	-
12	351	100	84	16	82	12	13	5

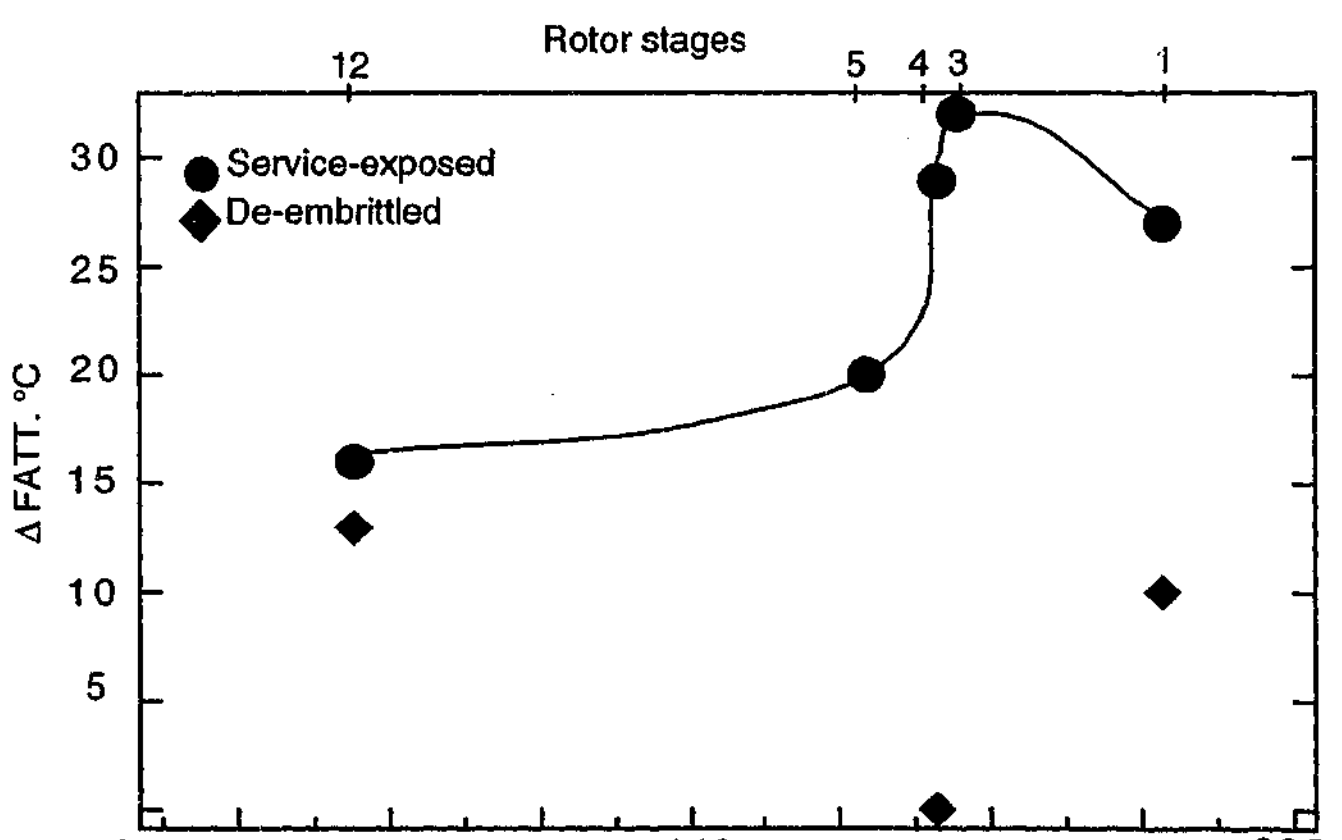

Figure 4.2 Relationship between the ΔFATT and operating temperature

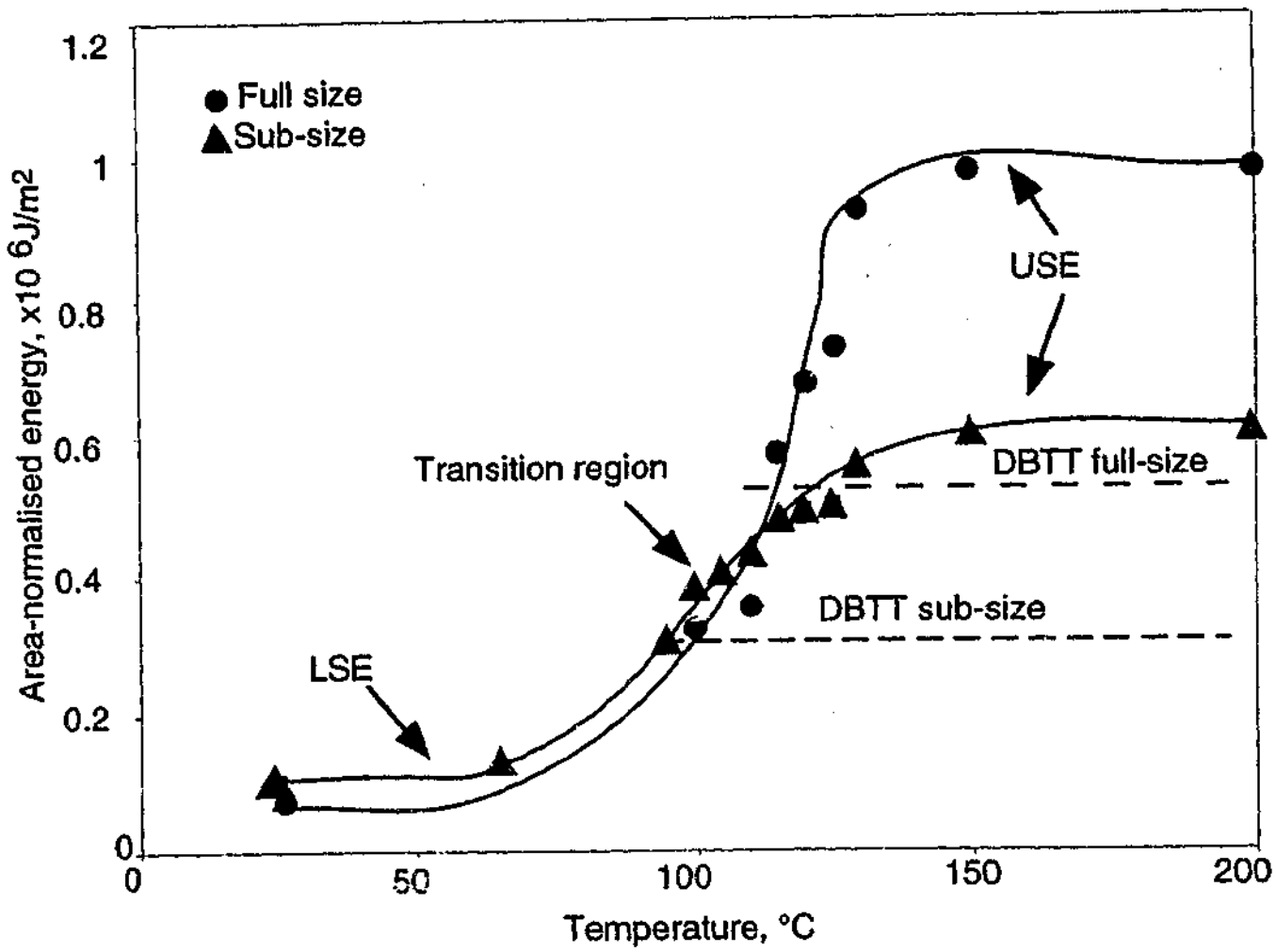

Figure 4.3 Area-normaisation of the absorbed energy cures for both full and sub-size specimens from stage 1 of the rotor

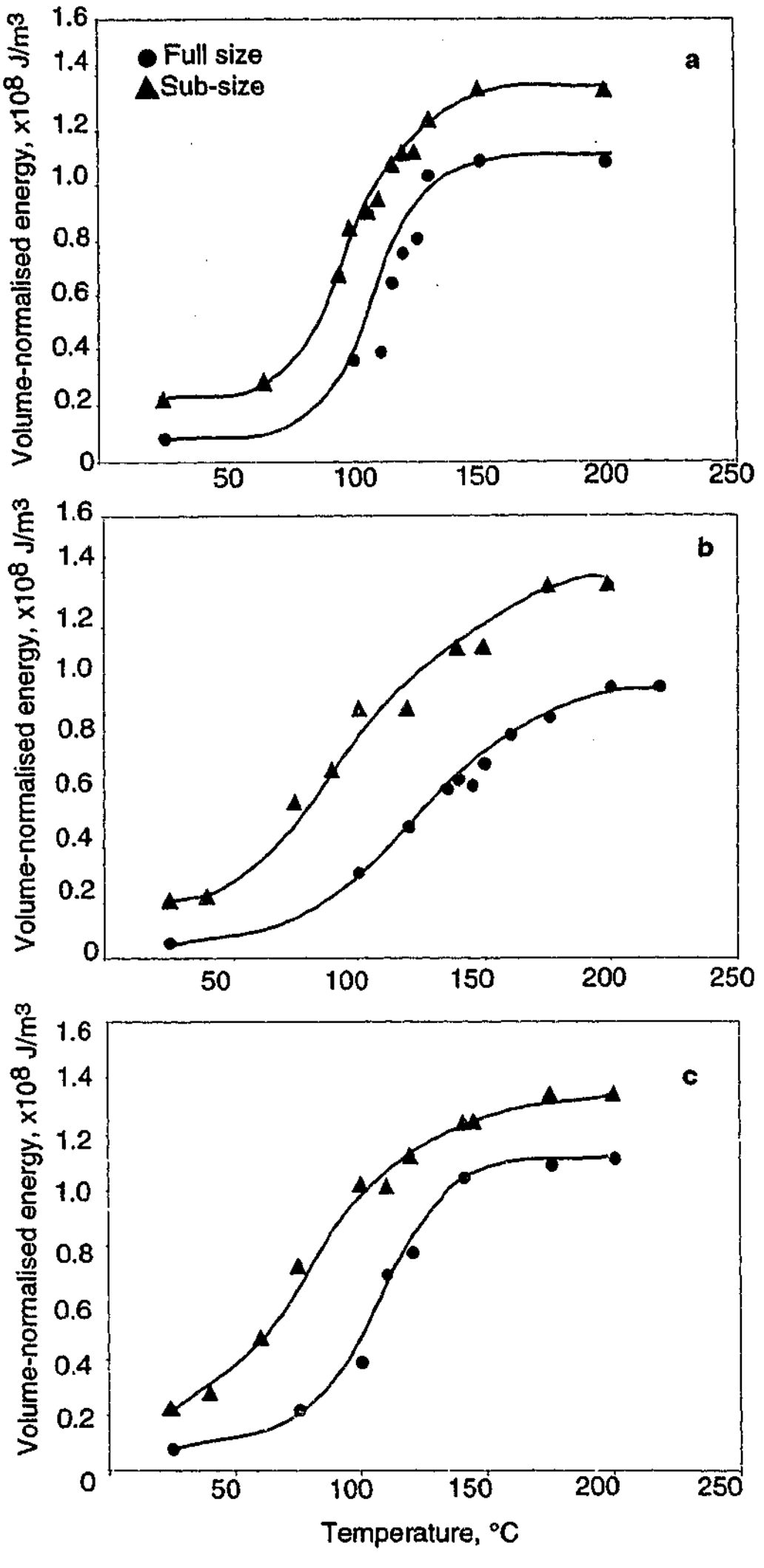

Figure 4.4 Volume-normalisation for the full and sub-size specimens: (a) stage 1, (b) stage 3 and (c) stage 12.

4.2.3 Fractography

Fractographical analyses were performed on full and sub-size specimens taken from the transition range for stage 3, representing the worst case of embrittlement. The results are provided in Figs. 4.5 (a-d). Figures 4.5 (a, b) are secondary electron images of a full-size specimen fractured at 150 °C. In Fig. 4.5 (a), an example of microvoid coalescence is clearly visible (arrowed), which resulted from the fracture mechanism changing from brittle to ductile fracture by microvoid initiation, growth and coalescence. Microvoids were initiated at interfaces between the matrix and particles such as carbides, precipitates and inclusions (Metals Handbook, 1974). The present result indicates that the ductile failure by microvoid coalescence had occurred prior to the onset of brittle failure by cleavage. In Fig. 4.5 (b), a fragment of intergranular fracture (arrowed) in a full-size CVN testing specimen is demonstrated. Intergranular fracture, described as grain-boundary separation accompanied by catastrophic brittle separation, is a characteristic of this damage mechanism since this specimen represents the most severe case of temper embrittlement. Here, the separation had occurred conjointly with the microvoid coalescence on the interfaces of grains.

Figures 4.5 (c, d) are SEM fractographs of sub-sized specimens fractured at 120 °C, which corresponds to the transition temperature for stage 3. Fig. 4.5 (c) shows a quasicleavage mode (arrowed), which is a consequence of true cleavage planes being replaced by smaller, ill-defined cleavage facets initiated at carbide particles or large non-metallic inclusions. Figure 4.5 (d) demonstrates an intergranular type fracture (arrowed) found in a sub-size CVN specimen. In contrast to the full-size examples of intergranular fracture, sub-size specimens exhibited a severe intergranular separation. Apparently, in the absence of river patterns, fracture proceeded along grain boundaries.

Figure 4.6 schematically demonstrates a "map" of a typical fracture surface topology representative for both types of specimens observed in the SEM. The lower edge of the fracture surface in Fig. 4.6 corresponds to the root of the V-notch in the specimens. The crack initiates near the notch-root and propagates through the surrounding grains in the quasicleavage mode. The river patterns, which represent steps between the different local cleavage facets, develop from the site of origin in the direction of crack propagation. This is followed by a transition region consisting of a combination of ductile and brittle surfaces, and is concluded by the fibrous zone at the outer edge of the fracture surface.

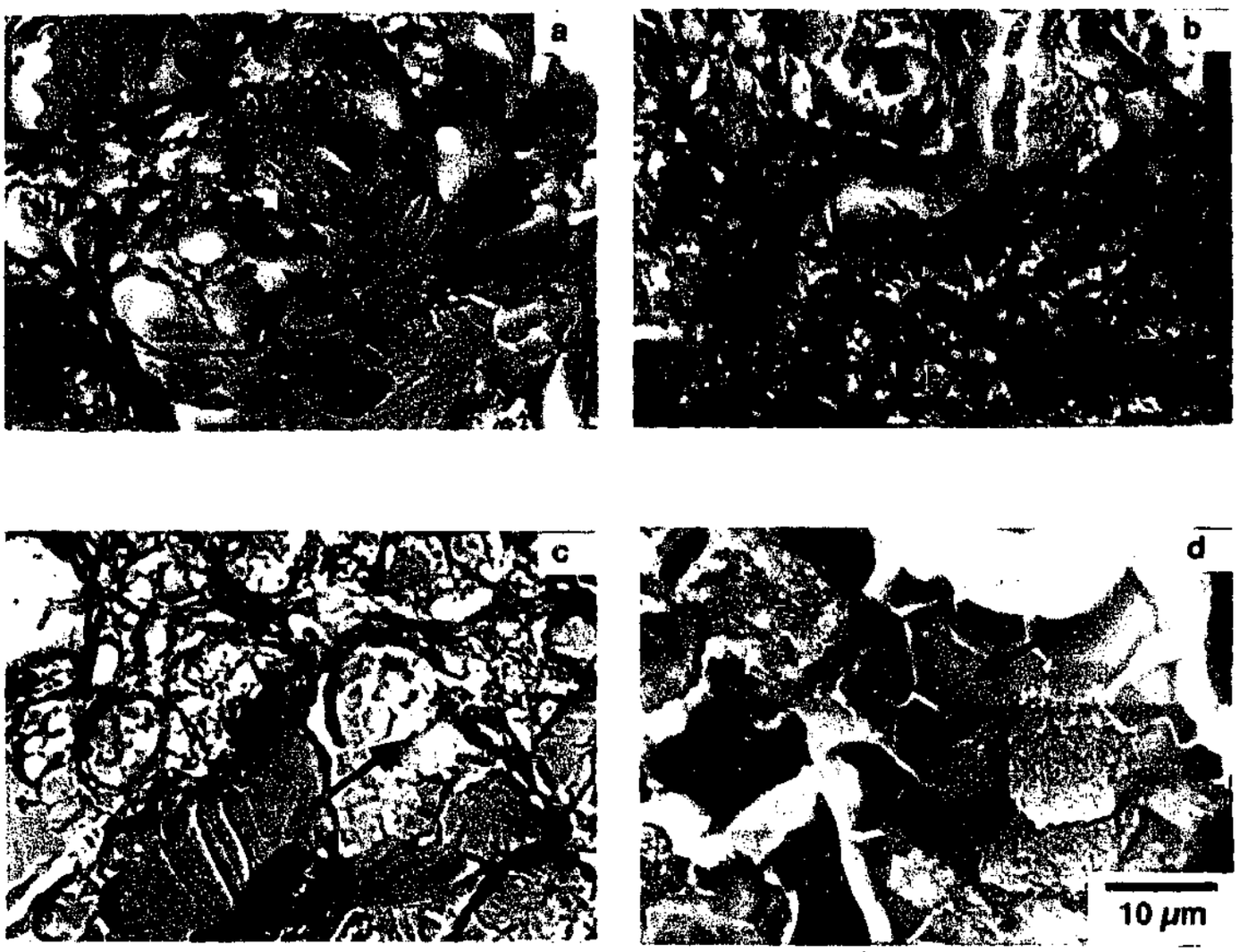

Figure 4.5 Secondary electron images of stage 3 specimens, following Charpy V-Notch testing, fractured at transition temperatures, showing (a) and (c)- a mixture of ductile and brittle fracture and (c) and (d) - intergranular fracture
(a) and (b) 150 °C - full size specimen, (c) and (d) 120 °C- sub-size specimen

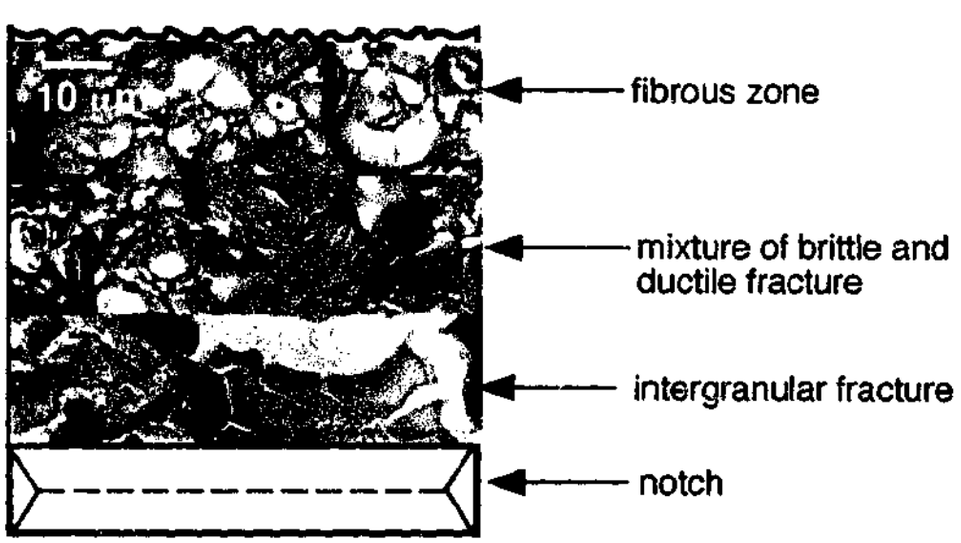

Figure 4.6: Schematic representation of the fracture surface observed in SEM

4.3 Discussion

4.3.1 Effect Of Temper Embrittlement On FATT Difference

The impact test data from both full and sub-size specimens indicates that stage 3 is the most embrittled stage. This may be correlated to a higher susceptibility to temper embrittlement since the nominal exposure of ~511 °C for this stage is near the upper limit of the critical temperature range within which this damage mechanism operates. Contrasting this, the FATT of stage 12 was the lowest for both specimen dimensions, which supports the initial assumption that this stage corresponds to the nominally "pre-service" material (Chapter 5 deals with this in great detail). Figure 4.2 refers to the relationship between the operating temperature and the change in FATT between full and sub-size specimens. The variation in ΔFATT with rotor stage/operating temperature is systematic and seems dependent on the degree of embrittlement of the various stages. Specifically, the nominally pre-service stage 12 exhibited the smallest magnitude of embrittlement and minimal dependence on the specimen size. On the other hand, stage 3 demonstrated the most embrittlement and the maximum ΔFATT. Intermediate points (rotor stages 4 and 5) in Fig. 4.2 emphasize the continuity of this tendency, which is further supported by the data from the de-embrittled samples. It is noteworthy that the ΔFATT values for the de-embrittled specimens are similar to that measured for stage 12. The origin of the dependence of the ΔFATT on the specimen size was not considered, experimentally. However, it is proposed that this effect is associated with the intergranular failure mode of temper embrittled samples. Since the prior austenite grain boundaries represent a two-dimensional array through the material, the fracture will be more sensitive to lineal thickness that the three-dimensional

volumes within which intra-granular fracture mechanisms operate. This is supported by the observation that volume normalisation of the data significantly converged the impact energy curves for sub and full-size specimens.

4.3.2 Effect Of Specimen Size On The Absorbed Energy

The full-size USE values in this study were ~6.5 times that of the sub-size. No agreement in the USE between the two specimen sizes was obtained by the area normalisation. However, the area-normalisation (E/Bb) did converge the lower shelf and the transition region for all three stages. For instance, the area - normalised absorbed energy for stage 1 was $1x10^5$ J/m^2 and $7.5\ x10^4$ J/m^2 in the lower shelf region and $3.75\ x10^5$ J/m^2 and $3.25\ x10^5$ J/m^2 in the transition region for the sub and full-size, respectively.

The volume-normalisation procedure is generally considered to be more suitable for the USE values, (Abe *et al*,1987; Alexander and Klueh, 1991) since samples fractured in the upper shelf demonstrate ductile failure, indicating the occurrence of large scale plastic deformation (Abe *et al*,1987). The volume-normalisation procedure for stage 1 produced values $1.11x10^8$ J/m^3 and $1.34x10^8$ J/m^3 for the full and sub-size specimens respectively in the USE. Although the curves for the full and sub-size specimens did not coincide quantitatively in the USE, they clearly followed the same qualitative trend. The difference between the impact energy values could be expressed as a linear equation of the type: $E_{sub\text{-}size} = kE_{full\text{-}size} + C$. Correlations of the volume-normalised absorbed energies for stages 1, 3 and 12 of the rotor yielded:

$$E_{sub\text{-}size} = 0.962E_{full\text{-}size} + 0.0386 \qquad \text{(Equation 4.1)}$$

Where $E_{sub\text{-}size}$ is volume-normalised absorbed energy for the sub-size specimen, and $E_{full\text{-}size}$ is volume-normalised absorbed energy for the full-size specimen.

Table 4.3 summarises the results from this and other sub-size CVN studies and compares the methodology used to correlate the data measured from sub and full-size specimens. Figure 4.7 utilises equation 1 so as to plot and compare the available data on size effect, summarised in Table 4.3. With the exception of report by Alexander and Kiueh, 1991, the data seem to support the volume-normalisation approach, and reasonable agreement with equation 4.1 is apparent. This supports the notion that limited correlations between various specimen sizes may be established for specific materials as mentioned in ASTM E-23, A 370.

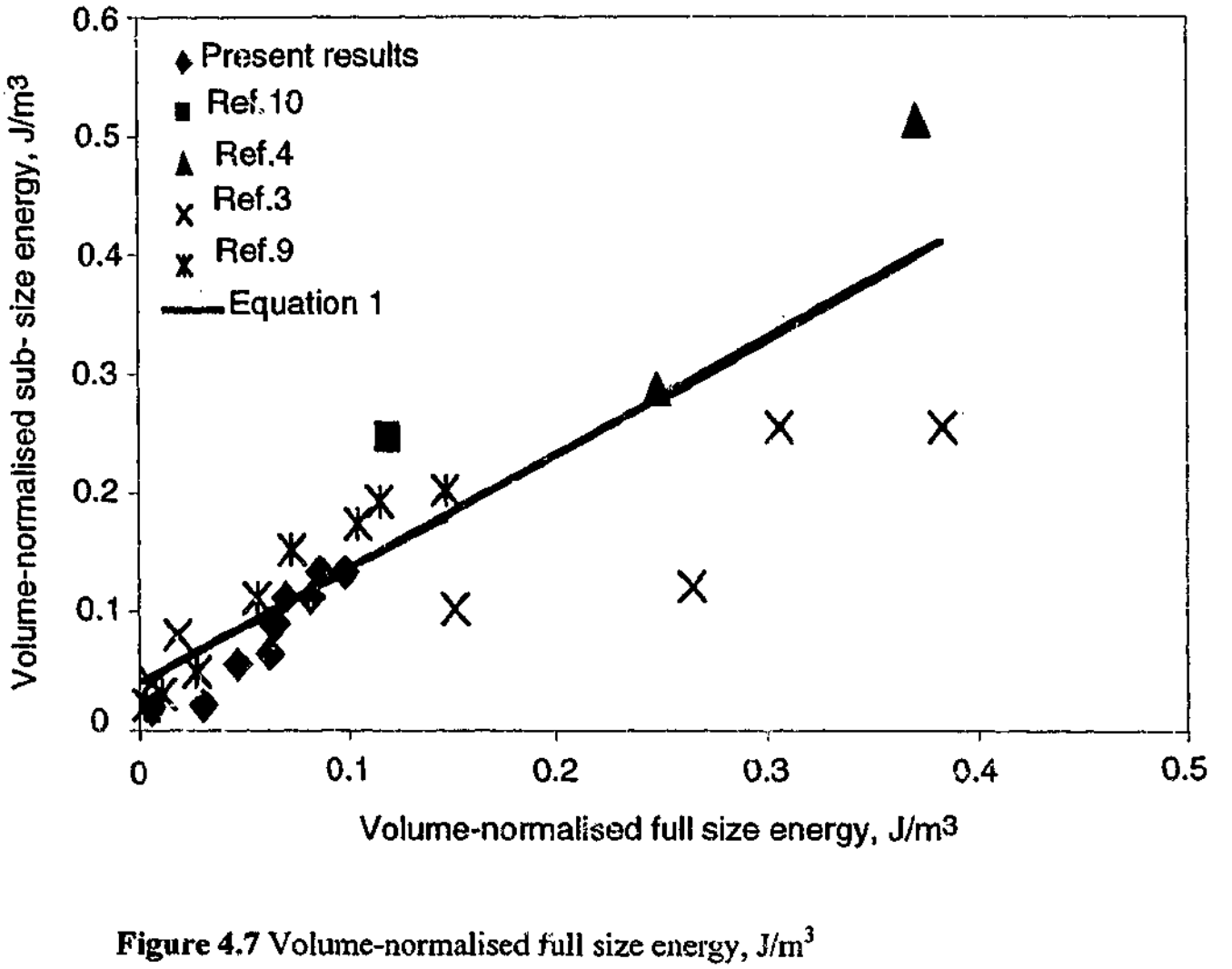

Figure 4.7 Volume-normalised full size energy, J/m^3

Table 4.3 Summary of Sub-seize Correlation Approaches

Steel Composition	*Sub-size specimen size, mm*	*Notch Radius*	*Correlation procedure*	*Region of the transition curve that correlation procedure is applicable to*	*Ref.*
9Cr- 1W 9Cr-2W 9Cr -4W	5x5x23.6	30°	E/Bb $E(Bb)^{3/2}$	LSE USE -	Abe *et al.*, 1987
9Cr-1Mo-V-Nb 9Cr-1Mo-V-Nb-2Ni	5x5x25.4	30°	$E(Bb)^{3/2}$	USE	Alexander and Klueh, 1991
9Cr-1Mo-V-Nb 9Cr-1Mo-V-Nb-2Ni	5x5x25.4	30°	$DBTT_{1/2}= DBTT_F + C_1$	Transition	Alexander and Klueh, 1991; Corwin and Hougland, 1986
9Cr- 1 Mo	5x5x25.4	30°	E/Bb $E(Bb)^{3/2}$	USE	Viswa-nathan, 1991
1 Cr-1 Mo-0.25V 12Cr -1Mo-0.25V	5x5xx55	45°	Energy vs specimen thickness	Room temperature tests only	Bashu, 1990
1 Cr- 1 Mo-0.25V	**5x5x55**	**45°**	**E/Bb** **$E_{1/2}= E_F + C_1$**	**LSE, Transition Whole curve**	-

Presents results are highlighted in bold.

4.4 Concluding Remarks

Following an investigation of the effect of temper embrittlement and specimen size on CVN testing of a 1Cr-1Mo-0.25V rotor steel it was concluded that:

- sub-size specimens exhibit qualitatively similar behaviour to the standard full-size specimens, although the USE levels and FATTs are reduced;
- variation in the ΔFATT with rotor stage/operating temperature is systematic and seems dependent on the degree of embrittlement of the various stages;
- fractography results suggest that the sub-size specimens tend to have more severe intergranular fracture than the full-size CVN specimens;
- area-normalisation yielded agreement for the lower shelf and the transition region for all three stages;
- volume-normalisation for full and sub-size specimen CVN data resulted in close matching in impact energies which was expressed in the linear equation form. This approach was applied to other available data and a material-specific correlation for specimen size was established.

Chapter 5:

Mechanical Testing and Property Correlations

This chapter presents the results from mechanical testing and describes the correlation methods used to derive a fracture toughness correlation based on the miniaturised testing technique.

5.1 Introduction

The remaining life analysis for power generation equipment is largely based on the determination of the critical crack size which is governed by fracture toughness K_{Ic}. This presents difficulties for plant operators since conducting fracture toughness experiments on the in-service high-temperature high-pressure reactor pressure vessels would be expensive and would require large volumes of material. Correlations between fracture toughness and small-scale test results are useful in assessing the structural integrity of pressure vessels due to cost, availability of material, ease of testing and because fracture toughness can be used directly in design analysis. The small-scale test results provide this information through correlation with the fracture toughness. Furthermore, K_{Ic} measurements involve use of large specimens which are difficult to excise from operating components. Thus there is a need to determine the fracture toughness by means of various predictive methods or correlations described in the "Literature survey" (Chapter 2). In the following chapter, the correlations between destructive methods CVN, K_{Ic} testing and SPT are examined and discussed.

5.2 Tensile Testing

Room and elevated temperature tensile testing was conducted to provide reference data for the fracture toughness testing.

The results from the room and elevated temperature tensile testing are summarised in Table 5.1 for the rotor material from stages 1, 3 and 12. The tensile properties for the material from all stages in all conditions, service-exposed, de-embrittled and re-embrittled appeared to be within the same proximity. Thus, Table 5.1 presents a single set of tensile properties.

Table 5.1 Tensile Testing Results

Temperature	*Yield strength, MPa*	*Max tensile strength*	*% Elongation*	*Modulus, GPa*
22	534	689.8	15.14	184.8
100	498.1	636.8	14.18	197.8
140	498	632.2	13.2	180.1
160	490.7	625.8	13.82	177.3
180	501	641	15.2	174
220	489	627	12.15	157
280	485	622	8.25	143

5.3 Impact Energy

5.3.1 Service-Exposed Material

Figure 5.1 provides the results from CVN and SPT data for the service-exposed condition of the rotor material from the core of the stages 1, 3 and 12. Here, CVN plots demonstrate the measured fracture energy vs testing temperature as well as the percentage of brittle fracture vs testing temperature. Small punch fracture energy versus testing temperature is plotted on the corresponding SPT graphs below.

Figures 5.2 are secondary electron images (SEI) of the fracture surface examined after testing at 200 °C and 25 °C, respectively, for stage 1. The photomicrograph in Fig. 5.2 (a) is a low magnification image, which exhibits an archetypal ductile character. Second phase particles appear to be embedded within the fully-fibrous fracture surface and a higher magnification image of these is seen in Fig. 5.2 (b). Energy dispersive X-ray spectroscopy identified Mn and S in association with the features. Also seen in Fig. 5.2 (b) is a fine and uniform distribution of dimples, representing a fraction of a microvoid that has opened during the fracture process. The photomicrograph in Fig. 5.2 (c) exhibits an archetypal brittle character, with ~ 100 % crystallinity. A higher magnification image of this fracture surface is seen Fig. 5.2 (d) showing crystalline flakes exhibiting chevron markings which follow the cleavage paths.

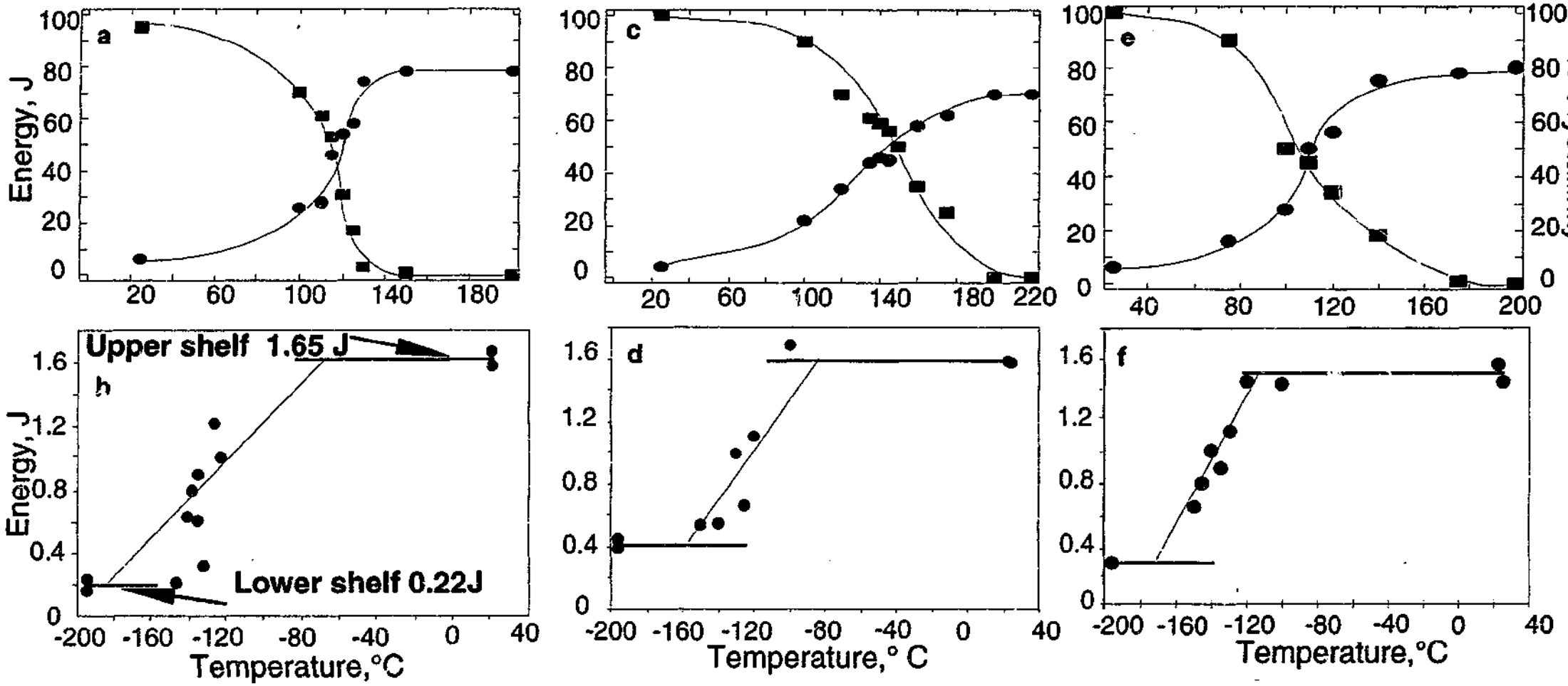

Figure 5.1 CVN Testing and corresponding SPT data for stage 1 (a and b), stage 3 (c and d) and stage 12 (e and f) in the service-exposed condition

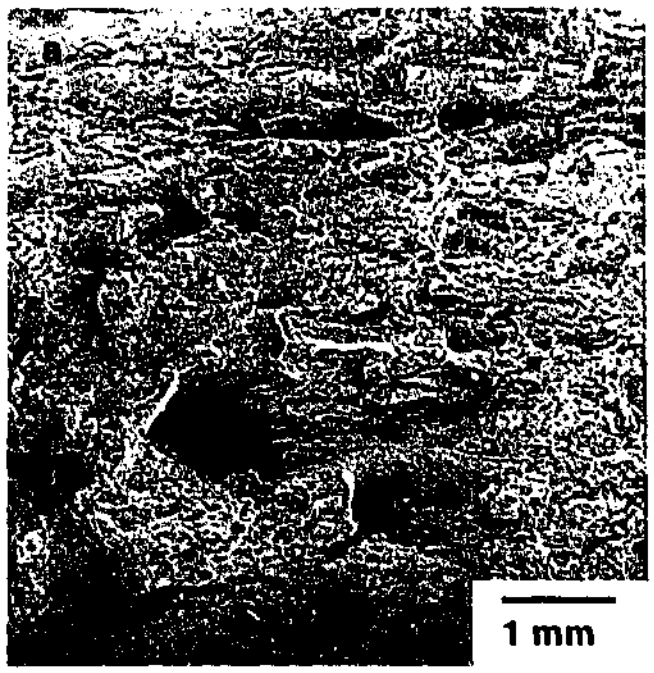

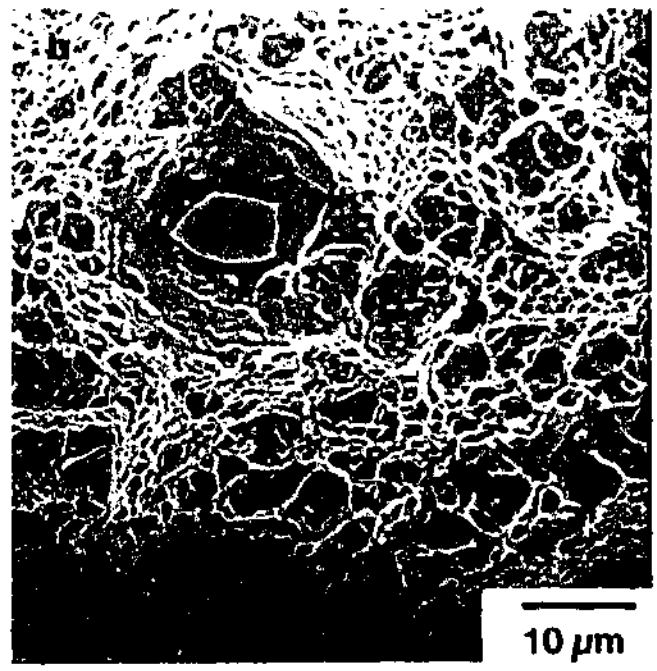

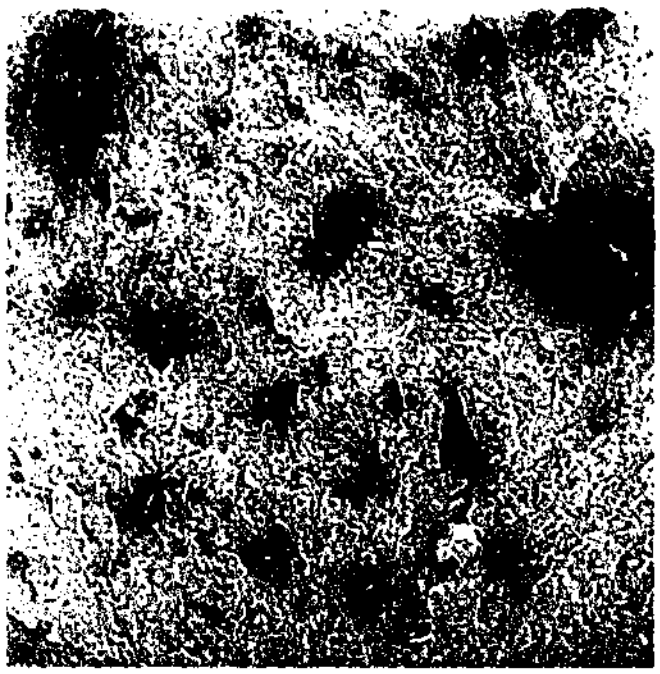

Figure 5.2 Secondary electron images of stage Charpy V-Notch specimens follwing testing at (a) 200 °C low magnification image indicating a fully fibrous, ductile appearance. Second phase particles were idnetified as containing Mn and S

(b) 200 °C higher magnification image showing the fine and uniform distribution of dimples in the fracture surface. A Mn and S containing particle is embedded in the fracture plane

(c) 25 °C low magnification image indicating a fully crystalline apperance

(d) 25 °C Chevron markings delineate the passage of cleavage across the fracture surface, revealing a fully brittle failure mode.

5.3.2 De-Embrittled Material

The results for all three stages of rotor steel in the de-embrittled condition are presented in Fig. 5.3 (refer to the following page). It shows the CVN and SPT results from samples taken near the core of stage 1, 3 and 12 in de-embrittled conditions, respectively. Fig.5.4 shows the light optical images of CVN samples in the as-received and de-embrittled conditions, respectively, tested at 100 °C. These images demonstrate the difference in the percentage of shear fracture for the service-exposed and de-embrittled material.

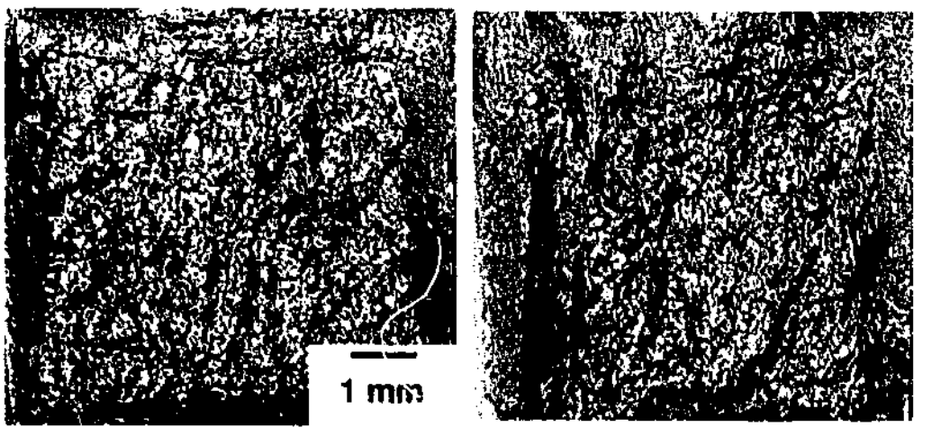

Figure 5.4 CVN fracture surfaces for specimens broken at 100 °C in (a) service-exposed condition and (b) de-embrittled condition.

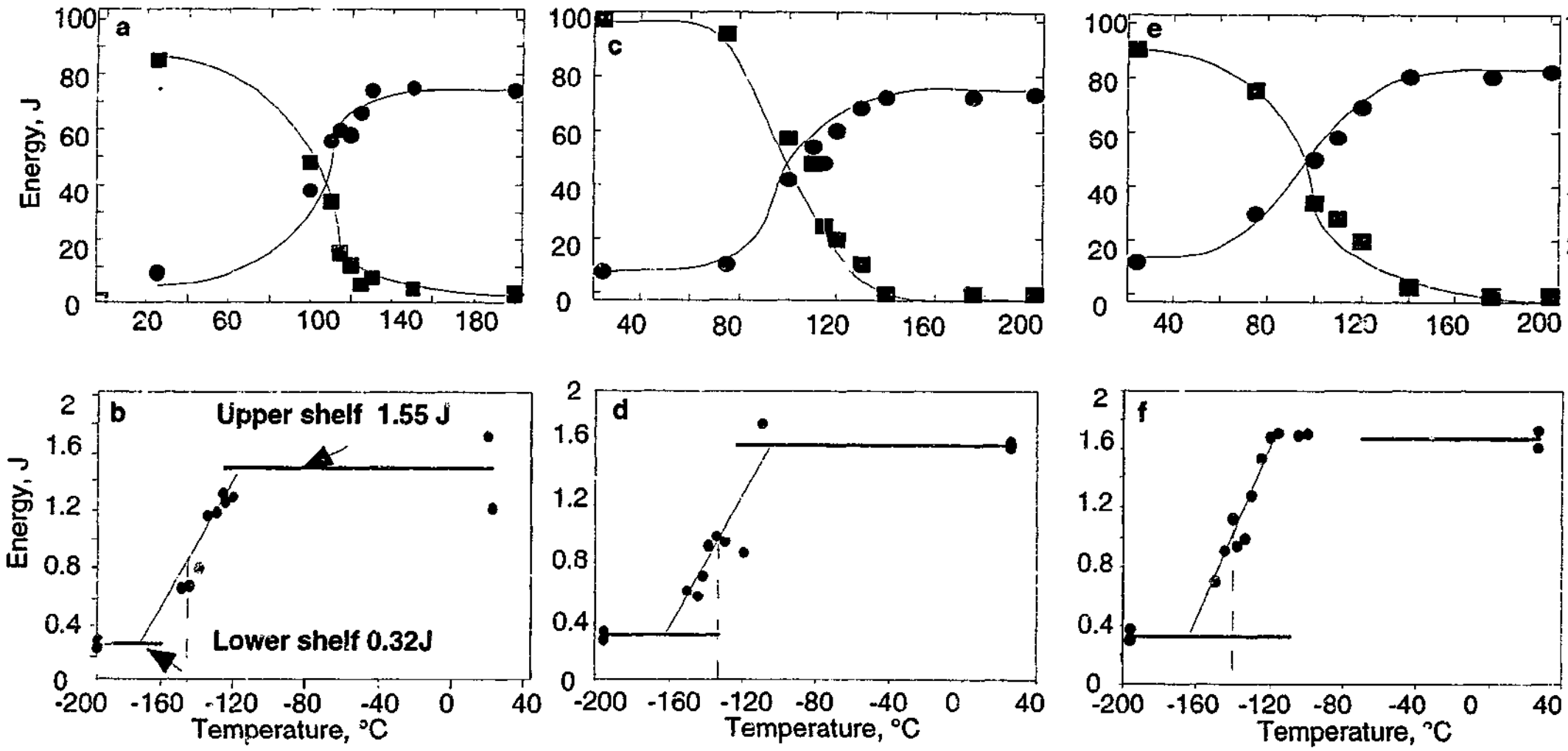

Figure 5.3 CVN Testing and corresponding SPT data for stage 1 (a) and (b), stage 3 (c and d) and stage 12 (e and f) in the de-embrittled condition

5.3.3 Re-Embrittled Material

The CVN and SPT results from the material in the re-embrittled condition are compiled in Fig. 5.5. The impact data presented here includes the results obtained for stage 3 and 12 only. Stage 1 was not subjected to the re-embrittled heat treatment since re-embrittling this stage represented little interest in studying the extremes of embrittlement. These were stages 3 and 12 yielding the highest and the lowest FATT in the initial screening tests, as described in Chapter 4, and also in this chapter (see section 5.3.1).

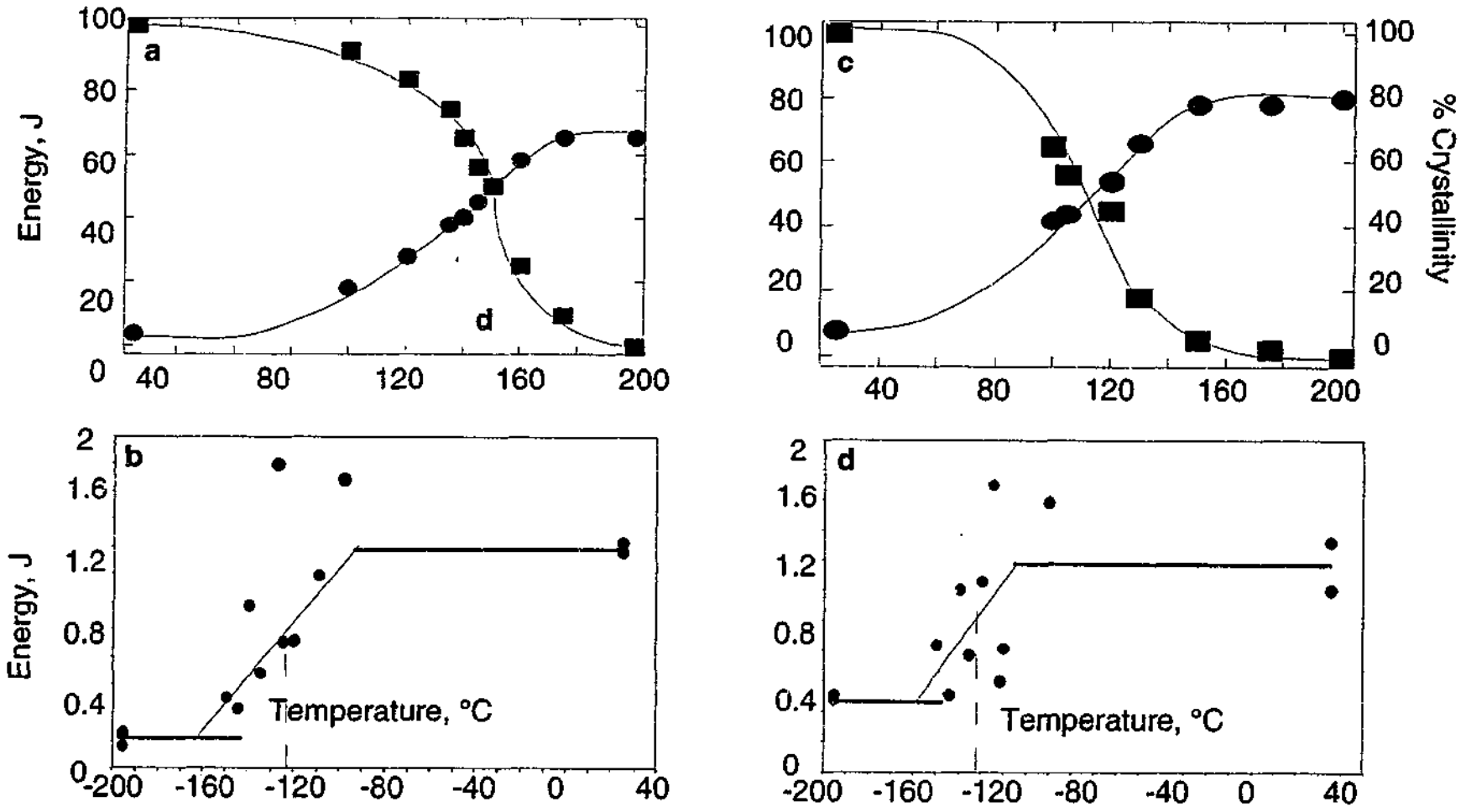

Figure 5.5 CVN Testing and corresponding SPT data for stage , stage 3 (a and d) and stage as (c and d) in the re-embrittled condition.

5.4 Fracture Toughness

Table 5.2 presents the experimental results of K_{Ic} fracture toughness measured at room temperature for ex-service, de-embrittled and re-embrittled samples of stages 1, 3 and 12 Appendix C describes the substantial data processing to calculate K_{Ic} from the load-displacement curves. All tests were valid according to the ASTM E 399-90.

Table 5.2 Summary of K_{Ic} Fracture toughness results

Condition	*Stage*	K_{Ic}, $MPa.m^{1/2}$
SE	1	35.8
SE	3	30
SE	12	49
DE	1	57
DE	3	55.5
DE	12	59
RE	3	52
RE	12	53

SE-service-exposed
DE-de-embrittled
RE-re-embrittled

Table 5.2 illustrates a change in fracture toughness values depending on the rotor operating temperature and material condition. The increase of K_{Ic} is clear in the rotor material in the service-exposed condition between the values of stage 3 (the most embrittled stage) and stage 12 (the nominally unmbtrittled stage). The result for stage 1 is in between the two extremes. The same trend is evident for the de-embrittled condition. The results for re-embrittled material do not appear changed from those of the de-embrittled, rendering the re-embrittling heat treatment ineffective.

5.5 Discussion

5.5.1 Impact Energy Correlations

Effect of the Exposure Temperature on the FATT and SPTT

Figure 5.1 details the FATT and SPTT results for the service-exposed rotor material. It is apparent from Fig. 5.1 that stage 3 (FATT = 150 °C and SPTT = -120 °C) represents the most embrittled case for this rotor. Moreover, the FATT value exceeds the ASTM recommended figure of 120 °C for rotors of this generation (ASTM A 470, Viswanathan and Jaffe, 1983). Similarly, the SPTT value recorded is the highest among the set of SPTTs for this condition. It should be noted that SPTT are shifted to much lower temperatures due to the specimen geometry and the slow strain rates involved in the deformation and rupture of the specimen during the SPT. A change in the strain rate causes a large effect on the transition temperature. As the strain rate increases, the yield strength increases and thereby increases the plastic stress intensification within the specimens (Baik, *et al.*, 1986). It was shown by Baik *et al.*, 1986 that a hunderedfold increase of the displacement rate leads to 20 % increase of the transition temperature. Therefore the higher strain rates promote brittle cracking over a wider temperature range (Baik *et al.*, 1986, Ha and Fleury, 1998 B).

The FATT value reported for stage 1 (the point of steam inlet) is 125 °C which is almost within the limit prescribed by ASTM. However the FATT of stage 12 (operating temperature 350 °C) is 100 °C which suggests that this stage had suffered virtually no embrittlement and is essentially an example of the "virgin" material (Bulloch, 1994).

The operating temperature of stage 3 in the HP section of the rotor is 525 °C. It is noteworthy that the range of temperatures within which the mechanism of temper embrittlement operates is 350-540 °C (Viswanathan, 1989). Thus, this stage becomes susceptible t temper embrittlement.

By closely examining the individual Charpy V-Notch Testing graphs for the three stages and separating the impact energy results into lower shelf, transition region and the upper shelf, it is possible to deduce that the lower shelf energy values appear to be the lowest for stage 3 (2 J) and so are the upper shelf values 72 J (as compared with stage 12 - 82 J).

While the lower shelf energy values for all three stages are approximately the same the transition region of a small punch curve is of interest. For stages 1 and 12 the transition starts as early as -160 °C. For stage 3 it does not to commence until ~-130 °C. Thus, the small punch test results are consistent with the CVN results and emphasize that stage 3 is the most embrittled stage of this rotor.

SPT-CVN Correlation

Table 5.3 Summary of correlated results between SPTT and FATT

Stage	*Condition*	*CVN FATT, ° C*	*SPTT, ° C*	*Predicted FATT from SPT using Cr-Mo-V correlation, ° C*
1	SE	125	-133	120.3
3	SE	150	-120	153.2
12	SE	100	-145	89.8
1	DE	100	-148	82.2
3	DE	110	-135	115.2
12	DE	95	-145	89.8
3	RE	145	-125	140.6
12	RE	95	-132	122.8

$$FATT\ (^{\circ}C) = 457.61 + 2.536\ T_{SP}\ (^{\circ}C) \qquad \text{Equation 5.1}$$

The Cr-Mo-V correlation approach method (Equation 5.1) that was applied here to derive the CVN-SPT correlations includes 17 C and D grade rotors with the 90% confidence interval of ±28 °C (Foulds and Viswanathan , 1994). Table 5.3 details the derived values of FATT in column 4. All predicted values of the FATT using small punch test are with the confidence limit approach. The de-embrittling heat treatment seemed to decrease CVN FATT and SPTT for all three locations, thus supporting the use of the heat treatment to remove the in-service incurred embrittlement.

With a few exceptions, the relationship between the experimentally measured and predicted FATT values is ±10 °C. The categories that do not fit the above temperature range are:

- stage 12 service-exposed
- stage 1 de-embrittled
- stage 12 re-embrittled.

These shall now be considered case by case. In case of the stage 12 SE, the discrepancy is 1 °C. The 18 °C variation in the stage 1 de-embrittled suggests that small punch test specimens were more sensitive to the de-embrittling heat treatment. Thus the correlations based on the small punch energy values yielded the FATT values of 82.2 °C, which seems to fit the experimental data better than the FATT actually measured form Charpy V-Notch test. The experimental difficulties with the re-embrittled heat treatment might have causesd those inconsistencies.

The brittle character of the fracture surface in Fig. 5.2 (d) represents the room temperature fracture appearance for these rotors. These images of brittle failure and the FATT values reported in Fig. 5.2 are of some concern, because of the similarity in age and composition of many in-service rotor steels.

The evolution of the small small punch test fracture energy results depending on the testing temperature is shown in Fig. 5.6.

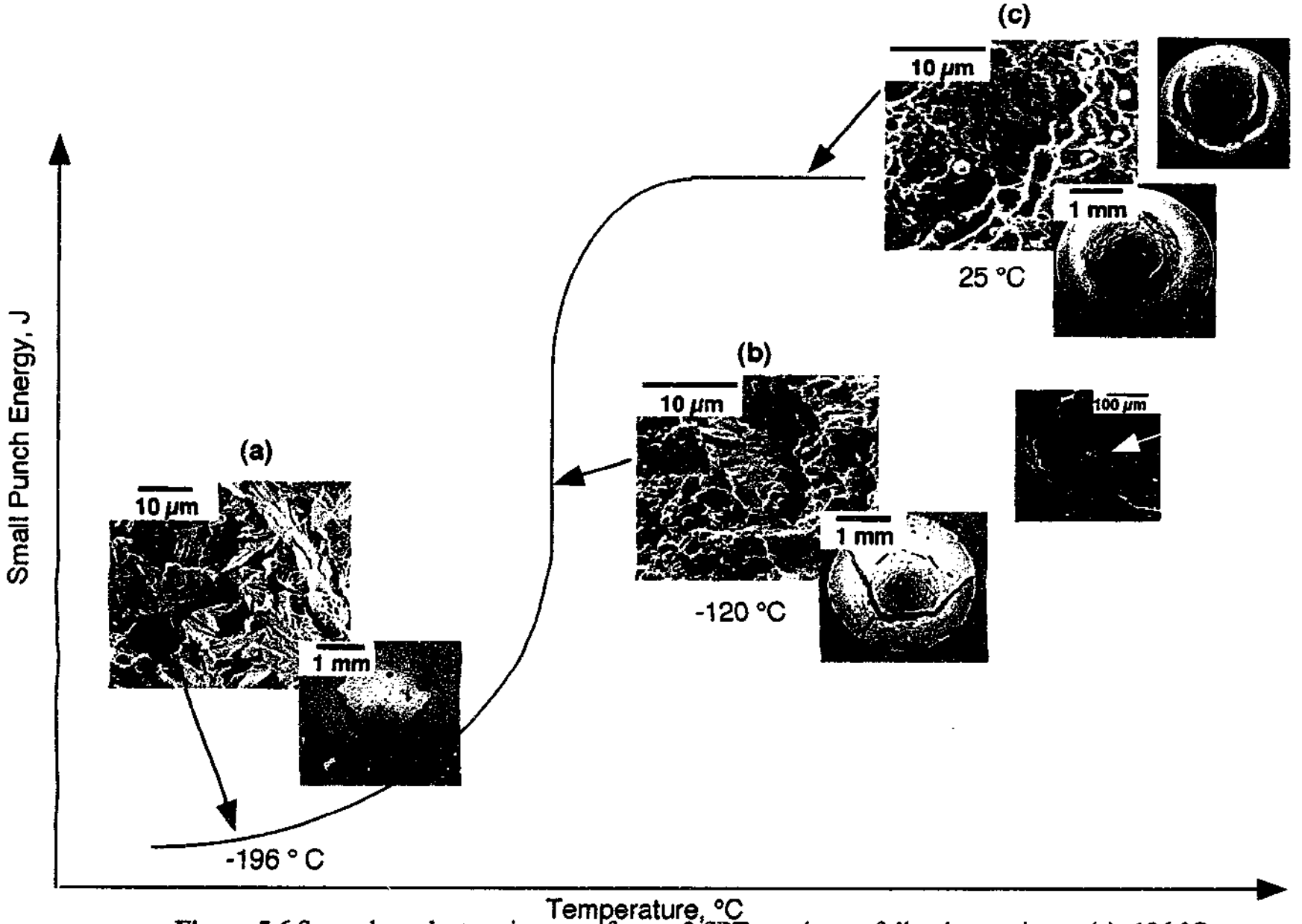

Figure 5.6 Secondary electron images of stage 3 SPT specimens following testing at (a) -196 °C indicating fulyl brittle failure mode, high and low (top view) magnifications, (b) -120 °C - transition temperature, showing a mixed fracture mode high and low (top view) magnifications, to the right is an image of the crack intitiation and (c) 25 ° C indicating a fully ductile appearance high and low (top view) magnifications, to the right is top view of the SPT specimen with the ball punch

As was explained in section 5.5.1 the transition temperature is shifted to much lower temperatures in the SPT. That is why full ductile fracture occurs at 25 °C while the same type of fracture happens at 200 °C in the case of CVN tests. A high magnification image is shown in Fig. 5.6(a) of mixed intergranular and transgranular mode while the lower magnification inset demonstrates the top view of the tested specimen with the fully brittle failure clearly evident. In the lower temperature range, cracks were initiated closer to the center of the specimen, and followed a straight and narrow propagation path. The resulting fracture surface exhibit transgranular cleavages.

A microvoid coalescence combined with the river patterns characteristic of brittle fracture are the intertwined features of this high magnification image of Fig.5.6 (b). The first low magnification inset shows a crack initiation while the second demonstrates the top view of the specimen and the evidence of the commencement of membrane stretching (arrowed). When the temperature is increasing, more plasticity is involved in the deformation, and this results in a modified crack initiation and propagation mechanisms (Ha and Fleury, 1998B).

The correlation between the CVN FATT and SPTT for three conditions of the rotor steel is depicted graphically in Fig. 5.7. The SPTT vs CVN FATT data by Viswanathan, is also presented in the figure in order to compare the experimental data with the results collected for 17 D grade rotors (Viswanathan, 1994). It is clear that the slopes for the linear fits are different for all three cases of the rotor material studied here (no slope is shown for the de-embrittled category, the explanation ensues). In the case of service-exposed steel the slope is similar to that obtained by Viswanathan and other researchers for ex-service material. The de-embrittled condition reveals virtually no change or trends in the SPTT-FATT correlation, thus no slope on the graph. This is

consistent with the idea of this heat treatment: to remove all the embrittlement, incurred in service and to return the material to a nominally pre-service state. The re-embrittled condition represents an anomalous case. While the increase for the SPTT and FATT for the service-exposed rotor material is quite gradual, the rise for the re-embrittled plot is sharp and does not appear to follow the regression described by Viswanathan for SPT This may be attributed to the difficulties associated with the re-embrittling heat treatment since this heat treatment may require up to 20,000 hours (Viswanathan,1989) of isothermal exposure in order to simulate the service performance. In this instance, the FATTs and corresponding SPTTs indicate that it was only possible to re-embrittle the rotor to the service-exposed FATT. Much longer heat treatment are possibly needed to bring it to the maximum embrittlement level (Shaw, 1981).

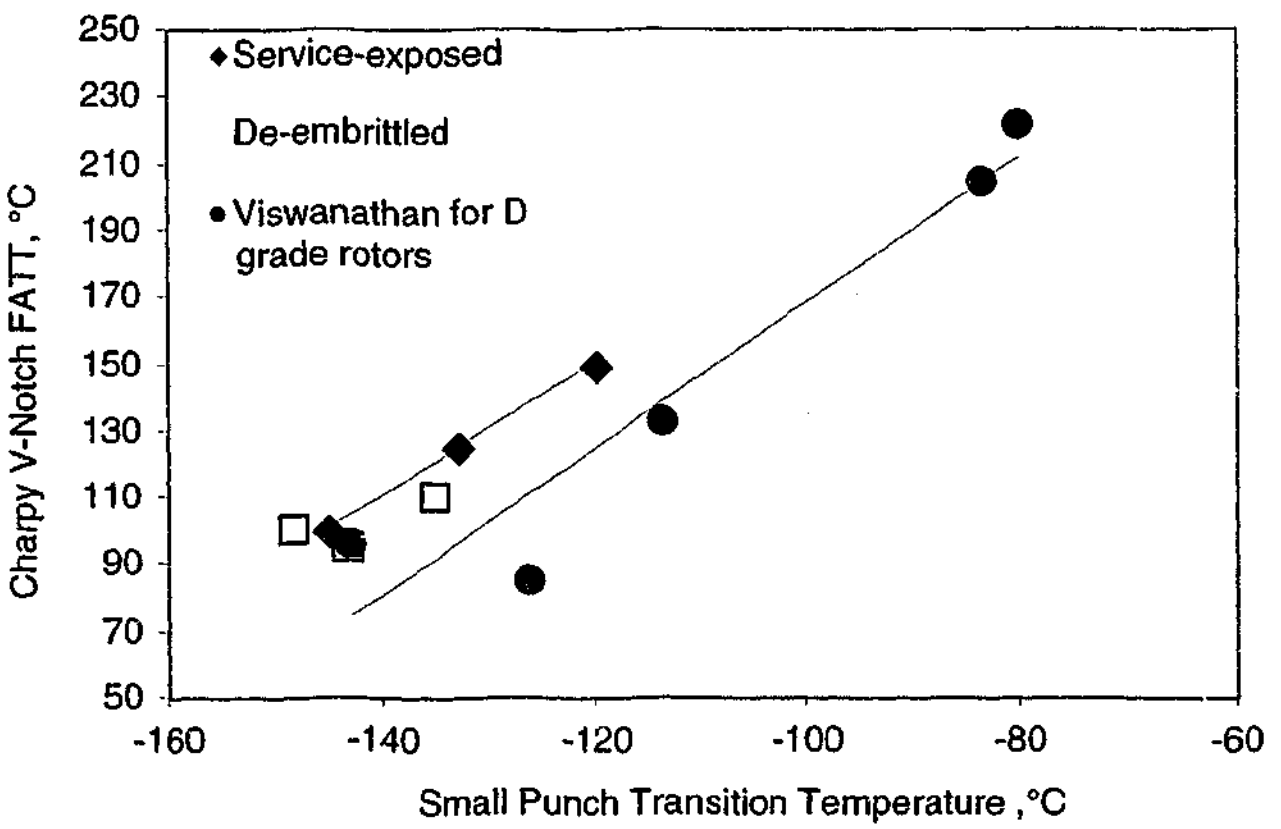

Figure 5.7 SPT-CVN correlation.

When analysing service-exposed and de-embrittled conditions, a shift in FATT of 50 °C has been measured between stage 3 service-exposed and stage 12 service-exposed, demonstrating the influence of material degradation in service due to the combination of high pressure and high temperature. However, this value of transition temperature shift obtained from SPT is lower (25 ° C) than the FATT shift determined from Charpy test on identical material. Thus the level of damage caused by temper embrittlement in aging rotor component appears more subtle to resolve from SPT in comparison to CVN. This constitutes a demerit when considering an application of this technique. This conclusion is consistent with the results by Ha and Fleury, 1998B.

5.5.2 Correlation Between Fracture Toughness and Impact Energy

Table 5.4 Selected published correlations relating CVN impact test data to K_{Ic}

Correlation title	*Equation*	*Region where applicable*	*Reference:*
Barsom- Rolfe	$K_{Ic}^2/E = 0.22\ (CVN)^{3/2}$	CVN energy between 3 and 82 J	(Roberts and Newton, 1981)
Sailors-Cortens	$K_{Ic} = 14.6\ (CVN)^{1/2}$	7-68 J	(Roberts and Newton, 1981)
Thorby- Ferguson	$K_{Ic} = 18.2\ (CVN)^{1/2}$	6-55 J	(Roberts and Newton, 1981)
Marandet-Sanz	$K_{Ic}=20\ (CVN)^{1/2}$	Lower shelf	(Roberts and Newton, 1981)
Begley-Logsdon	$K_{Ic\text{-}Ls}=0.093^* \sigma_{0.2}$ (F16)	Lower shelf	(Iwadate, *et al.*, 1994)
Jones, G.T.	$K_{Ic}=6600/60$-(T-FATT)	Lower shelf	(Jones, 1972)

In examining the adequacy of the fracture toughness correlations, the effect of data scatter, and the degree to which fracture toughness and the various alternative parameters can be related should be considered. A certain amount of scatter can be expected in the results of both alternative test methods and plane strain fracture toughness testing. This does not interfere with the use of the results. However, when the results of the two test methods are correlated, the scatter exhibited in the relationship is considerable. This scatter is due to the combined effects of the scatter of the two methods and the difficulties in developing such a relationship.

The experimental K_{Ic} values were compared in Fig. 5.8 to values derived by applying prediction methods discussed by other researchers (refer to Table 5.4). With the exception of Begley-Logsdon method all models appear to follow the same trend for all the conditions and locations of the rotor. Begley-Logsdon method takes into account the 0.2 % proof stress values, which in this work does not change depending on the condition and location, since temper embrittlement very rarely manifests itself in drastic changes of the tensile properties (Holtzmann, 1996).

The K_{Ic} predictions from the correlations proposed by other researchers (Table 5.4) are self-consistent. The experimental K_{Ic} values are also plotted as red squares in Fig.5.8 and results lie within the range of these correlations. The more steels incorporated into the correlation, the more conservative the predictions seem to be. For example, the Barsom-Rolfe method is the most conservative estimate of fracture toughness, since it relies on nine steels including rotor steels.

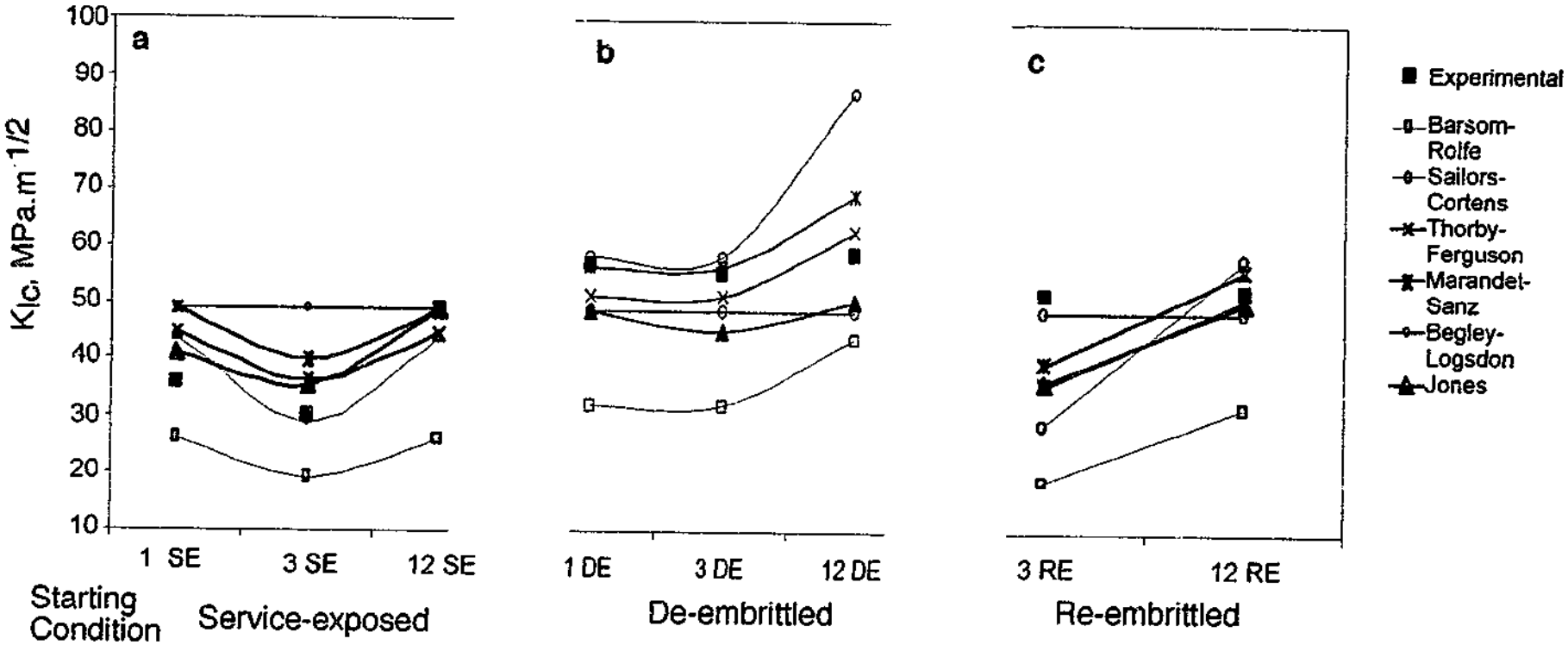

Figure 5.8 Summary of correlations for the three conditions of rotor steel: (a) service-exposed, (b) de-embrittled and (c) re-embrittled

The first five correlation methods listed in Table 5.4 are of the type whereby the prediction is based on a single LSE/USE Charpy value. The last method by Jones, 1972 incorporates the FATT values rather than an individual CVN value at corresponding temperature. This method is also called the excess temperature approach. Values predicted by Jones method appear to be closest in proximity with the experimental values obtained for this rotor. The use of FATT as a correlation variable is particularly useful since equipment manufacturers generally possess the records of the pre-service FATT. The use of the Jones expression is further warranted by the use of the lower-bound K_{Ic} values for Cr-Mo-V steels since these are the values that were measured in this work, i.e. room temperature K_{Ic} values.

As mentioned above, all correlation approaches show similar trends for each category of material condition. However, those trends are different between the service-exposed, Fig. 5.8(a), de-embrittled Fig. 5.8(b) and re-embrittled, Fig. 5.8(c) materials. Whereas the tendencies in each correlation in Fig. 5.8(b) follow a pattern involving an increase in K_{Ic} for each condition 12 DE compared to condition 1 DE and 3 DE, the experimental results show little variation across the de-embrittled materials. This suggests that de-embrittlement returns the material to a single "reference" condition regardless of the location in the rotor. Furthermore, the Jones approach for the de-embrittled material based on the excess temperature (the test temperature minus the FATT) follows the same pattern as the experimental K_{Ic} values. This implies that the FATT might be a more appropriate correlation variable than a single lower shelf Charpy energy value.

Figure 5.8 (c) describes the behavior of the re-embrittled material. All correlation methods appear to be in agreement here: the increase in K_{Ic} is predicted by all

derivations except Begley-Logsdon for the reasons described earlier. However, the experimental K_{Ic} values are unchanged compared to Fig. 5.8 (b). It is suggested that are-embrittling heat treatment of much longer duration should be used in order to achieve a full embrittlement effect.

The overall shape of the fitness curves for all three conditions of the rotor are also noteworthy. In the service-exposed condition, the plot decreases at stage 3 and increase towards the coldest stage 12. The de-embrittled fit of experimental data and the prediction models are different, as described above. The predictions tend to rise continuously while the experimental values remain the same for all locations of the rotor. Contrary to the experimentally measured values, the re-embrittled predicted values increase as predicted by other researchers which is consistent with the assumption made earlier in this chapter that stage 3 is the most embrittled stage in the rotor studied here.

Table 5.5 summarises correlation between CVN, SPT and K_{Ic}. The first column of Table 5.5 denotes the stage of the rotor (the precise locations where the specimens for mechanical testing were excised) while the second column provides the condition of the specimens. Column No.3 of the Table lists the FATT values as determined by Charpy V-Notch Testing. Similarly, column No.4 summarises the calculated SPTTs. Experimentally measured K_{Ic} fracture toughness results are presented in the fifth column of Table 5.7. Column No.6 lists the FATT values as predicted by Cr-Mo-V correlations (Equation 5.1). The Jones method (Jones, 1972) was used in triangular correlation, utilising the Foulds and Viswanathan SPTT-FATT relationship (Eq.5.1). The results of K_{Ic} values obtained using this method are summarised in the last column of Table 5.5.

Table 5.5 Fracture toughness Correlations between CVN, SPT and K_{Ic}.

Stage	*Condition*	*CVN FATT, ° C*	*SPTT, ° C*	*K_{Ic} MPa $m^{1/2}$*	*Predicted FATT from SPT using CrMoV correlation, ° C*	*K_{Ic} calculated from substitution into SPTT/CVN correlation*
1	SE	125	-133	35.8	120.3	42.5
3	SE	150	-120	30	153.2	35.1
12	SE	100	-145	49	89.8	52.8
1	DE	100	-148	57	82.2	56.3
3	DE	110	-135	55.5	115.2	43.9
12	DE	95	-145	59	89.8	50.8
3	RE	145	-125	52	140.6	37.6
12	RE	95	-132	53	122.8	41.8

5.5.3 Estimation of the critical crack size based on the small punch test

Calculation of Critical Crack Size from Experimental K_{Ic}

Using the K_{Ic} values obtained in this study, the calculation of the critical crack size is possible. The fracture criterion based on fracture mechanics is expressed by equation (5.2) in terms of crack length *a*.

$$a \geq a_{cr} \qquad \text{Equation (5.2)}$$

a_{cr} is the critical crack size for brittle fracture, which is governed by the fracture toughness K_{Ic} and applied stress σ (Iwadate *et al.*, 1985).

$$a_{cr} = \frac{K^2{}_{Ic}Q}{1.21\pi\sigma^2} \qquad \text{Equation (5.3),}$$

where a_{cr} is the critical crack size for brittle fracture, K_{Ic} is the fracture toughness and σ is the applied stress and Q is the flaw shape parameter.

A typical loading of the HP-IP rotor illustrating the variation in applied stress and temperature is shown in Fig. 5.9 (after Viswanathan and Jaffee, 1983). It shows that the highest risk of brittle fracture occurs during the transient conditions. The authors based this figure on the data obtained from Galatin rotor which failed catastrophically due to temper embrittlement. As with the rotor in the present study, the Galatin rotor was also manufactured in 1950s and had the same nominal chemical composition and microstructure (Viswanathan and Jaffee, 1983). Thus it became possible to use the loading sequence and conditions of stress and temperature for the critical crack size calculations for the Australian rotor investigated here. To identify the points of maximum stress for each stage/location of the rotor, the respective FATTs were used. Consequently, the points of maximum stress to be used in future calculation of the critical crack size were 450, 520 and 350 MPa for stage 1, 3 and 12, respectively. The

flow shape parameter Q was calculated using the determination procedure and a a/2c vs Q curve described by Dieter (Dieter, 1996). The values of the critical crack size a_{cr} are presented in column 4 of the following Table 5.6.

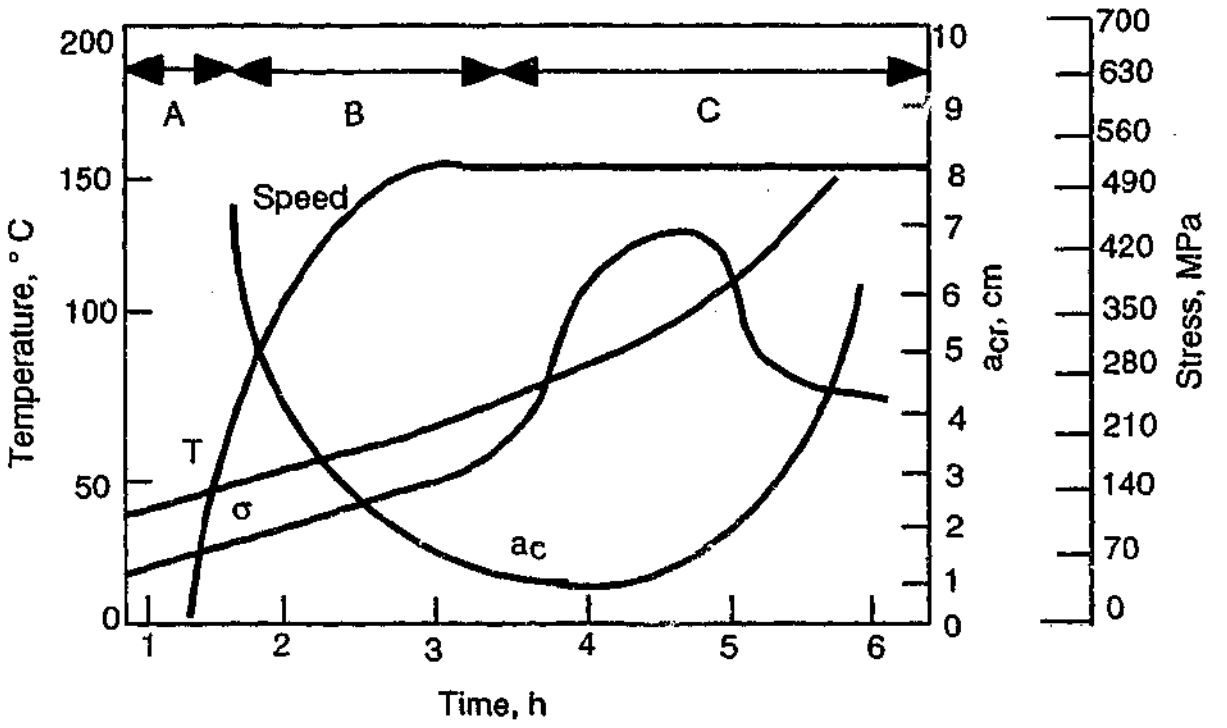

Figure 5.9 Illustration of cold-start sequence and associated variations in stress, temperature and critical crack size as functions of time from start (after Viswanathan and Jaffee, 1983).

Calculation of Critical Crack Size from SPT-Derived K_{Ic}

It is suggested to utilise the last column of Table 5.5 to calculate the critical crack size a_{cr} from the SPTT-derived K_{Ic} K_{IcSP}. Equation (5.4) them becomes:

$$a_{cr} = \frac{K^2_{IcSP} Q}{1.21\pi\sigma^2} \qquad \text{Equation (5.4)}$$

Table 5.6 summarises the critical crack size calculations. Column 1 of Table 5.6 denotes the stage/location of the rotor, column 2 describes the condition of the material. Column No. 3 presents the experimental K_{Ic} fracture toughness values. Column No. 4 reports the calculated critical crack size values, while the last column of tabulates the critical crack size values based upon the SPTT-K_{Ic} correlation.

Table 5.6 Summary of the actual critical crack sizes and SPT-correlated values

Stage	*Condition*	*K_{Ic}, MPa $m^{1/2}$*	*Critical crack size, a_{cr}, cm*	*Critical crack size, a_{cr}, mm based on the SPT values*
1	SE	35.8	1.33	1.88
3	SE	30	0.7	0.95
12	SE	49	4.12	4.8
1	DE	57	3.38	3.29
3	DE	55.5	2.4	1.5
12	DE	59	5.9	4.43
3	RE	52	2.1	1.09
12	RE	53	4.8	3

The comparison between the calculated critical crack size and the derived critical crack size is presented in Figure 5.10. A linear regression produced a correlation coefficient of 0.98 for the service-exposed rotor material. It is evident that a good agreement exists between the actual critical crack size and the derived remaining life assessment parameter based upon the SPT for all three conditions. Furthermore, the critical crack value obtained for stage 3, service-exposed (0.7 cm), coincides with the value given by Viswanathan in his analysis of the Galatin rotor (Viswanathan and Jaffe, 1983). However, the conservatism of the SPT-based a_{cr} derivation is of some concern, since these values are consistently higher than the experimental data.

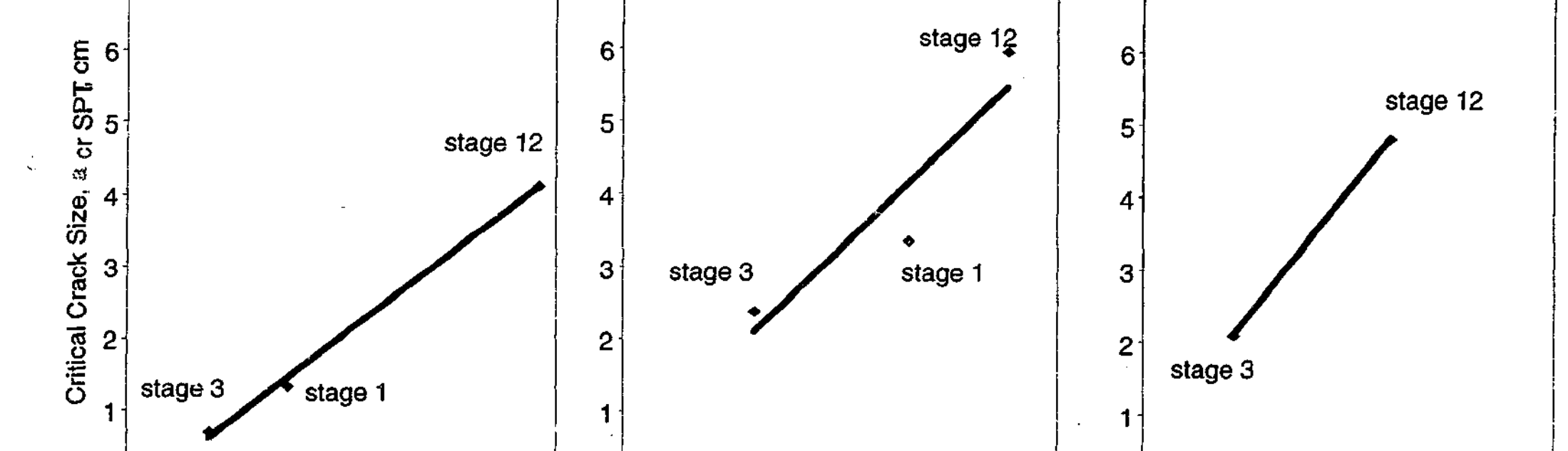

Figure 5.10 Correlations Between the actual and SPT-predicted crittical crack size

The fracture toughness K_{Ic} was related to FATT via empirical correlation (Jones, 1972) where the degree of uncertainty is unknown, and therefore, the correlation of lower-bound K_{Ic} estimated from excess temperature is interpreted conservatively (Foulds *et al*, 1991 and Viswanathan, 2001). In addition a K_{Ic} is a conservative estimation in its own right since it represents a lower limiting value of fracture toughness (ASTM E 399-90). So, there is a considerable number of safety factors already incorporated into these estimations.

By combining the results of the linear regression from all three conditions but keeping the constant from the service-exposed regression to maintain the degree of conservatism, a relationship emerges between the actual a_{cr} and the SPT-predicted a_{cr}:

$$a_{cr} = 1.16a_{crSPT} - 0.26 \qquad \text{(Equation 5.5)}$$

Correlation Approach vs Probabilistic Assessment and Finite Element Modeling Methods

The correlation procedure described here may be compared to the existing methodologies to predict fracture toughness.

The probabilistic assessment is based upon the theory that mechanical property measurements of materials under conditions when they behave in a brittle manner show a high degree of variability that requires statistical analysis (Dieter, 1992). An important aspect of the statistical behavior is that the strength of brittle solids demonstrates a pronounced size effect such that the strength decreases with increasing size or volume of the specimen. Moreover, it is more logical to expect a high frequency of occurrence of small cracks with a much lower number of large crack (Dieter, 1992).

The most generally applicable frequency distribution in fracture problems is the Weibull distribution (Weibull, 1952). Knott (1998) reviewed the probabilistic approaches to fracture toughness in pressure-vessel steels, which use microstructural indicators. The paper represents a major contribution to micro-mechanistic models of brittle fracture in search of "ideal" fracture toughness distributions (Knott, 1998). The approach relies an RKR model (Rice, Knott and Ritchie, 1973) that predicts the variation of K_{Ic} with temperature from known values of fracture stress σ_F and yield stress σ_Y, which is a function of temperature T.

Mao *et al.* (1991) derived a direct relationship between SPT and J_{Ic}/K_{Ic} fracture toughness. This approach is based on the estimation or measurement of equivalent fracture strain ε_{qf}.

$$K_{Ic} = C[\sigma_{f(SP)}]^{2/3} \qquad \text{(Equation 5.6)},$$

where C is an empirically determined constant. However, this method is known to have certain limitations. Firstly, the empirical constant is not expected to be material-dependent, as it might depend on the critical distance in the cleavage fracture stress RKR model (Foulds *et al.*, 1993). Secondly, and most importantly, the small punch fracture stress is empirically estimated form the peak load in the small punch load-displacement curve as described in Chapter 3. This assumes that fracture occurs at the maximum load. However, during the SPT experiments it was observed in the current study and in previous investigations (Foulds *et al.*, 1991; Fleury, 1998) that even when material behaves in a classically brittle fashion in CVN testing, it often does not exhibit a macroscopically brittle character when loaded in the small punch mode. Moreover, prediction of large-specimen brittle behavior cannot be made simply by macroscopic indications in the SPT. The maximum load-based estimation of fracture stress can therefore be in error (Foulds *et al.*, 1991). The approach employing a finite element

analysis (FEA) intends to overcome the empiricism and potential inaccuracies associated with the current prediction practices. It relates the unifying strain- and stress-based estimation of the fracture criterion by using an energy-based criterion, a purely analytical-based interpretation of the small punch load-displacement curve and the critical experimental aspect of identifying the point (temporal and spatial) of fracture initiation during the test. The three methods discussed above are compared in Table 5.7

Table 5.7 Comparison between different methods to predict fracture toughness

Method	*Merits*	*Demerits*
Probabilistic assessment	• Does not require material sampling • Complete models are available for a variety of pressure vessel steels	• Critical distance X is statistically-averaged • Initial frequency distribution is not known or cannot be sampled directly • Difficulties associated with extrapolation of low fracture probabilities
FEA	• Material-independent • Based on the analytical interpretation of the test results • Requires no prior knowledge of mechanical properties • Reduced prediction uncertainty	• Requires a database on materials with known stress-strain behavior or via a series of FEA of SPT • Difficulties associated with estimation of average distance, crack-tip strain energy averaging • Identification of crack initiation
Correlation-based	• Can be used directly in the RLA • Does not require large amounts of material • Can be used in conjunction with the existing miniature removal systems • Based on the actual fracture toughness data	• Material specific • Semi-non destructive • Requires a minor disruption of the plant operation • Degree of conservatism requires some refinement

5.6 Concluding Remarks

The key conclusions from CVN, SPT and K_{Ic} testing of an ex-service, de-embrittled and re-embrittled rotor steel are as follows:

- impact testing of service-exposed rotor material has shown that the rotor was in fact embrittled in several locations with FATT values as high as 150 °C in the case of stage 3.
- SPT and CVN property correlation yielded an excellent agreement and improved the cut-off level of the "Cr-Mo-V correlation" approach from ±28 °C to ±10 °C.
- experimental K_{Ic} fracture toughness results are consistent with the empirical estimates of K_{Ic} according to prediction methodologies described in literature
- critical crack size a_{cr} for the most embrittled rotor location was calculated and compared to that of a rotor that catastrophically failed due to embrittlement (0.7 cm). The coincidence of both values is of concern since many rotors similar to the one studied here remain in service. The critical crack sizes a_{cr} for several rotor locations was successfully correlated to the predicted a_{cr} based on SPT. This result supports the use of the SPT as a possible remaining life assessment tool.
- the present correlation method was compared to the probabilistic assessment and FEA method and the advantages/disadvantages of both methods outlined for the three methods. The present method's distinctions include miniaturisation, ease of testing and the fact that is based on the actual fracture toughness compilation. The main disadvantages of the proposed method include the prediction uncertainty and the fact that it's material specific.

Chapter 6 Microscopy and Microanalysis

This chapter presents the results of microstructural investigations of the rotor steel in the service-exposed condition. Attempts to characterise the temper embrittlement phenomenon with the aid of microstructural indicators are also presented and discussed.

6.1 Introduction

The main metallurgical problems involved in large rotor forgings are associated with the quality of ingots from which the forgings are made. The typical forging size in the 1960s and 70s, when most of the presently operating rotors were fabricated, was 200-240 t which requires ingots weighing between 350-500 t. Hence, casting defects such as coring, segregation and nonmetallic inclusions are difficult to avoid. Microstructural and microchemical heterogeneities also arise due to variations in cooling rate during fabrication. These types of processing induced variations in microstructure, microchemistry and properties have been reported for very early generation rotors, some of which are still in service, although less of this work has been performed on HP-IP rotors of the same generation as that studied here. The degradation of the properties owing to microstructural and microchemical variation during manufacturing in conjunction with the various temperature and stress regimes across the rotor due to time in exploitation exposure is complex. Microstructural modification during service may involve carbide coarsening, transformation, spheroidization, or secondary precipitation, all of which affect mechanical properties (Mitchell and Moss, 1998; Swaminathan, *et al.*,1994; Cheruvu and Malmfeldt,1990; Norton,1969).

In addition to the above factors, which relate to the fabrication and service of turbine rotors, the complex physical metallurgy of 1Cr-1Mo-0.25V (wt. %) steels also contributes to the formidable complexity of remaining life assessment of these components. Careful control of heat treatment and composition during fabrication produces a predominantly bainitic matrix. The combined presence of Fe, Cr, Mo and V results in the precipitation of as many as six carbide phases, each of which exhibits a

range of solid solubility for the metallic and interstitial elements (Senior, 1988). In an extensive metallurgical examination of a number of turbine rotors, Mitchell and Moss (1998) have detailed the compositional and morphological characteristics of the MC, M_2C, M_3C, $M_{23}C_6$, M_7C_3 and M_6C phases, observed in rotors having similar compositions to that studied here. By examining a number of rotors at various stages of service-life, they were able to follow the precipitate composition as a function of $\sqrt{t}$ for notionally "hot" and "cold" rotor stages. In common with laboratory based studies, they observed a complex precipitation process, involving the formation of more stable carbides at the expense of the M_3C precipitate, which is the main second phase following fabrication.

The following chapter presents microstructural characterisation of an ex-service rotor, where variations in microstructure from stage-to-stage (due to differing operating temperatures) and rim-to-core (due to fabrication and service stress states) are being examined.

6.2 Effect of Service Temperature on the Microstructure

6.2.1 Core-to-Rim Variations

Although there is uncertainty over the specific pre-service heat treatment processing, a widely used European practice involves final austenitisation treatment at ~975 °C (1787 °F) followed by an oil quench and tempering at ~700 °C (1292 °F). This was then followed by air cooling or oil quenching.. The CCT diagram (Refer to Fig. 2.5, Chapter 2) indicates that this processing would produce a upper bainitic microstructure with little lower bainite and almost no martensite. For air cooled rotors, Fig. 2.5. suggests that there would be a higher tendency to form upper bainite than for oil quenched components

While selected stage-to-stage investigations were reported previously there have been relatively few studies of the processing induced heterogeneities in microstructure and/or microchemistry between the rotor core and rim.

The initial work was conducted on the coldest stage, stage 12, which operated at ~ 351 °C (refer Chapter 3: Rotor Operating Temperatures Module). The relatively low operating temperature of this stage offers the closest opportunity to examine the pre-service rotor microstructure. Moreover, this operating temperature is generally considered to be below the threshold where damage mechanisms such as creep, creep embrittlement or temper embrittlement are operative and previous chapter has indicated that this stage exhibits a higher fracture toughness than any other.

Microstructural Investigation

At magnifications below ~1000, little or no distinct differences were observed between the core and rim microstructures. A typical optical micrograph of the microstructure is provided in Fig. 6.1. Prior austenite grain boundaries are clearly visible and are indicative of a grain size of approximately 30-40 μm. Within the prior austenite grains is a predominantly upper bainite structure, with M_3C carbides decorating the prior austenite and interlath boundaries.

Figure 6.1 Optical micrograph from stage 12 of the Cr-Mo-V rotor steel.

Figure 6.2 provides bright field (BF) TEM images from carbon replicas of the core and rim regions. The general microstructures were similar, exhibiting mixed ferritic and bainitic regions and copious carbide precipitation. Most of these carbides were the M_3C phase. The overall carbide distribution in the core region was slightly denser than in the rim. Coarse, equiaxed $M_{23}C_6$ carbides were also observed in the core region (arrowed, Fig. 6.2(a)), although their absolute fraction was very small. Precipitation was apparent within the intra-lath bainitic region as well as at inter-lath boundaries. Figure 6.3 provides BF TEM images of the microstructure of both the core and rim regions of thin foils of stage 12. The images are not necessarily representative since obvious variations between the core and rim were not apparent. However, these images do convey the typical microstructures observed.

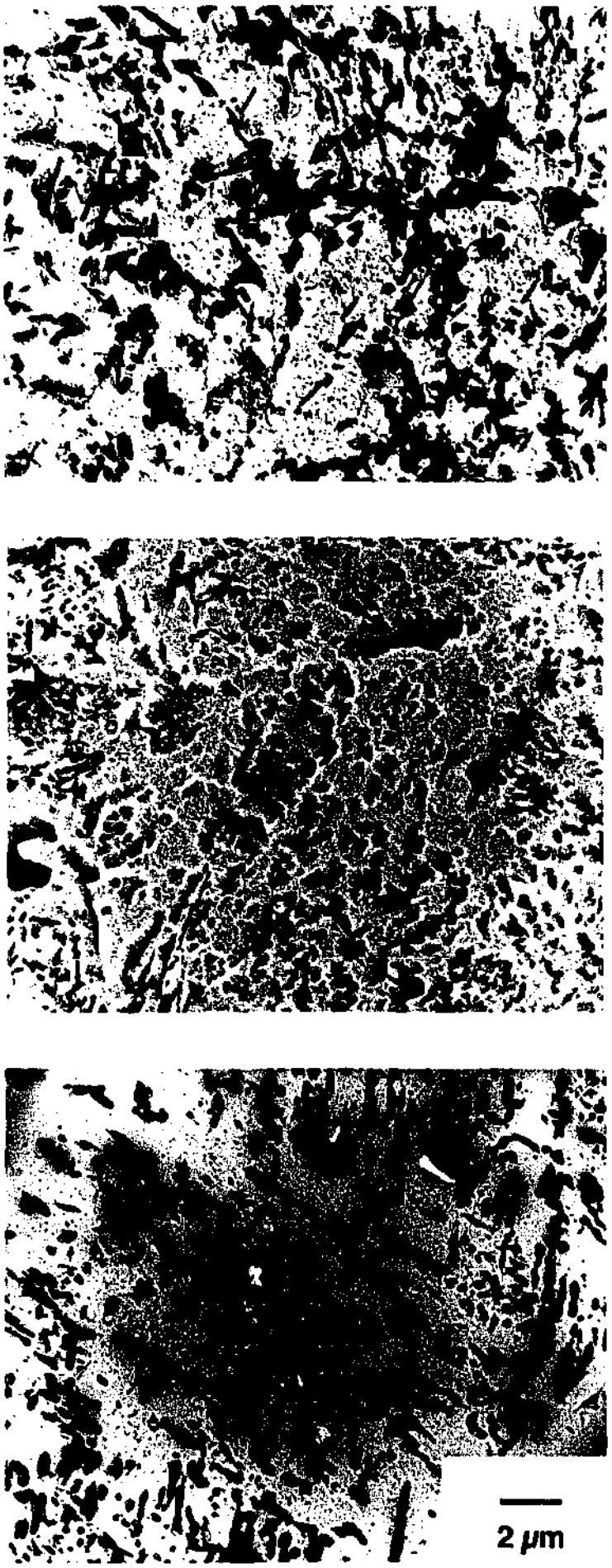

Figure 6.2 Typical microstructures of ex-service rotor steel (a) stage 1 (b) stage 3 and (c) stage 12.

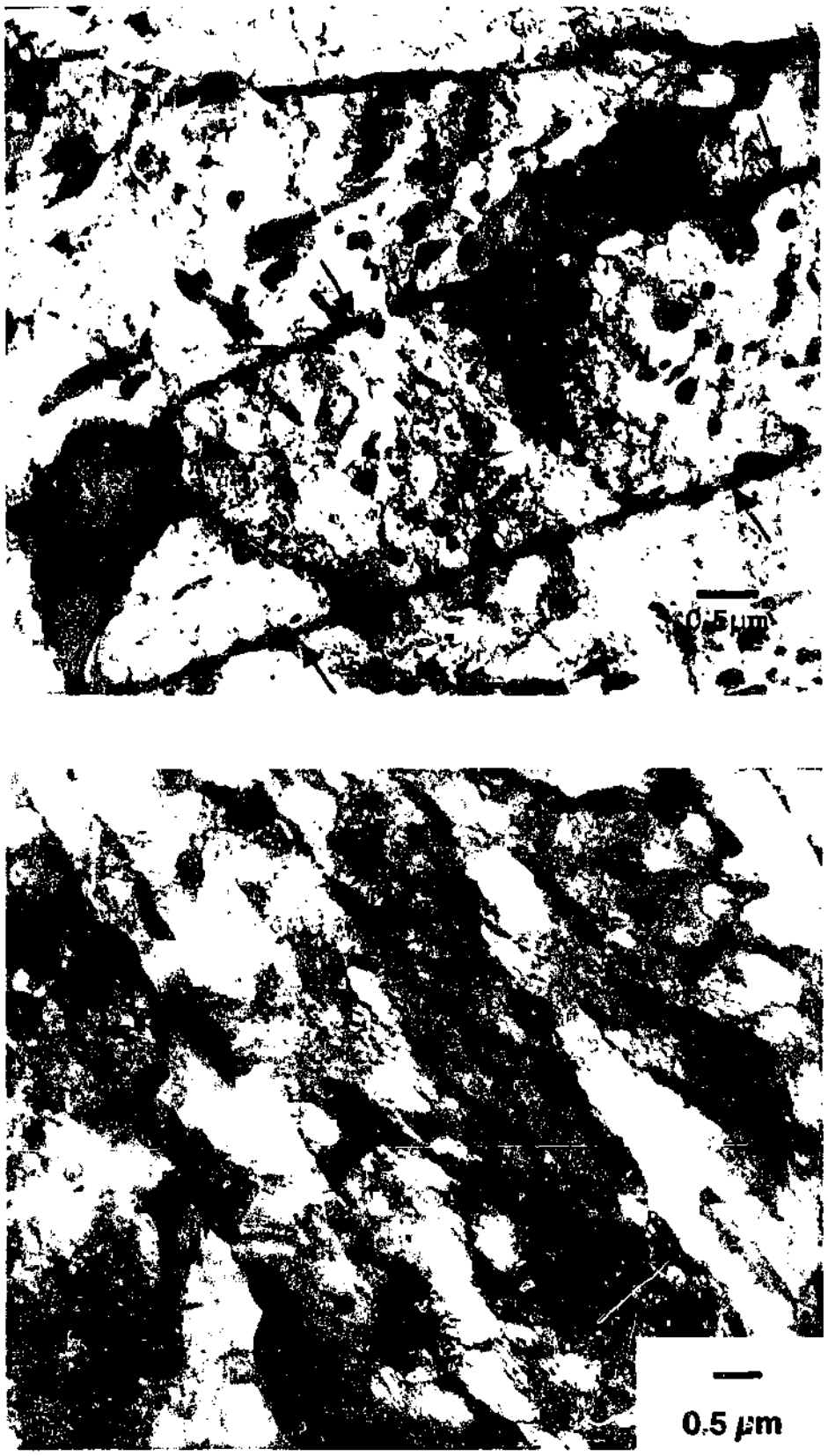

Figure 6.3 BF TEM images for (a) core and (b) rim regions. The arrows in (a) identify prior twin interfaces inside prior austenite grains.

6.3 Characterisation of Embrittlement Based on the Carbide Chemistry

Figure 6.4 (a,b) provides bright field (BF) TEM images of the extraction replicas taken from rotor stages 12, 3 and 1, respectively. Occasional ferritic regions were observed in the TEM as precipitate free regions. The microstructural results in Fig. 6.4(a) (stage 12) show the presence of carbides ≤ 1 μm, which were mostly M_3C in the form of spheroids or lath. Also observed were the distinctive H-type precipitates (arrowed) which possess an MC cuboidal core upon which M_2C needles nucleate (Collins, 1978). A magnified view of H-type carbides in stage 1 is provided in Fig.6.5.

The carbide growth along the grain boundary or inside of the grains was more evident for stage 1 and 3. However, carbides with a very large size up to ~10μm were more frequently found in stage 3. An example of such carbide is shown in Fig.6.6.

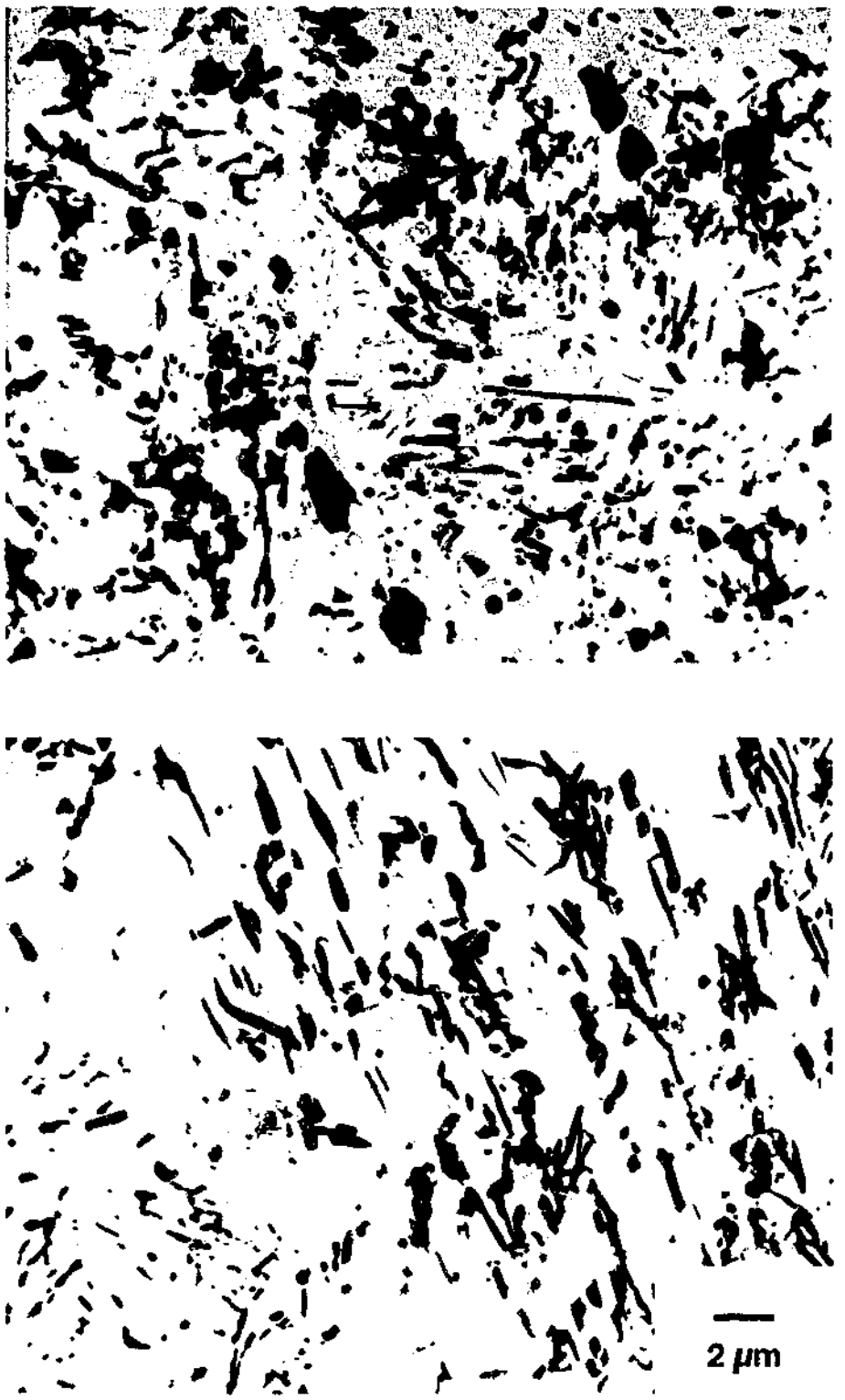

Figure 6.4 TEM images from carbon extraction replications of stage 12 of the rotor steel (a) core and (b) rim.

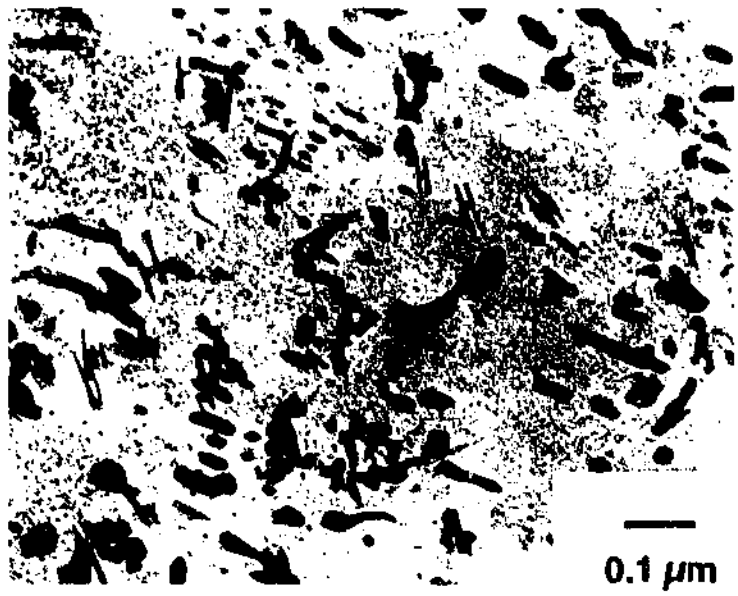

Figure 6.5 The secondary H-type carbides in stage 1 rotor steel.

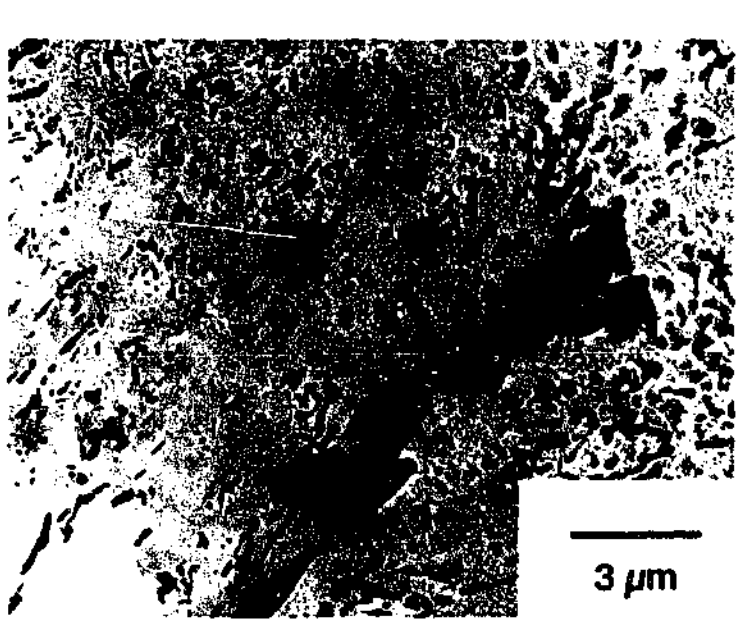

Figure 6.6 Large carbide due to carbide coarsening in stage 3 rotor steel

Figure 6.7 presents the elemental ratios within these precipitates, based on determinations of weight %, for Fe/Si, Fe/V, Fe/Cr, Fe/Mn and Fe/Mo. As seen in Fig. 6.4, the M_3C precipitates were either globular or lath-like and these forms were analysed randomly. The data shows a trend involving increased partitioning of solute such as Mo, Cr, V and Si for increased service temperature.

Table 6.1 summarises the results of localised EDXS analysis of the carbide precipitates. This data also suggested that Mn was slightly enriched in the matrix of the rim region. The tendency for a higher content of the elements Cr, Mo and Mn within the carbides of the rim, compared to the core is likely to be due to enrichment of M_3C carbides with these elements as the more thermodynamically stable compositions. This suggests that the rim sections operated slightly hotter than the core.

Table 6.1.Chemical concentrations of substitutional alloying elements in stage 12 (wt. %)

Stage	*Analysis*	*Fe*	*Cr*	*Mo*	*V*	*Mn*
12 (Core)	M_3C Carbide	79.9	14.0	4.6	0.2	1.2
12 (Rim)		75.4	15.7	7.5	0.1	1.3

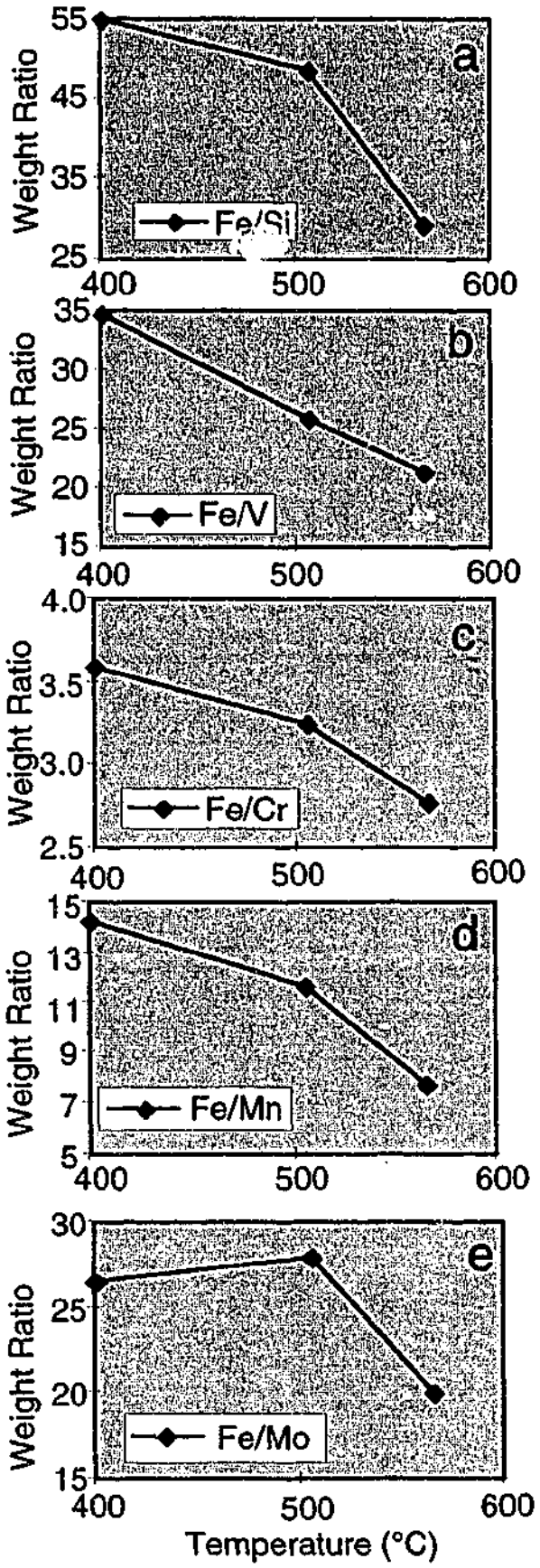

Figure 6.7. Compositional profiles showing the ratio of Fe and Si, V, Cr, Mn and Mo (by weight) as a function of service temperature. The data points represent stage 12 (350 °C), stage 3 (505 °C) and stage 1 (565 °C).

6.4 Characterisation of Embrittlement Based on Carbide Dimensions and Distributions.

To further examine the hardness and FATT variations recorded with thermal exposure history, an assessment of the carbide distribution was made using stereological techniques and image analysis from FEG SEM. Figure 6.8 contains high resolution FEG SEM micrographs of the material extracted from rotor disks/stages 1, 3 and 12.

Table 6.2 summarises the number of M_3C precipitates in the rotor stages 1,3, and 12 per unit volume as determined by stereological techniques

Table 6.2 Number of carbide particles per unit as calculated from image analysis of SEM images of the stages from different operating temperatures

Stage	*1*	*3*	*12*
No of particles (cm^{-2})	$2.77x10^{10}$	$2.41x10^{10}$	$19.8x10^{10}$

The volume fraction of the carbide particles decreased wit the operating temperature.

The information concerning morphology and distribution of the carbides combined with the microchemical information of these carbides could contribute to the search for microstructural indicators.

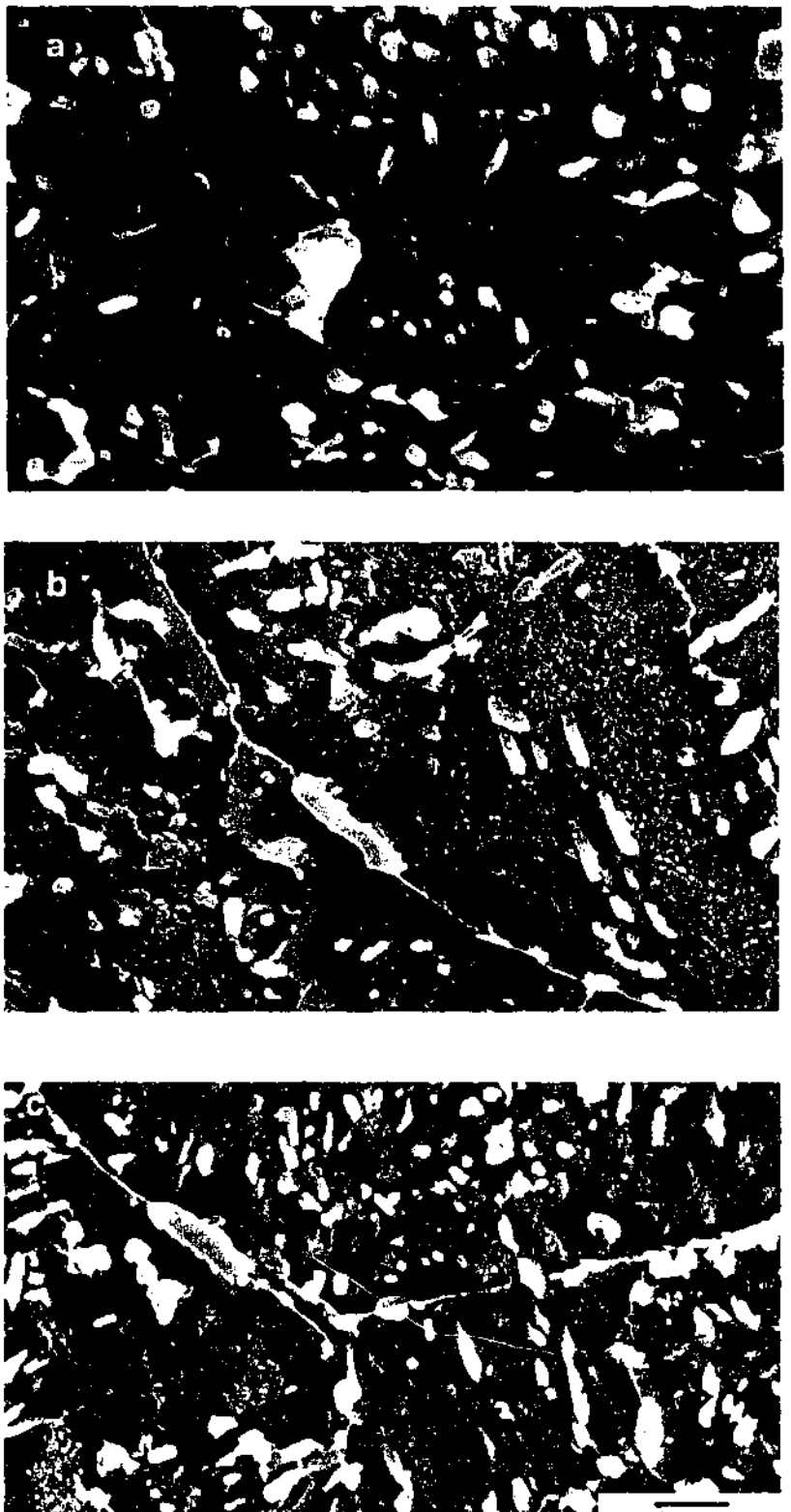

Figure 6.8 High resolution scanning electron microscopy images of (a) stage 1, (b) stage 3 and (c) stage 12 in the service-exposed condition.

6.5 Segregation of Phosphorus and Scavenging Effect of Molybdenum Using APFIM

The volume fraction of the matrix can be calculated from the chemical information of bulk, matrix and carbide. A summary of these results of this calculations are presented in Table 6.3. This calculation assumes that there is no phase other than the matrix and carbides.

Because of the low concentration of alloying elements in the matrix, it is difficult to acquire reliable data using EDXS analysis. In fact, the elements, such as P and S, and interstitials were eliminated from the analysis of mass balance due to detection difficulties in EDXS analyses. For these reasons, the chemical composition of the matrix was measured using 3DAP/FIM.

The first column of Table 6.3 defines an element that was subjected to analysis by the TEM, 3DAPFIM and bulk wet chemical analysis. Column No.2 lists the concentration of the element of interest in the matrix yielded by the 3DAPFIM. The results of the large area TEM analysis of the carbides are summarised in the next column. The results obtained from the wet chemical analysis are given in the column No.5 of the table. Lastly, column No. 6 contains the volume fraction of the matrix, calculated using: the microchemical information supplied by the TEM, concentration of the above elements in the matrix provided by the 3DAPFIM and the chemical composition of these elements in the bulk of the rotor material.

The volume fraction of the matrix estimated from the various analysis techniques for the different elements (except Mo) in the rotor steels are consistent with each other. This confirms that the other techniques applied were performed in systematic manner and their data are self-consistent.

Table 6.3. Concentration of alloying elements in matrix, carbide and bulk analysed by various techniques, and estimated volume fraction of matrix $F_{m,v}$ based upon the different elements for stage 3 rotor steel

Element	*Matrix, at %*	*Carbide, at %*	*Bulk, at %*	$F_{m,v}$
Fe	99.44	60.66	98.05	0.96
Cr	0.40	34.98	1.20	0.98
Mo	0.14	1.51	0.49	0.74
V	0.017	2.85	0.26	0.92
Total	100.00	100.00	100.00	

6.5 Preliminary APFIM Analysis on the Interface

The segregation of P into interfaces such as grain boundary is known to affect the embrittlement behaviour of Cr-Mo-V steels. Conventional analysis methods using EDXS present difficulties in reliability due to the limitation of beam size, detection efficiency issues and peak overlap between P and Mo. The 3DAP/FIM offers superior spatial resolution and was adopted for this analysis. The details of APFIM analysis are described elsewhere.

The FIM image for the rotor steel studied is shown in Fig. 6.9 The contrast difference between two phases is clear and makes further AP analysis unambiguous.

It was found that the dark right-hand-side area represented the ferritic matrix, whereas the bright contrast left hand side was the Mo-rich carbide. Although it is difficult to

identify this carbide based upon crystallography due to the complexity of image, this carbide is assumed to be M_2C type carbide since M_2C is known to be Mo-rich carbide.

A 3DAP analysis was performed across the interfacial region. The reconstruction of a ~ 30 x 30 x 30 nm three-dimensional atom map after atom probe analysis is shown in Fig. 6.10.

Figure 6.9 FIM image of stage 3 rotor steel. This image was obtained with Ne as the imaging gas at a voltage of 11.5 kV and temperature of 60 K.

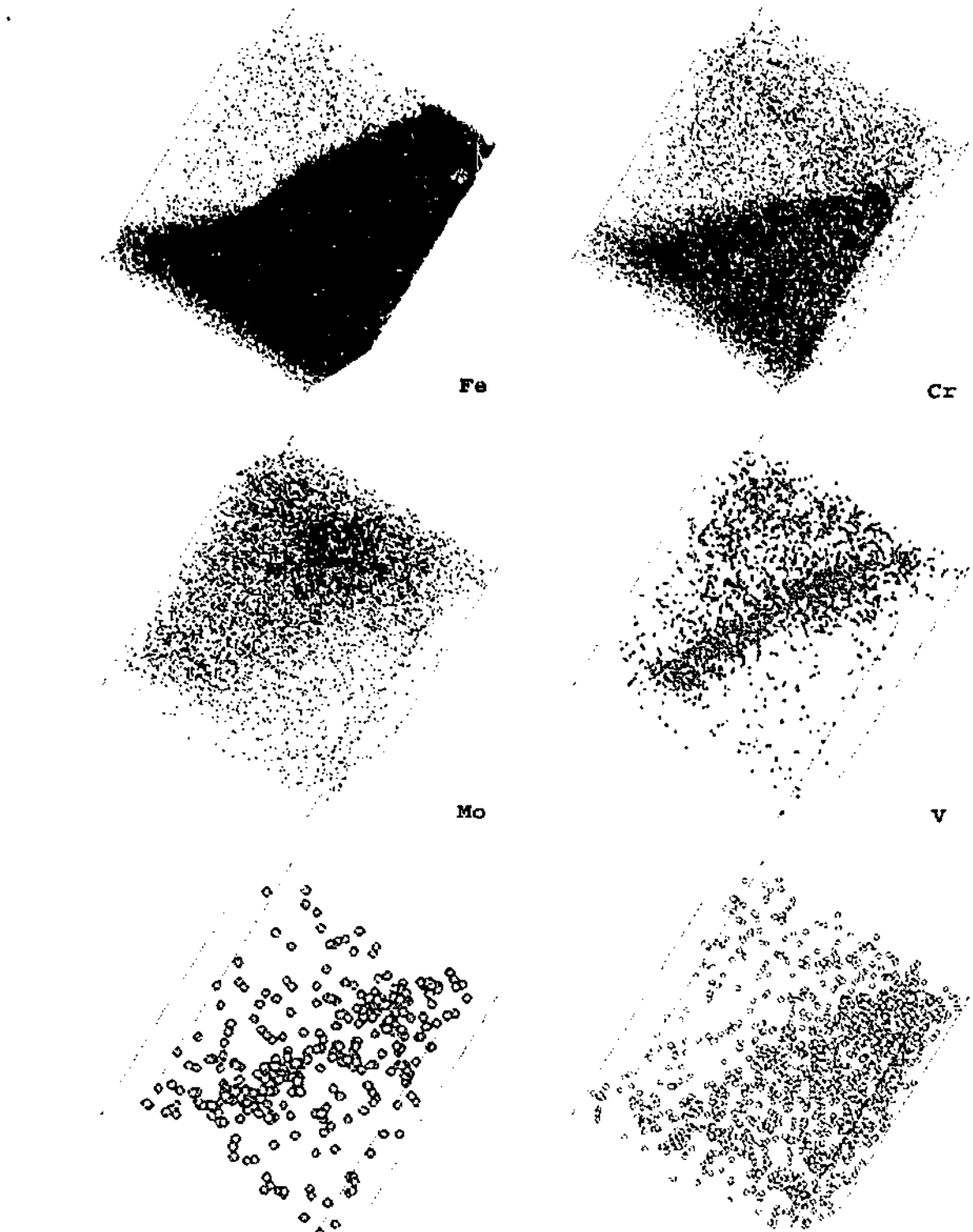

Figure 6.10 3D atom map of the alloying elements around interfaces for stage 3 rotor steel. The region shown is approximately 30x30x30 nm. Each dot represents an individual atom.

6.6 Discussion

6.6.1 General Microstructure

All three stages showed a similar, generally bainitic microstructure. There was no evidence of spheroidisation or grain boundary precipitation of large carbides suggesting that all microstructural changes were below the resolution of the optical microscope. The color etching brought out the differences in orientation of the prior austenite grain boundaries due to the preferential growth directions. The variation in color brightness is attributed to the different saturation of the carbides in the Fe- matrix.

The decoration of prior austenite grain boundaries was very clear. The linear arrangements of carbides which occurred in pairs (arrowed, Fig. 6.2 (a)) are thought to have occurred on a twinned segment in the prior austenite and these are interpreted as evidence supporting the identification of the prior austenite grain boundaries. This precipitation is associated with the pre-service processing. Electron diffraction was used to confirm that the matrix was mostly ferrite, which had transformed in patches of parallel laths typical of upper bainite, Fig. 6.2 (b). Within individual laths of ferrite, this figure also reveals a cellular network of slightly misorientated ferrite grains which contained a high dislocation density. This was more apparent after tilting experiments. This structure would be expected to also contain heterogeneously nucleated MC precipitation. The appearance of this ferritic cellular sub-structure was similar to that observed in recovered or recrystallised microstructures and suggests that the processing described above in the introduction imparts significant residual stresses in the microstructure. This is likely to be a further contribution to the higher hardness

observed in the core of stage 12 (Table 4.1, Chapter 4), since the operating temperatures of the other stages would be expected to anneal out most of these effects.

The previous chapter established that the FATT for rim samples of stage 3 of this rotor was ~ 150 °C. Therefore, it is not surprising to note that Fig. 6.2 (b) (stage 3) shows indications of thermal degradation. The microstructure is somewhat coarser in scale and there is extensive secondary precipitation of what was found to be mostly fine-scale MC cuboids and M_2C needles. Similarly, Fig. 6.2 (c) shows a coarser distribution of M_3C carbides and extensive secondary precipitation of the MC (see inset) and M_2C phases.

Core-to-Rim Variation

Both carbon replicas (Fig.6.3) and thin foils (Fig.6.4) of the core and rim of the rotor showed a generally similar microstructure. There was also no difference in the carbide composition between the core and the rim. This suggests that the rotor in study does not seems to be homogeneous microstructurally .

6.6.2 Effect of service history on the carbide composition

M_3C Carbides

The gross differences in M_2C precipitate number density between stage 1 and that of stages 3 and 12 suggested that changes in the microchemistry of this phase would not easily be interpreted in terms of service temperature. Their small size also introduced difficulties in analysis. Similar arguments were considered for the MC phase. Therefore, in seeking to follow compositional trends with selected microstructural phases from stage-to-stage, STEM-EDXS was performed on the M_3C carbides, which dominated all microstructures, Fig. 6.2.

These results are consistent with the thermodynamic data collated by Senior (1988), which shows that the stability of alloy carbides is greater than that for Fe_3C and that a strong driving force exists for the replacement of Fe. These results are also broadly consistent with those reported by Mitchell and Moss, 1994. Based the magnitude and continuity of the trends, the present work suggests that the most sensitive ratios were, in order: Fe/Si, Fe/V, Fe/Mn, Fe/Cr and Fe/Mo. Although the Si and V content changed by ~50% between the hot and cold stages, these are likely to be less reliable than (e.g.) the Mn due to their low overall fraction of the precipitate composition.

The carbide growth along the grain boundary or inside of the grains was more evident as well for stages 1 and 3. However, carbides with very large size up to ~10 μm were found much more in stage 3. An example of such carbide is shown in Fig. 6.6.

Large area analysis by EDXS is used as a simple tool for assessing the chemical composition changes during thermal exposures.

Because it is well known that the substitutional alloying elements, such as Cr, Mo, V and Mn, replace Fe in carbides as thermal exposure time increases, the compositional ratios of Fe and these alloying elements has been widely used for metallurgical assessments of pressure equipment. The compositional ratio for each stage is summarised in Table 6.4.

Table 6.4. Compositional ratios of Fe and substitutional alloying elements in the carbides analysed by EDXS

	Stage 1	*Stage 3*	*Stage 12*
Fe/Cr	1.42±0.08	1.87±0.21	2.33±0.12
Fe/Mo	14.33±1.31	26.45±7.49	28.32±6.75
Fe/V	18.04±3.84	24.67±5.95	24.07±1.68
Fe/Mn	10.98±1.23	2.31±0.12	2.56±0.05

H-Carbides

The H-like carbides were observed in extraction replicas from the three stages of the rotor examined and are shown (arrowed) in Fig. 6.2. These precipitates form during material fabrication (Senior, 1988, Mitchell and Moss,1998). Since they are present from the commencement of service and given their size and number density, changes in their morphology and composition were examined as a function of service temperature, with a view to using these parameters as potential indicators of service life. The spatial resolution of the EDXS analyses in STEM nanoprobe mode was well below that required to distinguish between the MC core and the heterogeneously nucleated M_2C wing-like components of the precipitate. Therefore, it was possible to analyse individual components of the H-precipitates from point-to-point. The analytical results varied somewhat within a given precipitate. Moreover, in common with recent results by Mitchell and Moss (1998) extensive analyses from H precipitates in all three rotor stages did not reveal significant differences, possibly due to averaging effects from segregation within precipitates. Given the close proximity of the MC/M_2C/matrix interfaces and the differing levels of solid solubility of solute within these phases, perhaps it is not surprising that the internal precipitate composition varies. In this situation, point analyses using EDXS, which seek to focus the electron beam on an arbitrary spot on the precipitate may be insensitive to the actual solute distribution in and around the precipitate phase, which is in a distinctly non-equilibrium state. Therefore, current efforts were focussed on the potential for EDXS mapping to reveal the distributed precipitate microchemistry in these steels.

The fine scale secondary precipitation appeared to be more prominent in the hottest stage, stage 1. Large numbers of H-type carbides, for example, which consist of square platelet shaped V-rich MC and rod shaped Mo rich M_2C carbide, were observed in this stage 1. A magnified view of H-type carbides, thought to be formed from secondary precipitation in stage 1 is provided in Fig. 6.5.

6.6.3 Carbides Distribution

The fraction of the carbides increased while operating temperature increased as depicted in Fig.6.7 and Table 6.2. The operating temperature of stage 1 (565 ° C) might have influenced the secondary precipitation of carbides. This result is consistent with the evidence of secondary precipitation in the hottest stage 1.

Given that interparticle spacing is inversely proportional to volume or area fraction of particles, the coldest stage, 12, has the smallest interparticle spacing whereas the hottest stage, 1, has the largest. This is also consistent with the decrease in hardness with increasing operating temperature (Kocks, 1966).

6.6.4 Scavenging Effect of Mo

It is known that Mo can interact preferentially with P so as to reduce the segregation of that element in the low alloy steels. It is speculated that the discrepancy measured in Table 6.3 arises from the Mo concentration into other locations such as grain boundaries, clusters or other interfaces which were not considered in this calculation. A more extensive characterisation is required to understand this behavior.

It is clear from Fig. 6.10 that the carbide is Mo rich and also possesses enrichment of V. What seems particularly interesting is the apparent segregation of P and V along the precipitate/matrix interface. The effect of Mo in mitigating against the embrittling effects of elements such as P is not well understood. The notion of a scavenging effect is often referred to (Viswanathan, 1989) but there is no clear mechanism for the basis of this effect and little, if any, direct evidence for it (Miller *et al.*, 1994). Results reported in Table 6.3 present grounds for further investigations. The kinetics of embrittlement may be related to the concentration of the alloying elements such as Cr and Mo in the matrix. Only 74 at % of Mo is present in the matrix thus allowing the remaining 26 % to be located elsewhere, most probably in the carbides. The formation of carbide such as M_2C, will severely deplete the amount of Mo is solution and the presence of significant amounts of either or both carbides will leave little Mo available to scavenge embrittling elements such as P (Moss and Kelly, 1998). Thus, there might a critical amount of Mo that needs to be present in the ferrite matrix in order to exercise the mitigating influence on the embrittling elements such as P.

The images in Fig. 6.10 suggest that one mechanism for the action of Mo in reducing the embrittling effects of elements such as P may be to lock these solutes at precipitate/matrix interfacial regions, thereby making them unavailable to diffuse to prior austenite grain boundaries. This data was recorded from stage 3, which was the stage which exhibited the highest FATT. The suggestion is that the effect of trapping P at the particle/matrix interface occurs to a lesser extent than in the other stages (e.g. stage 12).

6.6 Concluding Remarks

- It is clear that the Cr, Mo and V tend to replace Fe and partition into the carbide as operating temperature increases. However, Mn was found to have an opposite tendency by partitioning into matrix. It has been reported that Cr, Mo and V are strong carbide forming elements (V>Cr>Mo>Fe) ..It is considered that the hardness reduction shown in Table 4.1 is due partly to the reduction in solid solution hardening as solute elements are depleted from the matrix during the partitioning process. It is interesting to note that the trends in the FATT and hardness variations with service exposure (from the different stages) are likely to be the result of separate mechanisms. Whereas, the controlling mechanism for FATT variations is related to grain boundary segregation processes, the hardness changes are the result of changes in the amount of solute remaining in solution

- In the present investigation, the microstructure and microchemistry change was investigated using various analysis techniques. The results can be summarised as follows:

  - There was no substantial evidence of morphological differences of carbides in micron/sub-micron scale between the stages as shown by TEM and SEM analysis. However, detailed TEM characterisation suggested that microchemical information of the phases might vary for the three stages as they were exposed to different thermal histories.

- The carbide coarsening and secondary precipitation appear to be more clearly defined in the hotter stages 1 and 3 than stage 12. However, secondary precipitation was more prominent in stage 1 whereas coarsening is more evident in stage 3.

- EDXS analysis of the carbides showed that Cr, Mo and V tend to partition into carbides by replacing Fe as operating temperature increases.

- Solid solution hardening and interparticle spacing of carbides were found to be contributing factors to the hardness change with thermal exposure. There was no evidence found that volume fraction of the carbide any effect on the hardness change.

- Combining the results from SEM, TEM and 3DAP/FIM techniques may be applied to derive mass balances for most of the elements between the phases. This may subsequently provide a useful key for the assessment of the service history/remaining lifetime.

- Interface segregation was successfully analysed with 3DAP/FIM technique. It was apparent that P segregation along carbide and matrix interfaces was not negligible.

Chapter 7: Summary and Conclusions

This chapter summarizes the findings of this work lists the conclusions of the research and describes potential areas for further research

7.1 Embrittlement induced Microstructural Variation and Fracture Toughness

This work has examined two different approaches to temper embrittlement assessment in a power generating rotor: the mechanical correlations method and microstructural examination. The two methods were precipitated by the need to find an effective alternative to current remaining life assessment techniques and/or advance the current best practices for such evaluation. It is therefore of interest to visualise the relationship between the mechanical properties (as determined in Chapter 5) and microstructural indicators (as described in Chapter 6). The following figure, consisting of three parts (a), (b) and (c) allows to reproduce such a relationship.

Figure 7.1 (a) graphically depicts the relationship between the measured fracture toughness and the Fe/Mo ratio in the M_3C carbides. The variation of the ratio with fracture toughness and operating temperature is complex. As K_{Ic} fracture toughness decreases form stage 1 to stage 3, the Fe/Mp ration increases and continues to do so until it reaches its peak at stage 12, which also possesses the highest fracture toughness.

The overall picture created by Fig.7.1 (b) is different. Stage 12 is shown to contain the lowest number of precipitates per unit volume, whereas stage 1 emerges as having the highest amount of carbides. This is consistent with the assumption that stage 1 was subject to a prolonged thermal exposure at the highest operating temperature and thus the process of secondary precipitation had commenced.

Figure 7.1 (c) derives its data from the paper by Miller *et al*, 2000B. The researchers had studied a Cr-Mo-V reactor. The material was heat treated to produce unirradiated, neutron irradiated and thermally aged specimens. These categories were considered analogous to the rotor stages studied here as: unirradiated-to unembrittled stage 12, neutron irradiated – to the most embrittled stage 3 and thermally aged to the hottest stage 1. The average concentration of P in the matrix as determined by Miller *et al.*, 2000 using APFIM for Cr-Mo-V reactor was plotted against the K_{Ic} fracture toughness obtained in this work for Cr-Mo-V rotor steel. The resulting trend is consistent with the trend reported in the part (a) of the figure. It is proposed that this relationship might be connected with the scavenging effect of Mo and a complex relationship between the P and Mo.

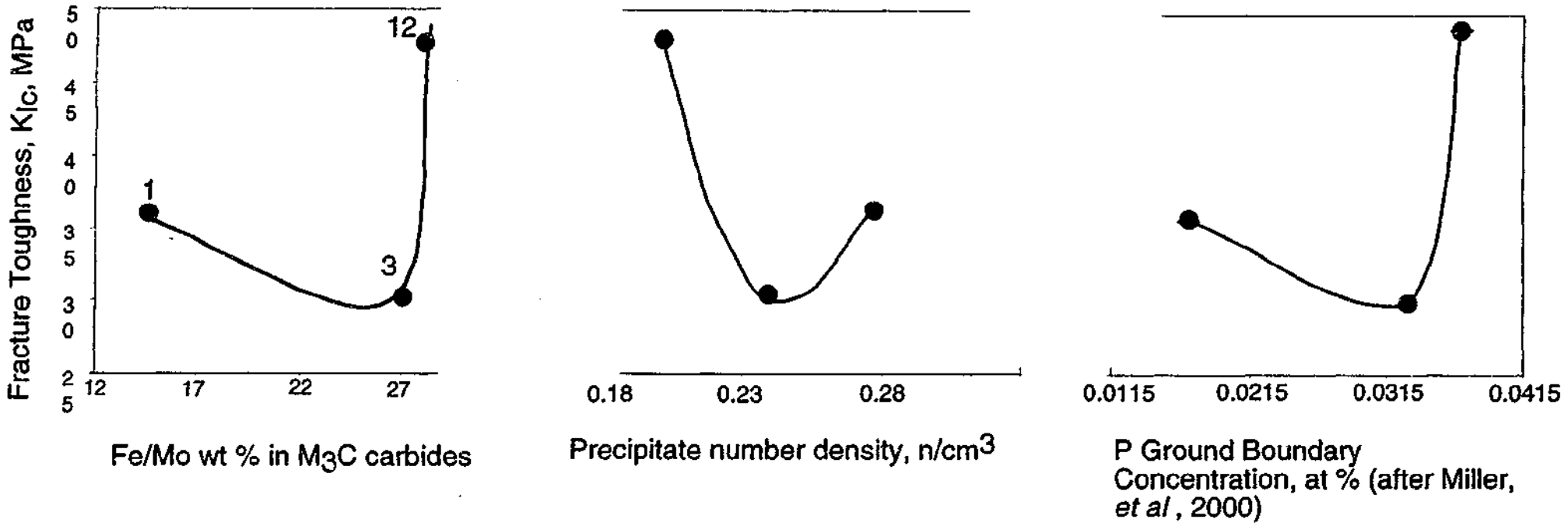

Figure 7.1 Microstrucutral indicators of embrittlement and fracture toughness

7.2 Conclusions

As a result of this study, a number of significant conclusion have been reached. Overall, it has been demonstrated that there exists a potential for the implementation of the SPT into remaining life assessment protocols. A number of relationships have been shown to support this proposal. In addition, the search for the microstructural indicators of temper embrittlement presents numerous possibilities for future exploration. More specifically, the following conclusions have been reached:

- The retired HP-IP rotor appeared to be subjected to the temper embrittlement damage mechanism whilst in service. This is supported by the FATTs measured for the entire rotor in the service-exposed condition. The FATTs exceed the limits specified in ASTM in most cases.
- Stage 3 that operated at nominal temperature of 505 °C emerged as the most embrittlement stage. This was documented by all three mechanical teschniques: CVN, SPT and K_{Ic} fracture toughness. This result is consistent with the previous reports for the operating window of temper embrittlement: 350–520 °C. Therefore stage 3 operating conditions coincide with these for this damage mechanism.
- The mechanical testing results generated for stage 12 suggested that this disk was virtually unembrittled. This is further supported by reports of similar FATT and K_{Ic} values for the rotors of this generation.
- The investigation into the relationship between the full and sub-size Charpy V-Notch Testing specimens concluded that the sub-size specimens qualitatively exhibit similar behavior to the standard full size specimens, although the USE levels and FATTs were reduced. Variation in the ΔFATT was systematic and seemed dependent on the degree of embrittlement of the various stages.

- The "Cr-Mo-V" correlation between the CVN an SPT was found to be within 90 % the confidence limit approach. Furthermore, the confidence interval was improved in this work from ±28 °C to ±10 °C.
- The reported correlations between the CVN and K_{Ic} were explored. These were found to be in good agreement with the experimental data.
- Since the CVN –SPT yielded an excellent working relationship, the SPT derived FATTs were used in a triangular correlation in order to predict fracture toughness K_{Ic}. Those values appeared to be consistent with the experimental K_{Ic} values.
- The critical crack size a_{cr} was calculated from K_{Ic} values for the three locations of the rotor. These were compared against the actual critical crack sizes of the failed rotor. Due to the successful triangular correlation based on the SPT it became possible to derive critical crack size from the miniature specimen technique. Since critical crack size is an important parameter in the remaining life assessment (RLA), this method has potential to be incorporated into the RLA protocols.
- The microstructure of the rotor was studied in detail. The microstructural uniformity of the core and rim sections was unexpected. Moreover, the rotor demonstrated an excellent microstructural homogeneity.
- The M_3C carbide dominated the rotor microstructure, and thus further microstructural investigation was based on this microstructural representative. The microchemical information that was derived from it suggested that its composition changed according to the thermodynamic driving force for solute partitioning. EDXS analysis for the carbides showed that Cr, Mo and V tend to partition into carbides by replacing Fe as operating temperature is increased.

- The carbide coarsening and secondary precipitation appeared to be clearly defined in the hotter stages 1 and 3 than 12. However, secondary precipitation was more prominent in stage 1 whereas coarsening was more evident in stage 3.
- The combined results from several microscopy tools such as FEG SEM, TEM and 3DAP/FIM may be used to derive mass balances for most of the key elements between the phases. This may subsequently provide a useful key for the service history/remaining life.
- Interface segregation was successfully analysed with 3DA/PFIM. P segregation along the carbide and the matrix was significant.

Chapter 8 Suggestions for Future Work

Several aspects of this study have provided potential avenues for future investigations.

- Improvement of the 95% confidence interval in CVN-SPT correlation. Since an excellent correlation was already obtained in this work, further research is possible to advance this relationship. Viswanathan and Foulds, 2001 reported that a reduction to ±10 °C instead of the ±28 °C currently adopted is possible. This work has demonstrated that the confidence interval is within 11 ° C. The reduction of the prediction uncertainty could contribute to the implementation of the SPT into the remaining life assessment protocols.

- It will be worthwhile to incorporate the data obtained from similar rotors into the K_{Ic} prediction based on the SPT and validate this relationship. It would be of interest to demonstrate that the three-way correlation of structural integrity was also applicable to other rotors. It would also be fascinating to implement this correlation method to predict fracture toughness of the rotors of both European and US manufacturing origin in order to examine the influence of the changes of the cooling rate and subsequently microstructure (lower vs upper bainite) onto such a correlation.

- Measurement of elevated temperature fracture toughness in order to construct a full transition curve and implement the triangular correlation. This would contribute towards the credibility of the correlation based on SPT and could also give rise to new improved correaltions based on the entire transition curve between CVN, SPT and K_{Ic}.

- Studies of the mechanism of de-segregation (de-embrittled) with the use of APFIM. Since the kinetics of solute desegregation during the de-embrittled heat treatment have not been extensively studied it would assist in establishing the effectiveness of such a heat treatment and better justify the results in impact properties that it produces. This could be achieved by conducting comparative matrix analyses of severely embrittlement vs de-embrittled material. The calculations that such analysis would allow for the determination of the concentration of the embrittling species at the grain boundaries and inside the matrix. The 3DAP/FIM results could also be correlated with the de-embrittled fracture toughness.

- Studies of scavenging effect of Mo with the use of APFIM. The relationship of P and Mo is complex and causes the migration of the P to the grain boundaries and vice versa. 3D/APFIM experiments would give insight into the mechanism of the action. The analysis should be conducted both inside the matrix and on the grain boundaries

- FEA of SPT results obtained here and implementation of the FEA approach described in Chapter 5 (5.5.3). The resultant fracture toughness could then be compared to the fracture toughness obtained from the correlation method described in this thesis and the advantages/disadvantages of using either of the methods further explored.

References

Abe, F., Noda, T., Araki, H., Okada, M., Narui, M. and Kayano, H., (1987). "Effect of Specimen Size on the Ductile-to-Brittle Transition Behaviour and the Fracture Sequence of 9Cr-W Steels", Journal of Nuclear Materials, **150**, pp. 292-301.

Abe, T., Tsukada, K., Tagawa, H. and Kozasu, I., (1990). "Grain Boundary Segregation Behaviour of Phosphorous and Carbon under Equilibrium and Non-Equilibrium Conditions in Austenitic Region of Steel", ISIJ International, **30**, (6), pp. 444-450.

Alexander, D., and Klueh, R., (1990). "Specimen Size Effects in Charpy Impact Testing", Charpy Impact Test: Factors and Variables", ASTM STP 1072, John M. Holt Editor, ASTM, Philadelphia, pp. 179-191.

Bagnoli,, D.L., Leedy, J.W., Wada, T., (1988). "Embrittlement of 1 Cr-1/2 Mo and 1 1/4 Cr-1/2 Mo Alloys After long Time Service", Corrosion **88**, March 21-25, pp. 160/1-160/18.

BaikJ-M., Kameda, J. and Buck, O. , (1986). " Development of Small Punch Tests for Ductile-Brittle Transition Temperature Measurement of Temper Embrittled Ni-Cr Steels", ASTM STP **888**, pp. 92-111.

Bashu, S.A., (1990). "Impact Energy/Specimen Thickness Relationships for Two Turbine Steels", Journal of Testing and Evaluation, **18**, (5), pp. 363-368.

Bayomi, , M.R. and Bassim, M.N., (1983). "Study of the Relationship Between Fracture Toughness J_{Ic} and budge ductility", International Journal of Fracture, **23**, pp.71-79.

Berg,V., Bertilsson, J.E., Friedla, K.H. and Scarlin, R.B., (1982). "On the Limits of the Design of Large Steam Turbine Rotors Operating at Elevated Temperatures", Rotor Forgings for Turbines and Generators, R.I. Jaffee Ed., Pergamon Press, New York, pp. 3-147.

Bhadeshia, H.K.D.H. and Christian, J.W., (1990). "Bainite in Steels", Metallurgical Transactions A, **21A**, pp.767-797.

Bodnar, R.L., Ohhashi, T and Jaffe, R.J. (1989). "Effects of Mn,Si, and Purity on Design of 3.5NiCrMoV, 1 CrMoV, and 2.5Cr-1Mo Bainitic Steels", Metallurgical Transactions A, **20A**, , pp.1445-1460.

Bruemmer, S. and Viswanathan, R., (1992). "Quantitative Characterisation of Grain Boundary Composition in Steels", Proceedings of the Robert Jaffee Memorial Symposium on Clean Materials Technology, ASM Materials Week, Chicago, Illinois, USA, pp.91- 99.

Bruemmer, S.M.: (1988)."Grain Boundary Composition Effects on Environmentally Induced Cracking of Engineering Materials", Corrosion Science, **44**, pp.364-370.

Bulloch, J.H., (1994). "An Appraisal of Certain Factors Which Influence Toughness Restoration (De-embrittlement) in Some Temper-embrittled Low Alloy Steels", International Journal of Pressure Vessels and Piping, **58**, pp.231-247.

Bulloch, J.H., (1999). "Reverse Temper Embrittlement , RTE, in Low Alloy Steels: A Substantive Study Concerning the Influences of Grain Size, Bulk Phosphorus and Accumulated Service Strain", International Journal of Pressure Vessels and Piping, **76**, pp.63-78.

Bulloch J.H., (1994). "Reverse Temper Embrittlement A Common Source of Perplexity in Low Alloy Steels", Materials at High Temperatures, **12**, pp.312-321.

Bulloch, J.H., (1999). "The Embrittlement Characteristics of Large Turbine Casing Bolts: The Influence of Service Induced Strain", International Journal of Pressure Vessels and Piping, **76**, pp.79-90.

Cane, B.J. (1986). "Present status of Predictive Methods for Remanent Life Assessment and Future Developments", Materials Forum, Vol.9, pp.5-101.

Carruthers, R.B. and Collins, M.J., "The Application of a New Microstructural Technique for the Assessment of Effective Operating Temperature", CEGB Confidential report, (Dr Moss).

Chenm J.H. and Wang, G.Z., (1998). "On Scattering of Measured Values of Fracture Toughness Parameters", International Journal of Fracture, **94**, pp. 33-49.

Cheruvu, (1989). "Degradation of Mechanical Properties of Cr-Mo-V and 2.25Cr-1Mo Steel Components After long-Term Service at Elevated Tempertures", Metallurgicla Transations A, pp. 87-9

Cheruvu, N.S., Malmfeldt, L.R., (1990). "Metallurgical Characterisation of a High-Pressure Rotor for Remaining Service Life Assessment After 26 Years of Service", Journal of Engineering for Gas Turbines and Power, pp.543-549.
Collins,M.J. Met. Technol., 5, 1978, p. 325.

Comon, J., Martin, P.F. and Bastien, P.G., (1968). "Statistical Study of Factors Influencing Impact Strength of Turbine Generator Rotors-Influence of Temper Embrittlement", ASTM-STP 407, pp.74-89.

Cook, T.S., Pennick, H.G., and Wells, C.H., (1978). "Lifetime Prediction Analysis System" in "Steam Turbine Rotor Reliability", EPRI, Report NP923,

Croker, A.B.L., Hellier, A.K.H., (1997). Small Punch Testing of a Turbine Rotor Steel.

Cunnane, D.J., Lyell, G.D. and Strong, A. "Metallurgical Examination of Material from the Bore of a retired Belgian 1CrMoV IP Steam Turbine Rotor", GEC, (Dr Moss).

Ellis, F. V., Hilton, S.O., Henry, J.F., Bynum, J.E., (1982). "Influence of Service Exposure on Base and Weld Metal of 1/2 Cr-1/2 Mo-1/4 V High-Pressure Steam Inlet Piping", Transactions of the ASME. pp. 120-129.

Erwin, W.E. and J.G. Kerr " The Use of Quenched and Tempered 2 1/4 Cr-1Mo Steel for Thick Wall Reactor Vessels in Petroleum Refinery Processes: An Interpretive Review of 25 Years of Research and Application", WRC Bulletin 275, pp.1-63.

Faulkner, R.G., Song, S.-H. and P.E.J. Flewitt, (1996). "Combined Quenching and Tempering Induced Phosphorous Segregation to Grain Boundaries in 2.25Cr-1Mo Steel", Materials Science and Technology, pp. 818-822.

Fleury, E., (1997). "Small punch test for Fossil Power Plant", Workshop "Life Assessment and Management", Taejon,

Foulds, J. and R.Viswanathan, (1994). "Small Punch Testing for Determining the Material Toughness of Low Alloy Steel Components in Service", Transactions of ASME, Journal of Engineering Materials and Technology, **Vol.116,** pp. 457-465.

Foulds, J.R. and Viswanathan, R., (1996). "Nondestructive Material Sampling and Mechanical Strength", Journal of Testing and Evaluation, 15, **3/4,** pp.151- 162.

Foulds, J.R., Jewett, C.H. and Bisbee, L.H., (1992). "In-Service Stem Turbine Rotor Material Evaluation by Small Punch Testing", PWR, **Vol.18,** Steam Turbine -generator Developments for the Power Generation Industry, pp.151-157.

Foulds, J.R., Jewett, C.W., Bisbee, L.H., (1992). "Miniature Sample Removal and Small punch testing", reprinted from Clean Steels Technology, Proceedings of the Robert I. Jaffee Memorial Symposium on Clean Materials Technology ASM/TMS Materials Chicago, Illinios, USA.

Foulds, J. R., Woytowitz, P.J, Parnell, T.K., Jewett, C.W., (1993). "Fracture Toughness by Small Punch testing", Third EPRI Turbine-Generator Workshop, New Yorsk, pp. 2-22.

Foulds, J.R and Viswanathan, R., (2001). "Determination of the Toughness of In-Service Steam Turbine Disks Using Small Small Testing", Journal of Materials Engineering and Performance, **10 (5),** pp. 614-619.

Giglio, M., (1995). "Life Prediction of Notched Components", Transactions of the ASME, **Vol.117**, pp.50-55

Gladh, M., Wallen, P., "Embrittlement of a steam turbine rotor", Pergamon Press, pp.297-305.

Gordon, J.R., Skeleton W. J., (1985). "The Effect of Temper Embrittlement on the Fracture Properties of a Pressure Vessel Steel", Transactions of the 8th International Conference on Structural Mechanics in Reactor Technology, pp. 425-431.

Gray, J.L., "Investigation into the Consequences of the Failure of a Turbine-Generator at Hinkley Point 'A' Power Station", Proceedings of the Institute of Mechanical Engineers, **186**, 32/72, pp. 379-390.

Ha, J.S and Fleury, E. (1998). " Small punch tests to estimate the mechanical strength of steels for steam power plant: I. Mechanical Strength", International Journal of Pressure Vessels and Piping, **75**, pp. 699-706.

Ha, J.S and Fleury, E, , (1998). " Small punch tests to estimate the mechanical strength of steels for steam power plant: I. Fracture Toughness", International Journal of Pressure Vessels and Piping, **75B,** pp.707-713.

Habraken, L.J., (1967). "Bainite Microstructures in Low-Carbon Alloy Steels nd Their Mechanical Properties", Climax Moly, Co, pp.69-107.

Hellier, A.K., Smith, G.K., (1997). "Charpy Impact Testing of Materials from Four Turbine Rotors",

Hippsley, C.A., (1985). "Brittle Intergranular Fracture at Elevated Temperatures in Low Alloy Steel", Materials Science and Technology, **1,** pp. 475-479.

Holdsworth, S.R., "A Review of Manufacturer Route on the Properties of 1Cr-Mo-V Steels", (Dr.Moss).

Holtzmann, M., Vlach, B. and Krumpas, J., (1996). "Degradation of mechanical properties of Cr-Mo-V and Cr-Mo-V-W steam turbine rotors after long-term operation at elevated temperatures. Parts I and II: tensile properties, intergranular fracture strength and impact tests", International Journal of Pressure Vessels and Piping, pp.99-111.

Irvine, K.J., Pickering, F.B., "High-carbon Bainitic steels", (1965). Physical Properties of Martensite and Bainite, Special Report 93, The Iron and Steel Insitute, pp.110-125.

Iwadate, T., Karushi, T. and Watanabe, J. (1977). "Prediction of Fracture Toughness K_{Ic} of 21/4 Cr- 1Mo Pressure Vessel Steel from Charpy V-Notch Test Results", STP **631**, ASTM pp.493-506.

Iwadate, T., Tanaka, Y. and Takemata, H., (1994). "Prediction of Fracture Toughness K_{Ic} Transition Curves of Pressure Vessel Steels From Charpy V-Notch Impact Test Results", Journal of Pressure Vessel Technology, **116**, pp.353-358.

Iwadate, T., Watanabe, J., (1985). "Prediction of the Remaining Life of High-Temperature/Pressure Reactors made of Cr-Mo Steels", Transactions of the ASM, , pp.230-238.

Iwadate, T., Watanabe, J., Tanaka, Y., (1985). "Prediction of the Remaining Life of High-Temperature/ Pressure Reactors Made of Cr-Mo Steels", Transactions of the ASME, **107**, pp.230-238.

Joarder, A., (1994). "On the Bainite Structure in Cr-Mo-V Steel", Steel Research 65, No 8, pp. 345-349

Jones, D.P.,. Hoppe, R.G.,. Hechmer, J.L. and James, B.A., (1994). "An Experimental Study on the Effects of Compressive Stress on the fatigue Cracj Growth of Low Alloy Steel", Transaions of ASME, Journal of Pressure Vessel Technology pp.317-323.

Jones, G.T., (1972). "Discussion on D. Kalderon and J.L. Gray", Proceedings of the Institute of Mechanical Engineers, **186,** 31-2/72, pp. D122-D123.

Kadoya, Y., Goto, T., Takei, M., Haruki, N., Ikuno, K., .Nishimura, Y., (1991). "Nondestructive evaluation of temper embrittlement in Cr-Mo-V rotor steel", PWR-Design, repair nad Refurbishment of Steam Turbines, ASME, pp229-234.

Kadoya, Y., Goto, T., Takei, M., Haruki, N., Ikuno, T., Nishinura, Y., (1992). "Nondestructive evaluation of temper embrittlement in Cr-Mo-V Rotor Steel", JSME International Journal, Series I, , pp.226-237

Kalderon, D., (1972). "Steam Turbine Failure at Hinkley Point 'A"", Proceedings of Institute if Mechanical Engineers, **186 (31),** pp.341-377.

Kameda, J. and Mao, X., (1992). "SMALL PUNCH and TEM-disc testing techniques and their application to characterisation of radiation damage", Jouranal of Materials Science, **27,** pp.983-989.

Kim, G.S., Indacochea, J.F., Spry, T.D. (1991). " Metallurgical Aspects I welding Cr-Mo-V turbine Rotor Steels, Part 1 Evaluation of Base Material and Heat Affected Zone", Materials Science and Technology, pp.42-49.

Kim, H.J., Kim, Y.H. and Morris, J.W., Jr., (1998). "Thermal Mechanisms of Grain and Packet Refinement in a Lath Martensitic Steel", ISIJ International, **38,** pp.1277-1285.

Knott, J.F., (1998). "Probilistic Assessments of Fracture Toughness In Pressure-Vessel Steels", Lifetime Management and Evaluation of Plant, Strucutres and Components, Eds. Edwards, Flewitt, Gasper, McLarty, Stanley and Tomkins, Emas Publishing, pp. 77-85.

Kocks UF. Acta Metall. 1966; 14: pp. 1629-1651.

Kuniya, J., Masaoka, I., Itoh, H., Okazaki, T., (1985). "Stress Corrosion Cracking Susceptibility of Low Alloy Steels Used for Reactor Pressure Vessel in High Temperature Oxygenated Water", pp.431-435.

Low, J.R. Jr, (1964). "Fracture of Engineering Materials", American Society for Metals, Metals Park, Ohio,

Lucas, G.E., (1990). " Review of Small punch techniques for Irradiation Testing", Metallurgical Transactions A, **21A,** pp.1105-1119.

Manahan, M.P., (1983). "A New Postirradiation Mechanical Behaviour Test-The Miniaturised Disk Bend Test", Nuclear Technology, pp. 295-315.

Mao, X., Saito, M., Takahashi, H., (1991). "Small Punch Test to Predict Ductile Fracture Toughness J_{Ic} and Brittle fracture Toughness K_{Ic}", Scripta Mettalurgica, pp. 2481-2485.

Mao, X., Shoji, T., Takahashi, H., (1987), "Characterisation of Fracture Behaviour in Small Punch Test by Combined Recrystallization-Etch Method and Rigid Plastic Analysis", Journal of Testing and Evaluation, pp 30-37.

Mao, X., Takahashi, H. and Kodiara, T., (1991). "Estimation of Mechanical Properties of Irradiated Nuclear Pressure Vessel Steel By Use of Subsized CT Specimen and Small Punch Specimen", Scripta Metallurgica, **25,** pp.2487-2490.

Marandet, B., Phelippeau and Rousellier, G., " Effect of Speciemen Size on J_{Ic} for a Ni-Cr-Mo Rotor Steel", Ref ?????, pp.871-878.

Marandet, B., Phellippeau and Sanz, G., "Experimental Determination of Dynamic Fracture Toughness by J Integral Method", Ref.??????, pp. 375-382.

Maropoulos, S., Paul, J.D. and Ridley, N., (1993). "Microstructure-Property Relationships in Tempered Low Alloy Cr-Mo-3.5Ni- V Steel", Materials Science and Technology, **9**, , pp.1014- 1019.

Mayer, K.H., Beger, Ch., Heinrich, D. and Scarlin, B., (1992). "Evaluation by fracture mechanics of ultrasonic indications in turbine and generator rotors", Nuclear Engineering and Design", pp.277-289.

McMahon, C.J., Jr., Gentner, D.H. and Ucisik, A.H., (1968). "An Investigation of the Effects of Grain Size and Hardness in Temper-Embrittled 2 1/4 Cr- 1 Mo- Steel", Transactions of ASME, **106**, pp.66-70.

Mercaldi, D.W., 1989, "Surface Sampling Device", US Patent 4, 845, 896, Failure Analysis Associates, Inc.

Miller, M.K., Jayaram, R. and Russell, K.F., (1995). "Characterisation of Phosphorous in Neutron-Irradiated Russian Pressure Vessel Steel Weld", Journal of Nuclear Materials, **225**, pp.215-224.

Miller, M.K., (2000A). " Atom Probe Tomography: analysis at he atomic level", Kluwer Academic/Plenum Press.

Miller, M.K., Russell, K.F., Kicok, J. and Keilova, E., (2000b). "Atom Probe Tomography of 15kH2MFA Cr-Mo-V Steel Surveillance Specimens", MMEM,

Mitchell, D.R.G. and Moss, C.J (1997). "Metallurgical Examination of Seven Power Generating Turbine Rotors Using Microscopy-Based Techniques", Rotor Journal, pp. 1-25.

Mitchell, D.R.G. and Moss, C.J., (1998). "Characterisation of Seven Power-Generating Turbine Rotors Using Microscopy-Based Techniques", Journal of Materials Engineering and Performance, **7**, (5), pp. 621-631.

Moss, C.J., Croker, A.B.L.,. Harrison, R.P.,"A Perspective of Pressure Paint Life Management in Australia", Advanced Materials Program.

Moss, C.J., Kelly, P.M., (1994). "The mechanisms and detection of embrittlement in Cr-Mo pressure vessel steels", Fatigue Fract. Eng Mater. Struct. pp.369-380,

Moss, C.J.,. Kelly, P.M., "Deteciton of embrittlement in Cr-Mo Pressure Vessel steels", Advanced Materials, Fax Communications.

Murza, J.C. and McMahon, C.J., (1980). "The Effects of Composition and Microstructure on Temper Embrittlement in 2 1/4 Cr-1 Mo Steel", Journal of Engineering Materials and Technology, **102**, pp.369-375.

Myers, D.E., Chen, F.C., Zhang, J. and Ardell, A.J. (1993). "Optimisation of Test Parameters for Quantitative Stress measurements Using the Miniaturised Disk-Bend Test:, Journal of Tensing and Evaluation, pp263-271.

Narayan, R. and. Murphy, M.C., (1973). "Temper Embrittlement in Rotor Steels", JISI, part 7.

Newhouse, D.L. and Holtz, H.G., (1968). "Temper Embrittlement of Rotor Steels", ASTM-STP **407**, pp.106-126.

Nishizaka, Y., Hara, Y., Hori, A., Tsukahara, H., Miyano, K., Wada, T. and Cox, T.B., (1985). "Changes in Microstructure and Mechanical Properties of Cr-Mo Reactor Vessel Steels During Long-Term Service", Journal of Pressure Vessels Technology, **107**, pp.285-294.

Nishizaka, Y., Nara, Y., Nori, A., Tsukahara, H., Miyano, K., Wada, T.,.Cox, T.B., (1985), "Changes in Microstructure and Mechanical Properties of Cr-Mo Reactor Vessel Steels During Long-Term Service", , pp.285-294.

Nogata, F., and Seo, K., (1991). "Evaluation of Material Degradation In-Service High temperature Structural Component by A Chemical Etching Test", Int. J. Pres.Ves & Piping, pp. 369-379.

Norton, J.F., Strang, A., (1969). "Improvement of Creep and Rupture Properties of Large 1%Cr-Mo-V Steam Turbine Rotor Forgings", Journal of the Iron and Steel Institute, pp.193-201.

Parker, J.D. and James, J.D. (1993). " Disc-Bend Creep Deformation Behaviour of 1/2Cr1/2Mo1/4V Low Alloy Steel", Creep and Fracture of Engineering Materials and Structures, pp. 651-660.

Pickering, F.B., (1967). "The Structure and Properties of Bainite in Steels", Climax Moly Co, pp. 109-133.

PuzakP.P., Eschbaher, E.W, and Pellini, W.S., , (1952). "Initiation and Propagation of Brittle Fracture in Structural Welds", Welding Journal Research Supplementary, pp.561S.

Pyun, S., Kim J-T., Lee, S-M., (1991). "Effects of Phosphorous Segregated at Grain Boundaries on Stress Corrosion Crack Initiation and Propagation of Rotor Steels in Boiling 40 wt% NaOH Solution", Materials Science and Engineering, A **148**, pp. 93-99.

Qu, Z., McMahon, C.J., Jr, "The Effects of tempering Reactions on Temper Embrittlement of Alloy Steels", Metallurgical Transactions A, pp.1101-1108.

Rana, M.D., (1994). "Structural Integrity Assessment of Carbon and Low-Alloy Steel Pressure Vessels Using a Simplified Fracture mechanics Procedure", Journal of Pressure Vessel Technology, pp.324-330.

Raoul, S., Marini, B. and Pineau, A., (1998). "Effect of Microstructure on the Susceptibility of a 533 Steel to Temper Embrittlement", Journal of Nuclear Materials, **257**, pp. 199-205.

K., Geiger, T., (1967). "Influence o Microstructure and Heat-Treatm
Relander ent on Impact and Creep Properties of a Low Alloy CrMoV Turbine Steel", Transactions of ASME, pp. 238-246.
Ritchie, R.O., Knott, J.F. and Rice, J.R., Journal of Mechanical Physics and Solids, **21**, 1973, p. 395.

Roberts, R. and Newton, C., (1981). "Interpretive Report on Small-Scale Test Correlations with K_{Ic} Data", WRC Bulletin **265**, pp.1-18.

Rolfe, S.T. and S.R. Novak, Slow Bend K_{Ic} Testing Medium Strength, High Toughness Steels, STP, **463**, ASTM, 1970, pp.124-129.

Sawada, S., Ohhashi, T., Okamoto, M. and Watanabe, J., "Temper Embrittlement Charactersitics of 2 1/4 Cr-1 Mo Steels Used in Hydrogenation Units for 30,000 and 60,000 Hours at About 660 to 840 °F", Report, Research Laboratory, Muroran Plant, The Japan Steel Works, Ltd., Hokkaido, Japan.

Senior, B.A., (1988). "A Critical Review of Precipitation Behaviour in 1Cr-Mo-V Rotor Steels", Materials Science and Engineering, A **103**, pp.263-271.

Sevc, P., Janovec, J. and Katana, V., "On Kinetics of Phosphorus Segregation in Cr-Mo-V Alloy Steel", Scripta Mettalurgica, pp.1673-1678.

Shaw, B.J., (1981). "Characterization Study of Temper Embrittlement of Chromium-Molybdenum Steels", Procedgins of the American Petroleum Institute, Devision of Refininf, 60 ,API, Washington, pp.225-247.

Smith, D.J., Ayatollahi, M.R., Davenport, J.C.W. and Swankie, T.D., (1998). "Mixed Mode Brittle and Ductile Fracture of a High Strength Rotor Steel at Room Temperature", International Journal of Fracture, **94,** pp.235-250.

Suresh, R.K., Ramakrishnan, N., Srinivas, M. and Ramarao, P., (1999). " On the Determination of J Using the Stretch Zone Width Method", Journal of Testing and Evaluation, **27,** (3), pp. 211-218.

Swaminathan, V.P., Cheruvu, N.S., Saxena, A., (1990). "Life assessment of an HP-IP Rotor Under Creep Service Conditions", Journal of Engineering for Gas Turbines and Power, **112/237**, pp. 237-242.

Swaminathan, V.P., Viswanathan, R. and. Clark, C.P.,(1994). "Material Property Studies of Two High-Pressure Turbine Rotors for Remaining Life Assessment", Journal Of Engineering Materials and Technology, **116**, pp.19-26.

Takahashi, H., Shoji, T., Mao, X., Hamaguchi, Y., Misawa, T., Saito, M., Oku, T., Kodaira, T., Fukaya, K., Nishi, H., Suzuki, M., (1988). "Recommended Practice for Small Punch Testing of Metallic Materials (Draft)", JAERI_M 88-172.

Timo, D.P., Curran, R.M., Placek, R.J., (1982). "The Development and Evolution of Improved Rotor Forgings for Modern Large Steam Turbines", Rotor Forgings for Turbines and Generators, R. I. Jaffee, Ed. Pergamon Press, New York, pp. 115, 128.

Tomita, Y., (1991). "Development of Fracture Toughness of Ultrahigh Strength Low Alloy Steels for Aircraft and Aerospace Applications", Materials Science and Technology, 7, pp.481-489.

Tu, L.K., and Seth, B.B., (1978). "Effect of composition, strength, and residual elements on toughness and creep properties of Cr-Mo-V turbine rotors", Materials Technology, pp.79-91.

Tungdong, X., (1999). "The Critical Time in Temper Embrittlement Isotherms of Phosphorous in Steels", Journal of Materials Science, **34**, pp. 3177-3180.

Viswanathan, R., (1989). "Damage Mechanisms and Lie Assessment of High-Temperature Components, ASM International.

Viswanathan, R. and Bruemmer, S. M. (1986) "In Service Degradation of Toughness of Stem turbine Rotors", EPRI, 6-25-6-45.

Viswanathan, R. and Bruemmer, S.M. 1985 "In-Service Degradation in Toughness of Steam Turbine Rotors", Journal of Engineering Materials And Technology, **107**, pp.316-324

Viswanathan, R. and Foulds, J.R., (1994.) "Nondestructive Evaluation of the Fracture Appearance Transition Temperature of Rotor Steels", Presented at the 12th IFM Conference, Chicago, USA, Sep 11-17.

Viswanathan, R. and Gehl, S., (1991) " A Method for Estimation of the Fracture Toughness of CrMoV Rotor Steels Based on Composition", Journal of Engineering Materials and Technlogy", **113**, pp.263-270.

Viswanathan, R. and Gehl, S., "Nondestructive Assessment of Temper Embrittlement in Turbine Rotor Steels", EPRI Report.

Viswanathan, R. and Gehl, S., "Nondestructive Evaluation of the Fracture Appearance Transition Temperature of Rotor Steels", EPRI Report.

Viswanathan, R. and Gehl, S., (1992). "Temper Embrittlement of Rotor Steels", Proceedings of the Robert Jaffee Memorial Symposium on Clean Materials Technology, ASM Materials Week, Chicago, Illinois, USA, November, pp.59-67.

Viswanathan, R. and Jaffe, R.I, (1983). "Toughness of Cr-Mo-V steels for steam turbine rotors", Transactions of ASME, Journal of Engineering Materials and Technology, **105**, pp 286-294.

Viswanathan, R., (1971) "Temper Embrittlement in a Ni-Cr Steel Containing Phosphorous as Impurity", Metallurgical Transactions, 2, pp. 809-815.

Viswanathan, R., Bruemmer, S.M., (1985). "In-Service Degradation in Toughness of Steam Turbine Rotors", Journal of Engineering Materials And Technology, **107**, pp.316-324.

Viswanathan, R., Dooley, B., and Saxena, A., (1988) "A Methodology for Evaluating the Integrity of Longitudinally Seam-Welded Steam Pipes in Fossil Plants", Journal of Pressure Vessel Technology, **110**, pp.283-290.

Viswanathan, R. and Wells, C.H., (1993). "Life prediction for turbine generator rotors", Technology for the nineties, invited review paper, ASME, pp.1-33.

Viswanathan, V. Rosinski, S., Fould, J. and Williams, J. 'Taking Stock of Component Condition", Reprinted from the November 1997 edition of Power Engineering, Copyright 1997 by Penn Well.

Wada, H., (1986). "Thermodynamic Properties of Carbides in 2.25 Cr- 1Mo Steel at 985 K", Metallurgical Transactions A, 17a, pp. 1585-1592.

Watanabe, Y., Shoji, T., (1991). "The Evaluation of In-Service Materials Degradation of Low Alloy Steels by the Electrochemical Method", Metallurgical Transactions A, **22A**, September, pp.2097-2106.

Werner, F.E., (1956). " Transformation Characteristics of CrMoV Steel", Research Memo, Westinghouse Research Laboratories,

Weibull, W. (1951). Journal of Applied Mechanics, 18, ,pp .293-297.

Williams, K.R., "Microstructural Examination of Several Commercial 1/2Cr1/2Mo1/4V Casts in the As-Received and Service Exposed Conditions", CERL.

Yang, L. and Fatemi, A., (1996). "Impact Resistance and Fracture Toughness of Vanadium-Based Microalloyed Forging Steel in the As-Forged and Q&T Conditions", Journal of Engineering Materials and Technology, 118., pp.71-79.

Yu, J. and MacMahon, C.J.,Jr., (1980). "The Effects of Composition and Carbide Precipitation on Temper Embrittlement of 2.25 Cr- 1 Mo Steel: Part I: Effects of P and Sn", Metallurgical Transactions A, 11A, pp.277-289.

APPENDICES

APPENDIX A:

CUT-UP DOCUMENTATION

Stage 1 Cut-Up Plan

1C1- sub-size J_{Ic} specimens
1C2-1C4 – sub-size Charpy specimens
1C5-1C10 – full-size Charpy specimens
1C11-1C12 – full-size K_{Ic} specimens
1C13-1C14 – Tensile Specimens

Scale: 1:1.5

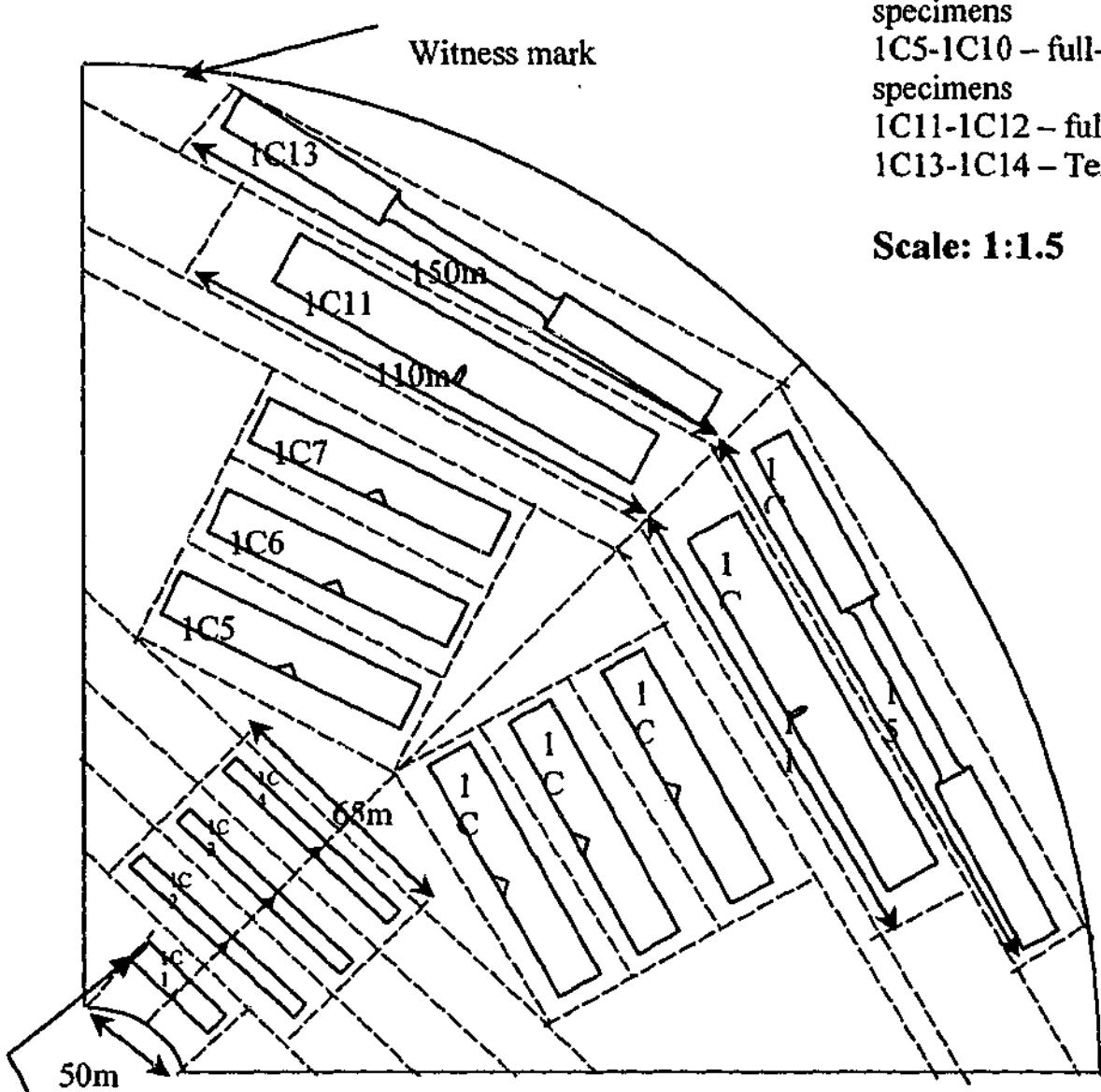

Witness mark this

Sectioning of _ of the core of stage 1
Blocks for mechanical samples were cut in radial orienation
1C witness sample

Stage 3 Cut-up Plan

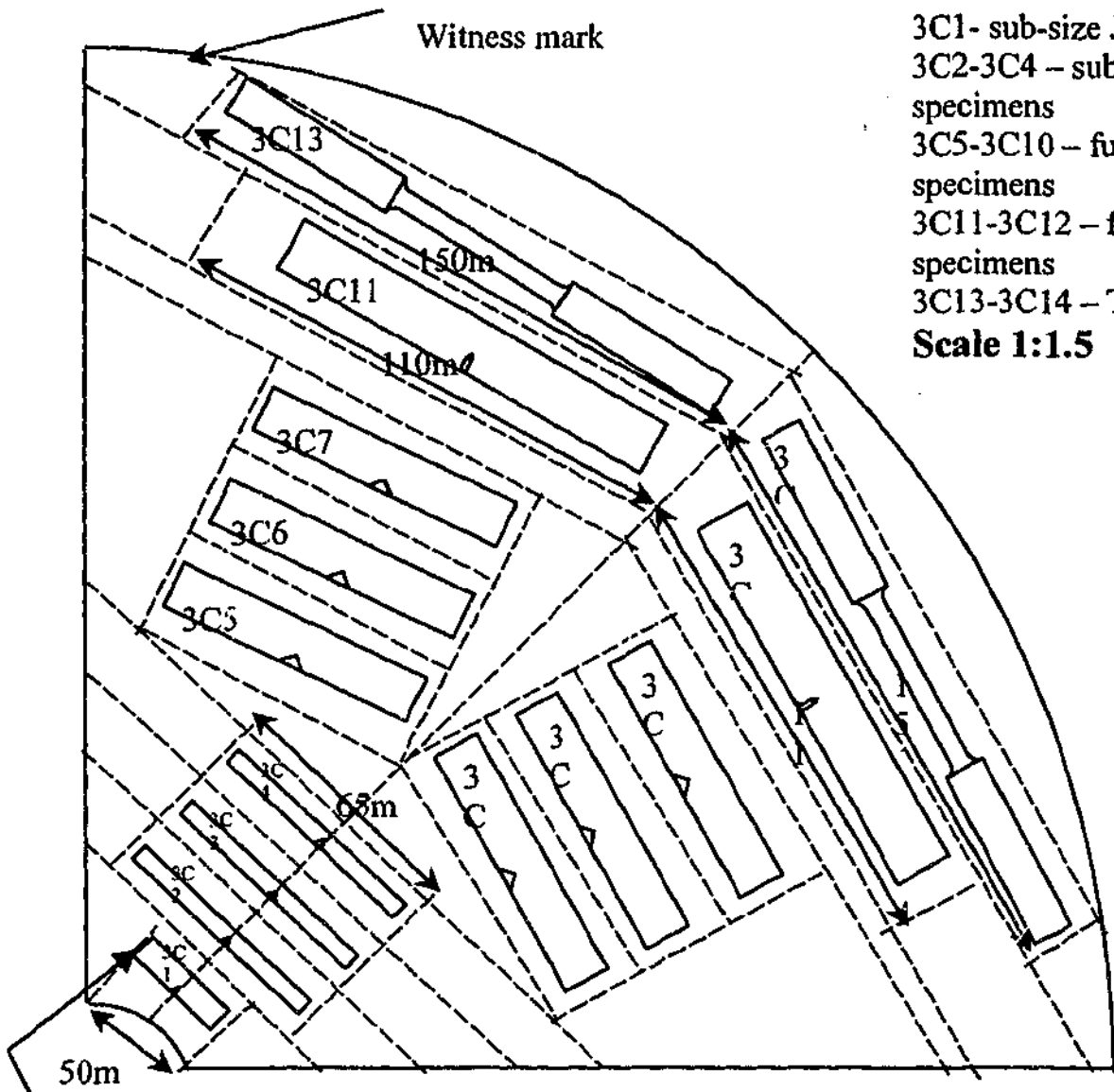

3C1- sub-size J_{Ic} specimens
3C2-3C4 – sub-size Charpy specimens
3C5-3C10 – full-size Charpy specimens
3C11-3C12 – full-size K_{Ic} specimens
3C13-3C14 – Tensile Specimens
Scale 1:1.5

Stage 12 Cut-up Plan

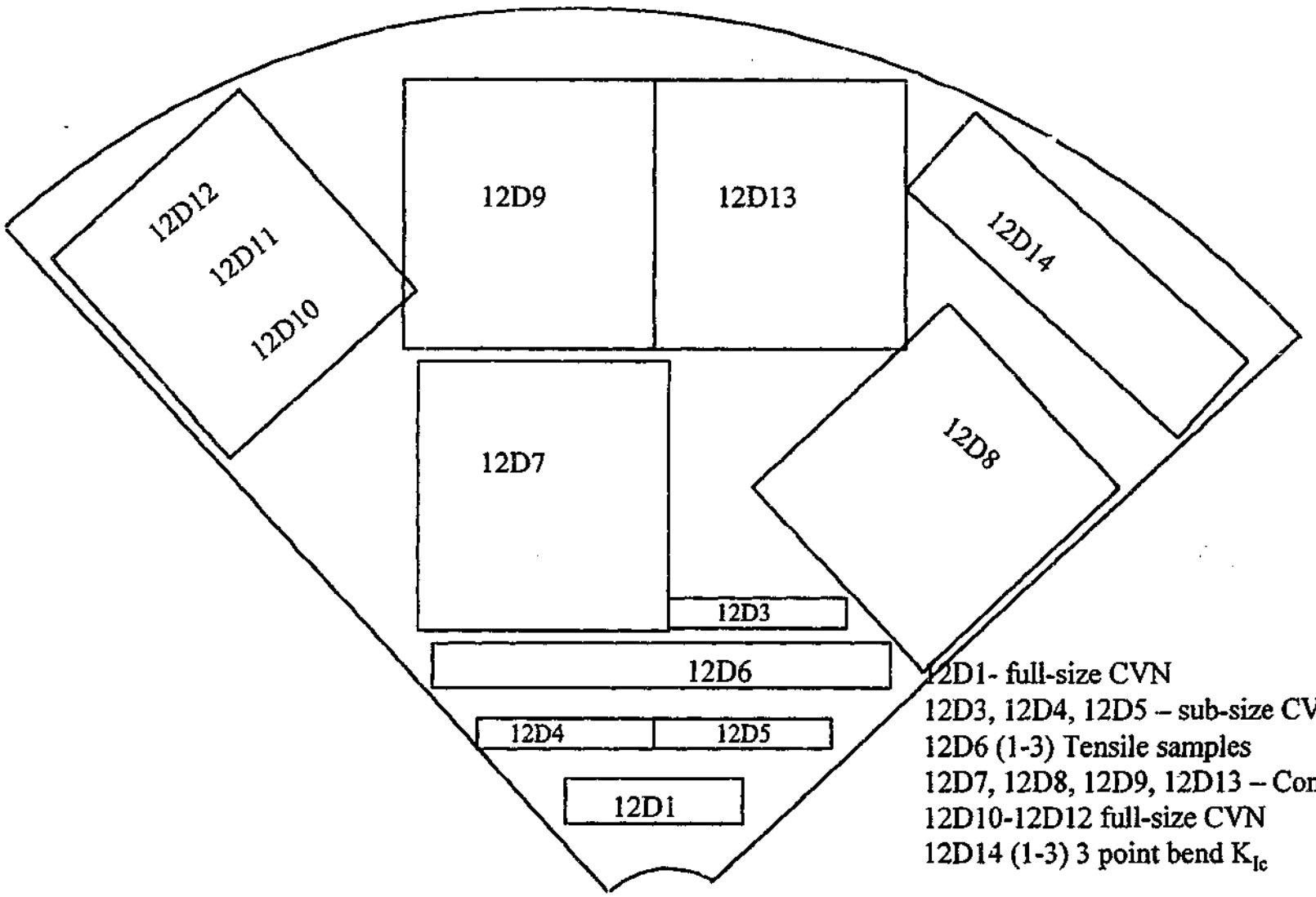

12D1- full-size CVN
12D3, 12D4, 12D5 – sub-size CVN
12D6 (1-3) Tensile samples
12D7, 12D8, 12D9, 12D13 – Compact J_{Ic}
12D10-12D12 full-size CVN
12D14 (1-3) 3 point bend K_{Ic}

Scale 1:2

APPENDIX B:
SPECIMEN CONFIGURATIONS

Dimensions of full-size Charpy Specimens

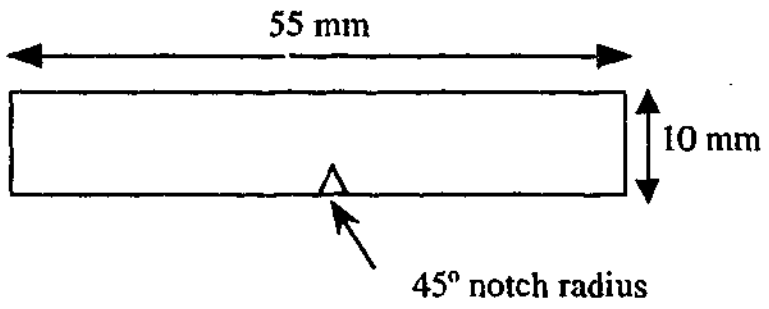

Dimensions of sub-size Charpy specimens

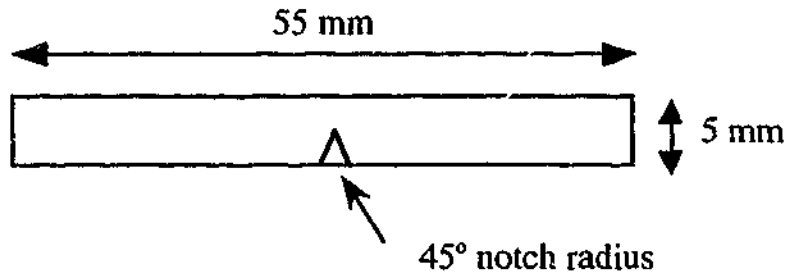

Dimensions of full-size K_{Ic} Specimens

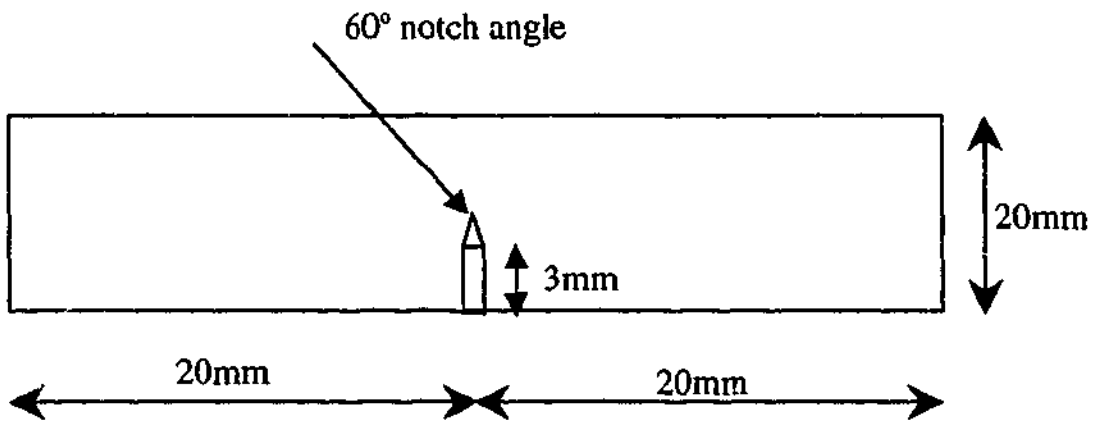

Dimensions of Tensile Test Specimen

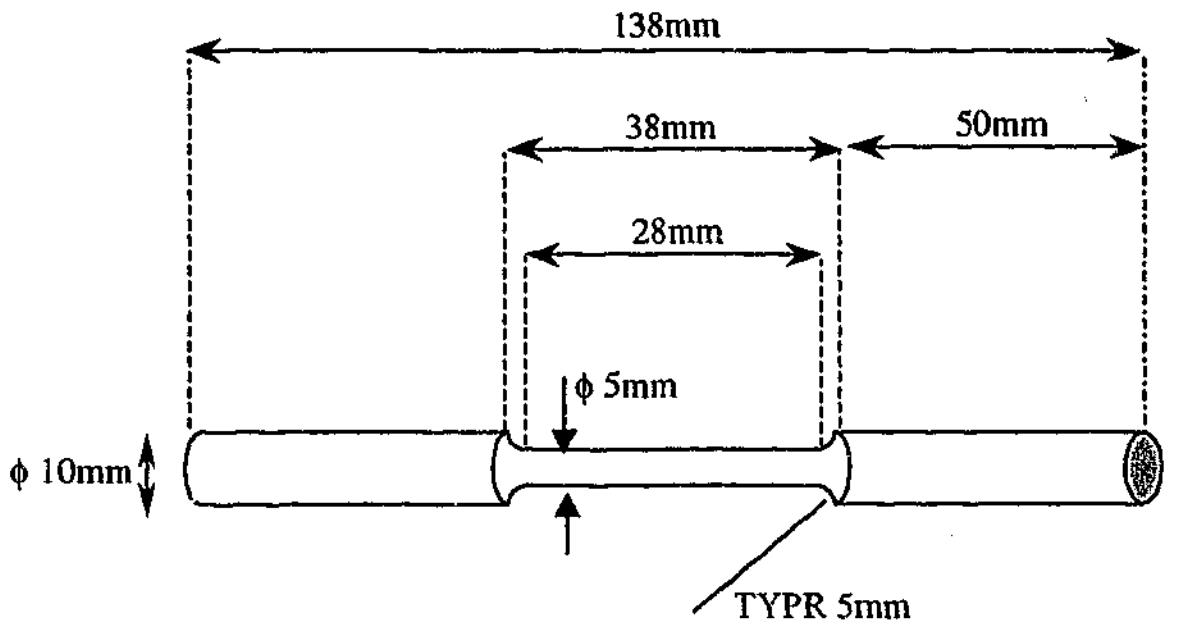

APPENDIX C: K_{Ic} Measurement

ASTM E399-90 was followed when conducting K_{Ic} testing. The procedure involved the following:

- Pre-cracking the three-point bend specimen (Re: Appendix B for specimen configuration). (Annex A2 of the AST, E 399-90). The following table summarises the fatigue loads used to create a fatigue crack from starter notch. Fig. C1 illustrates the three-point bend setup and the fatigue pre-cracking procedure.

Table C1: Fatigue Load Calculations

Fatigue interval	*Maximum Load, kN*	*Minimum Load, KN*	*Mean Load, kN*	*Amplitude*	*R*
First 1.05 mm from the the notch tip	2.26	0.226	1.243	1.017	0.1
Second 0.25 mm from the notch tip	1.71	0.171	0.9405	0.7695	0.1

Please note: K_{max} estimates were based on K_{Ic} values of ~30 $MPa^{1/2}$ (using values for ex-service rotors of similar age and composition: Viswanathan, 1989; Roberts and Newton, 1981).

- The specimens were loaded until the specimen could no longer sustain an increase in load. An example of the load vs displacement curve is given in Fig. C2.
- The determination of P_{max}/P_q is also shown in Fig. C2 and its validity was checked against the ASTM requirement.

Figure C1: pre-cracking of K_{Ic} specimen

- K_q was calculated using Annex 3 of ASTM E399-90. MS Excel was employed for calculations of f(a/w) and K_q. Its validity was assessed according to the ASTM requirements
- Specimens were heat-tinted and broken and the crack examined and measured. The crack front edge and surface were measured according the ASTM validity requirements (section 8.2.2 of the ASTM E 399-90). Figure C3 shows a crack comprising of a starter notch, fatigue pre-crack and crack propagation.
- The K_{Ic} value was calculated using an average of at least three valid K_{Ic} values according to ASTM E 399-90.

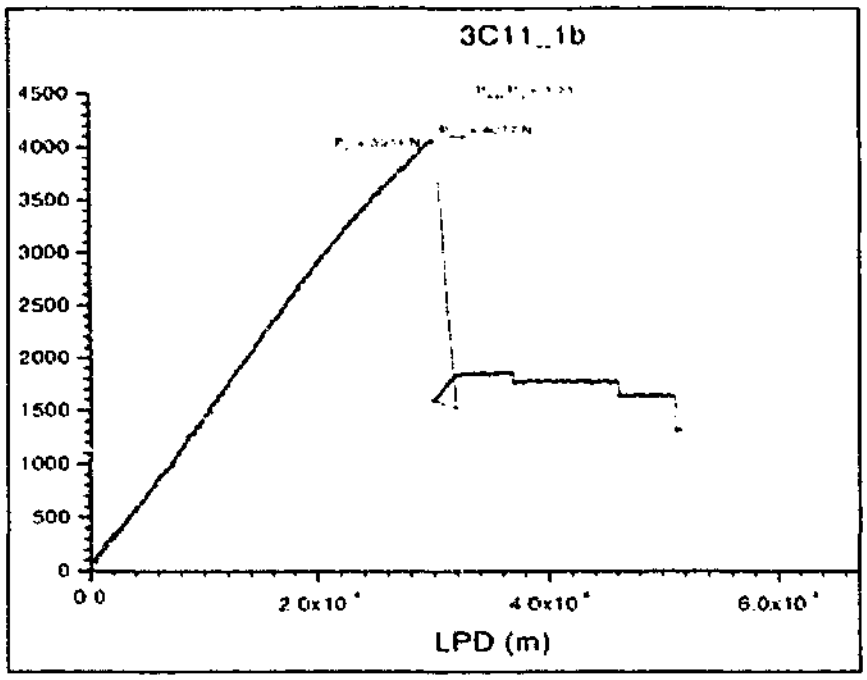

Figure C2: Typical Load vs Displacement curve used to calculate P_{max} and subsequently K_Q.

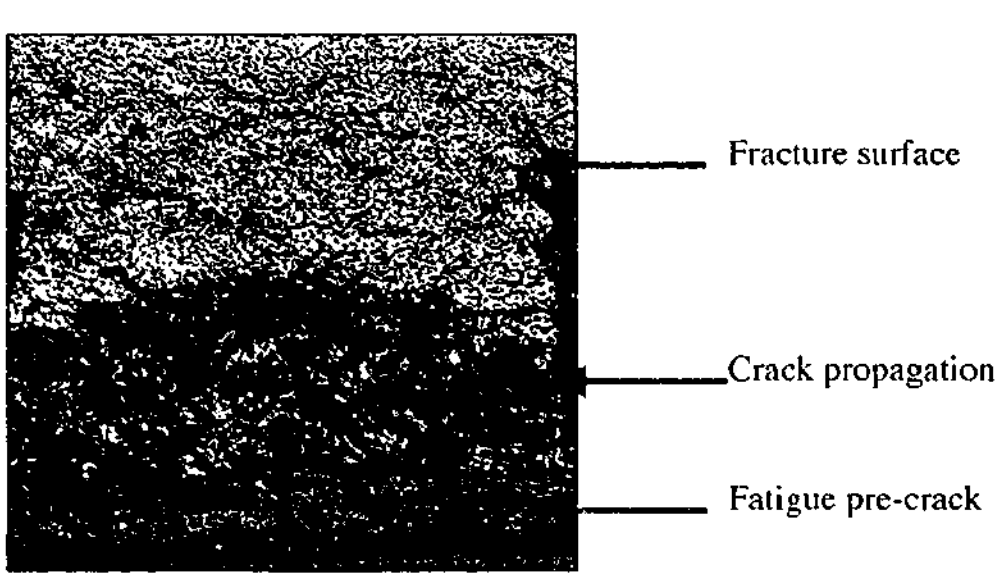

Figure C3: Fracture surface of a tested K_{Ic} specimen, showing the fatigue pre-crack, crack propagation and the brittle fracture surface.

APPENDIX D: PUBLICATIONS

A. Shekhter, A.K. Hellier, M.Drew, C.J. Moss and S.P. Ringer (1997) "Management of embrittlement issues in turbine rotor steels", Proceedings of Operating Pressure Equipment, Brisbane, Australia, IMMA, pp. 83-87.

C.A. Pullen, A.Shekhter, A.K. Hellier, C.J. Moss and S.P.Ringer, (1997). "Microstructure of a 200 MW HP/IP 1Cr-1Mo-0.25V Ex-Service Rotor", Proceedings of Materials Research Forum, Materials Conservation, IMMA, Melbourne, pp.119-122.

A. Shekhter, A.K.Hellier, C.J. Moss and S.P. Ringer, (1998). "Fracture Toughness of an Ex-Service Power Generating Rotor", Lifetime Management and Evaluation if Plant Structures and Components, Proceedings of the 4th International Conference on Engineering Structural Integrity Assessment, Churchill College, Cambridge, September, , Emas Publishing, pp.87-94.

A. Shekhter, A.B.L. Croker, A.K.Hellier, C.J.Moss and S.P. Ringer, (1999)."An Approach Towards the Assessment and Correlation of Fracture Toughness in an Ex-Service Power Generating Rotor", Proceedings of Operating Pressure Equipment, Melbourne, Australia, IMEA, pp. 271-277.

S. Kim, A. Shekhter and S.P. Ringer (1999). "Pre-service Processing and Microstructure of a Power Generating CMV rotor", Proceedings of Materials Research Forum, Melbourne Australia, November, pp.121-127.

A. Shekhter, A.B.L. Croker, A.K.Hellier, C.J.Moss and S.P. Ringer (2000). "Towards the Assessment and Correlation of Fracture Toughness in an Ex-Service Power Generating Rotor", International Journal of Pressure Vessels and Piping, 77/2-3, pp.113-116.

A. Shekhter, E.V. Pereloma and S.P.Ringer (2001). "Effect of Temper Embrittlement and Specimen Size on Charpy Impact Testing of HP-IP rotor" Journal of Materials Science and Technology, 17, pp.141-147.

A. Shekhter, S. Kim, D.C. Carr, A.B.L. Croker and S.P. Ringer, (2002). "Assessment of Temper Embrittlement in an Ex-Service 1Cr-1Mo-0.25V Power Generating Rotor by Charpy V-Notch Testing, K_{Ic} Fracture Toughness and Small Punch Test", ", International Journal of Pressure Vessels and Piping, 79, pp. 611-615.

S. Kim, A. Shekhter and S.P. Ringer (2002). "Microstructure and Microchemistry Variation During Thermal Exposure of Low Alloy Steels", International Journal of Pressure Vessels and Piping, 79, pp. 571-576.

A.Shekhter, A.B.L. Croker and S.P.Ringer (2002). "Assessment of Fracture Toughness in Power Generating Rotor Using Mechanical and Microstructural Techniques", Proceedings of the International Conference on Failure Analysis 2002, Melbourne, Australia.